공학박사학위논문

점소성 복합재료의 비선형 손상 모델과 해석 연구

Nonlinear Damage Modeling and Analysis of Viscoplastic Composite Materials

2014 년 8 월

서울대학교 대학원

협동과정 계산과학전공

박 일 경

ABSTRACT

Recently, polymeric composite materials have been widely used as the primary structures for saving the weight and increasing the efficiency in the aerospace industry. As the application of composite airframes is promoted, it is almost equipped that the engineering properties and analysis method for the composite structural design for the quasi-static and linear conditions. However, analysis methods for of the dynamic and nonlinear behaviors of composite materials are relatively deficient to fully predict structural responses, and which nonlinear behaviors are typically caused by the impact or crash conditions. Therefore, appropriate analysis methods for the rate-dependent and nonlinear behaviors of composite materials can improve the crashworthiness performance of aerospace structures.

The present study aims at the nonlinear damage models for the explicit finite element method with respect to strain rates which are to predict nonlinearly damaging behaviors of polymeric composite materials. The damage model for prior to material failure, which represents the rate-dependent damage modeling for polymeric composite materials with the viscoelastic and viscoplastic constitutive

model using a multi-scale approach. Phenomenologically, the nonlinear response of a composite under the in-plane shear loading condition is originated from the viscoplasticity of a matrix and the damage behavior of composite materials. In case of dynamic loading conditions, the strain-rate effects the change of the damage behavior of composite materials, as well as the behavior of the matrix. The enhanced micromechanical model which improves the in-plane shear behavior, is used for analyzing the rate-dependent behaviors of the fiber and matrix constituents. The rate-dependent elastic damage model based on orthotropic continuum damage mechanics theory at the macromechanical level is applied to improve the accuracy of the analysis model.

The damaging behavior after the material failure in this study, which represents the degradation after the composite failure. The rate-dependent composite failure criteria based on Hashin failure model is employed in this study. In order to degrade the stiffness and reduce the stresses, the enhanced damage progression model is proposed in this study. This model is suitable for the progressive failure analysis of composite materials using the explicit FE analysis, because it has one more variable than the original model which can adjust the progressive failure behaviors of composite laminates.

Predictions by presented the rate-dependent damage model are shown to agree fairly well with experimental results over a wide range of strain rates. The enhanced damage progression model is shown that it is quite suitable for the progressive failure model for the explicit finite element method.

Keywords : Enhanced damage progression model, Multi-scale approach, Polymeric composite, Progressive failure analysis, Rate-dependent damage model

Student number : 2010-30954

TABLE OF CONTENTS

LIST OF FIGURES

LIST OF TABLES

1. INTRODUCTION

Fiber reinforced composite materials with a polymeric matrix have rapidly become the primary materials for aircraft structures, due to the high specific stiffness and strength. Furthermore, increasing demands for eco-friendly transportation systems have encouraged automotive industries to adopt composite materials to improve fuel efficiency.

As crashworthiness is the crucial factor of the design requirements for the structures of the transportation vehicles, it is significant to study design/analysis methodologies of composite structures under severe loading conditions, such as crashes or impacts.

For laminate composite structures composed of orthotropic and heterogeneous fiber reinforced polymeric composite materials, the optimal stacking sequence a laminate is typically designed based on dominant static loads under the normal operating conditions. In the events of collisions or crashes, however, transportation vehicles may encounter extreme load conditions with very high strain-rates up to several hundred per second in unexpected directions. Therefore, in order to

improve the crashworthiness of composite structures, it is necessary to predict the nonlinear behaviors of composite materials caused by impacts or crashes loading conditions and material failures.

The variational stress-strain response with respect to strain rate, nonlinear deformation under in-plane shear loading, and the material failure and progressive failure can count as the dominant nonlinear behaviors of polymeric fiber reinforced composite materials under the impact or crash events. The nonlinear behaviors prior to material failure are known as the results from the viscoelastic and viscoplastic properties of polymeric matrix constituents and the micro-crack within the matrix and interface of constituents. The post failure behavior, namely, the progressive failure of laminate composite materials is in consequence of very complex phenomena such as lamina failure progression, inter-laminar shear failure and delamination etc. However, the appropriate prediction for the progressive failure is important to evaluate the crashworthiness performance of aerospace structures, because it is the prominent means of energy dissipation due to the material facture.

The present study aims at the nonlinear damage models for the explicit finite

element method with respect to strain rate up to several hundred per second which are to predict nonlinearly damaging behaviors of polymeric composite materials. The damage behavior prior to material failure, which represents the rate-dependent damage model (RDM) for polymeric composite materials with the rate-dependent constitutive model using a multi-scale approach. Phenomenologically, the nonlinear response of a composite under the in-plane shear loading condition is originated from the viscoplasticity of a matrix and the damage behavior of composite materials. In case of dynamic loading conditions, the strain-rate effects the change of the damage behavior of composite materials, as well as the behavior of the matrix. The enhanced micromechanical model which improves the in-plane shear behavior, is used for analyzing the rate-dependent behaviors of the fiber and matrix constituents. The rate-dependent elastic damage model based on orthotropic continuum damage mechanics (CDM) theory at the macromechanical level is applied to improve the accuracy of the analysis model.

The progressive failure analysis (PFA) model in this study, represents the material failure detection and the stiffness and stress degradation after the composite failure for the application on the crash and impact simulation of aircraft composite structures. The rate-dependent composite failure criteria is employed in

this analysis model based on the Hashin failure model. To account for the progression of damage, the ply-discounting material degradation approach with the enhanced damage progression model (EDPM) based on the CDM approach using internal state variables is employed in this study. The ply-discounting material degradation is general method for the PFA in the explicit finite element method, because each layer in laminate composites is expressed as each integration point. In order to degrade the stiffness and reduce the stresses in the level of lamina, the EDPM based on the Yen's damage model (or MLT model) is proposed in this study. This model is efficient method for the PFA of composite materials, because it has one more variable than the original model which can adjust the post failure behavior. Through applying this damage model, we can approximately account for the progressive failure behavior caused by the interaction between layers in laminates and delamination into the analysis using multi-integration points shell elements.

1.1 Backgrounds

Several experimental studies have been carried out to study the strain rate effects on the material properties of polymeric fiber reinforced composite materials

[1-3]. The rate-dependent behavior of composite materials originated mostly from the rate-dependence of each constituent. Carbon fiber widely used in aerospace applications, is known to be rate insensitive, while the glass fiber has the rate-dependent material property [4]. Polymers have been widely employed as the matrix of advanced composite laminates. Polymers are known to have not only nonlinear rate-dependent deformation in range beyond one or two percent strain, but also the rate-dependent rupture strength at wide range of strain rates [5-7]. Another principal factor is the hydrostatic stress that generates the nonlinear behavior of polymers [8,9].

At the early stage of the research, viscoelasticity models have been used to represent the rate-dependent polymer behavior [10]. Thereafter, mature plastic and viscoplastic constitutive equation for metals have been adopted on predicting the behaviors of rate-dependent polymers and polymeric matrix composite materials [11-13]. However, there is a demerit that the nonlinear model based on metals could not accurately describe the polymer's response to hydrostatic stresses. Goldberg et al. [14] has modified the Bodner-Partom viscoplastic state variable constitutive equation, which was originally developed for metals, to account for the effects of hydrostatic stresses with a state variable.

Polymeric matrix fiber reinforced composite materials have been modeled by means of macromechanical approaches or micromechanical approaches to analyze rate sensitive behaviors. Sun et al. [11,12] developed a macromechanical approach to obtain transversely isotropic viscoplasticity model to analyze the nonlinear deformation of polymeric composite materials. Kim and Oden [15] applied the "unmixing-mixing" method which is the micromechanical approach to account for viscoplastic behaviors, to the materials of type N using the modified Bodner-Partom model. Thereafter, "unmixing-mixing" method was used to predict the viscoplastic behavior of thermoplastic composite materials at elevated temperature and low strain rates by Kim and Cho [16]. Goldberg [17] analyzed the nonlinear behavior at low strain rates based on the micromechanical approach of Sun and Chen [18], but this method was available only for the cases of low strain rates. After several years, Goldberg [19] developed the advanced micromechanical approach using slice algorithm of Mital et al. [20], which worked fairly well at strain rates from 10-5/s to 400/s. Thereafter, Goldberg [14] and Zheng [21] applied this micromechanical method to analyze the rate-dependent deformation of polymeric composite materials.

The non-linearity observed in the stress-strain curve of off-axis composite

materials is known to be caused by viscoplastic behaviors of the matrix and micro-cracks in the matrix or at the fiber/matrix interface before failure [22,23]. In order to describe this non-linearity, traditionally, Petit and Waddoups [24] presented the nonlinear stress-strain curve as the piecewise linear. Hahn [25] superposed the nonlinear term upon the in-plane shear constitutive relationship and Hashin et al. [26] adapted Ramberg-Osgood parameter on the ply under off-axis loading to predict the nonlinear deformation. Sandhu [27] got the accurate results through employing the piecewise cubic spline Interpolation function in constitutive equations.

The plastic, viscoplastic or continuum damage theory was employed to predict the nonlinear deformation of composite materials under off-axis loading [28-30]. Ladeveze and Dantec [31] have devised the degradation model for off-axis composite materials with a plastic flow equation coupled with the damage values which is in proportion to the stress in each ply. This nonlinear model is appropriate to apply on the thermoset composite materials.

When the dynamic loading in non-fiber direction on polymeric fiber reinforced composite materials, the in-plane shear nonlinear behavior and the rate sensitivity

simultaneously arise, since the contribution of polymers among the material properties of composite materials is enlarging [32,33]. Thiruppukuzhi and Sun [32] developed the macromechanical model and the rate-dependent failure criteria based on experimental studies of glass fiber reinforced composite materials under off-axis loading at low strain rates. Goldberg [17] and Zheng [21] expanded the micromechanical model and the rate-dependent failure criteria into carbon fiber reinforced composite materials.

From a phenomenological point of view, it should be applied on laminate composite materials under the in-plane shear dynamic loading that the nonlinear model contains not only viscoelastic and viscoplastic behaviors and micro-crack development of polymers, but also the strain rate sensitivity of these nonlinear elements. However, in previous studies for rate-dependent polymer matrix composite [11,12,14,17,19,21], the degradation caused by the damage in the matrix and at the matrix/fiber interface was not considered on off-axis and angle-ply composite materials. Deenadayalu et al. [34] proposed the phenomenological model which employed the modified state variable inelastic equations for polymers in order to account for the effects of damage in the matrix of polymeric composite materials with a micromechanical approach. However, this model had limitations

as the phenomenological approach for the composite damage, because the macromechanical model was not implemented to account for the damage at the matrix/fiber interface.

The PFA methodology typically consists of damage and failure detection, damage progression, and crack simulation. Crack simulation of laminate composite materials is typically considered in the finite element analysis scheme using a three dimensional meshing model. In case of two dimensional finite element approach, the crack propagation is altered as appropriately computational methods.

Numerous efforts have been conducted previously to develop damage and failure detection theories for composite materials. Mostly common failure criteria, namely, the maximum stress criteria, the maximum strain criteria, the Tsai-Wu failure polynomial, and the Hashin criteria [35-39] were widely used for composite strength analysis. Among above a sort of criteria, the Tsai-Wu failure polynomial and Hashin model are an interacting failure criterions, then Hashin failure criteria has been widely applied in the explicit finite element method, also it was employed in this study. In the 2000's, Paris have done a thorough survey on the failure criteria of fibrous composite materials [40]. During the World Wide Failure

Exercise (WWFE), Soden et al. [41,42] investigated the accuracies of several failure criteria based on a comparison to experimental results. As a result, the failure criteria developed by Puck and Schurmann [23], Zinoviev et al. [43], Kuraishi et al. [44], and Sun et al. [45] displayed good predictive capabilities.

Through many experimental studies, it has been shown that strain rate has great effect on the polymer's deformation behavior such as the increasing of the modulus, yielding stress, and ultimate stress [5,6,7,33]. As previously described, Thiruppukuzhi and Sun [32] developed the rate-dependent failure strength model for polymeric composite materials, then Goldberg [17] and Zheng [21] have applied this rate-dependent failure strength model to the rate-dependent failure criteria for carbon fiber reinforced composite materials based on Hashin model.

Damage progression strategies provide material degradation. Various material degradation models have been proposed and demonstrated for laminated composite structures [37,41,42,46-53]. These models may be generally categorized into two main groups: heuristic models based on a ply-discounting material degradation approach and models based on a CDM approach using internal state variables [54]. Among CDM approaches, the Matzenmiller, Lubliner and Taylor (MLT) model is

known as the most popular damage progression methodology. MLT model was proposed by Matzenmiller et al. [55] such a model based on the use of a Weibull function [56] to describe the statistical nature of internal defects and the ultimate strength of a fiber bundle within a composite lamina. Creasy [57] developed a different model based on the Weibull function, and Moas and Griffine [50] used Weibull functions in their degradation model. Yen [77] proposed the alternative damage growth model, which model is more straight forward and consistent then the original MLT model. Yen's model was modified as more functionality to simulate the damage progression in this paper. The MLT model was applied in LS-DYNA as material MAT58 [58].

Zhu et al. [59] proposed the stiffness degradation model suitable for the micromechanical model. This model employed Hashin failure criteria as damage and failure detection, and three dimensional (3D) sectional micromechanics model of the polymer matrix composite materials is discussed.

1.2 Scope of this works

The objective of this research is to develop the phenomenologically enhanced, effective and accurate nonlinear damage models for polymeric composite materials

to implement into the explicit finite element method, which model can predict the nonlinear and rate-dependent behaviors whenever it is pre or post failure. In order to attain the objective, the present study introduces nonlinear damage models for the analysis of nonlinear behaviors before and after material failure.

In Chapter 2, the RDM with the state variable inelastic equation for polymers using a multi-scale approach will be introduced with the background on the phenomenological description about the rate-dependent behavior of polymeric composite materials and the nonlinear behavior under in-plane shear loading. An enhanced micromechanical model using the modified slicing algorithm is also introduced to improve the accuracy of prediction of in-plane shear stresses. For the verification of the modified slicing algorithm, obtained material properties using proposed model are validated with experimental results [67-69]. The RDM based on an orthotropic continuum damage using a multi-scale approach, predicts the degradation of composite laminates under dynamic loading, it has scalar damage variable which is calculated from the stresses in each ply. From macromechanical point of view, scalar damage variable is implied into constitutive equations of composite elementary ply which is generated by the enhanced micromechanical approach.

The damage model for post failure and the PFA methodology using this damage model for UD composite materials will be given in Chapter 3. It is fit for a multi-scale approach and an explicit finite element methodology. The strain rate dependent failure criteria based on the Hashin model will be implied into the PFA model, then the EDPM, which is based on the Yen's damage model is introduced in this chapter. The methods for degradation of stiffness and reduction of stress which are most suitable for the multi-scale approach including the micromechanical composite model, are presented also.

In Chapter 4, the implementation in the explicit finite element method and validation process of the proposed damage models and verified results with experiments will be introduced. For the verification, developed models are implemented as a UMAT (User Material Subroutine) linked to explicit finite element software, LS-DYNA, and then the computed results are compared to experimentally obtained results for several representative polymeric UD carbon epoxy composite materials.

In Chapter 5, the discussion of the examined and compared results will be presented. Finally, the study will be summarized in Chapter 6.

2. RDM MODEL FOR POLYMERIC COMPOSITES

Under in-plane shear dynamic loading, polymeric composite materials typically show the rate-dependent and nonlinear stress-strain response simultaneously. It is known as the effect of polymeric matrix constituent. Polymers have the characteristics of viscoelastic and viscoplastic as well as relatively high plastic deformation. In case of in-plane shear loading on polymeric composite materials, the micro-cracks in the matrix or at the fiber/matrix interface generate the degradation of stiffness. To effectively simulate these nonlinear behaviors of polymeric composite materials, the RDM using a multi-scale approach is introduced in this study. The RDM is composed of the micromechanical model with the viscoelastic and viscoplastic matrix constitutive equations and the macromechanical damage model based on the CDM of a composite lamina.

2.1 Phenomenological description for polymeric composite materials under in-plane shear dynamic loading

To develop the analysis model for the nonlinear behavior of polymeric composite laminates under arbitrarily directional dynamic loading conditions, the phenomenological inquiry presented for the source of nonlinear deformations such as anisotropic behavior, rate-dependent characteristics, and the initiation and evolution of the micro-cracking of composite laminates.

2.1.1 Orthotropic behavior of fiber reinforced composite materials

Due to heterogeneity of fiber reinforced composite materials, the orthotropic deformation and failure mechanism of individual layers can be typically observed. It is known that these are derived from the large discrepancy of the stiffness and strength between fiber and matrix. When a UD composite lamina is loaded in fiber direction, the largest portion of the load is transferred by the fibers due to their high

stiffness compared to the matrix and it has the linear and brittle manner of behaviors. Also, the transmission of tensile loads in the fiber is not influenced by the state of damage in the matrix [70]. In UD composite materials, fiber failure trigger structural collapse almost immediately. Under compressive load in fiber direction, the composite failure is considered to be a micro-buckling problem. This phenomenon is influenced by several factors such as fiber geometry, fiber waviness, fiber-matrix bonding, and the stiffness and strength of fiber and matrix [71]. The effective stiffness and strength of matrix significantly affect the carrying capability for compressive load. The matrix works as an elastic base for the fibers under compressive load condition [70]. Under compressive load in fiber direction, micro-cracks close up and they do not influence the behavior in fiber direction.

The transverse behavior of UD composite materials is highly anisotropic with low strength and stiffness in the matrix direction. In the transverse direction, the normal and shear stresses are transmitted by both matrix and fiber. Under transverse tensile loading, $\sigma_{22} > 0$, in-plane shear stress, σ_{12}, existing defects such as small de-bond, voids, and resin rich regions in the matrix or at the fiber/matrix interface trigger a transverse crack, which extend through the ply thickness. The nonlinear behavior before failure originates from these defects as

well as viscoplasticity of the matrix [22,23,72]. Under transverse compressive load, $\sigma_{22} < 0$, matrix cracks in the sense of "fragmentation" of brittle matrix materials [70]. As same in fiber direction, there is no effect of micro-cracks under the compressive loads in matrix direction.

2.1.2 Nonlinear behavior of in-plane shear loaded composite materials

The stress-strain behavior of in-plane shear loaded composite laminae depend on the difference of each constituents, the inclined loaded angle with fiber direction, and the nonlinear behavior caused by micro-cracks and viscoplasticity of the matrix. Fig. 2.1 shows the stress-strain curves for a glass fiber [32] and carbon fiber [17] reinforced composite materials under off-axis loading. As the off-axis angle increases, degradation and non-linearity become more dominant. Beyond 45 degree of inclined angle, both of materials converge to a similar range of stress-strain behavior.

Lafarie-Frenot and Touchard [22] have conducted a comparative study of the in-plane shear behavior of the AS4/PEEK thermoplastic and T300/914 thermoset materials. Herein, the phenomenological study is presented for the behavior of thermoset polymeric composite materials by means of the detailed investigation

about the nonlinear behavior and damage accumulation characteristic presented in Ref. [22].

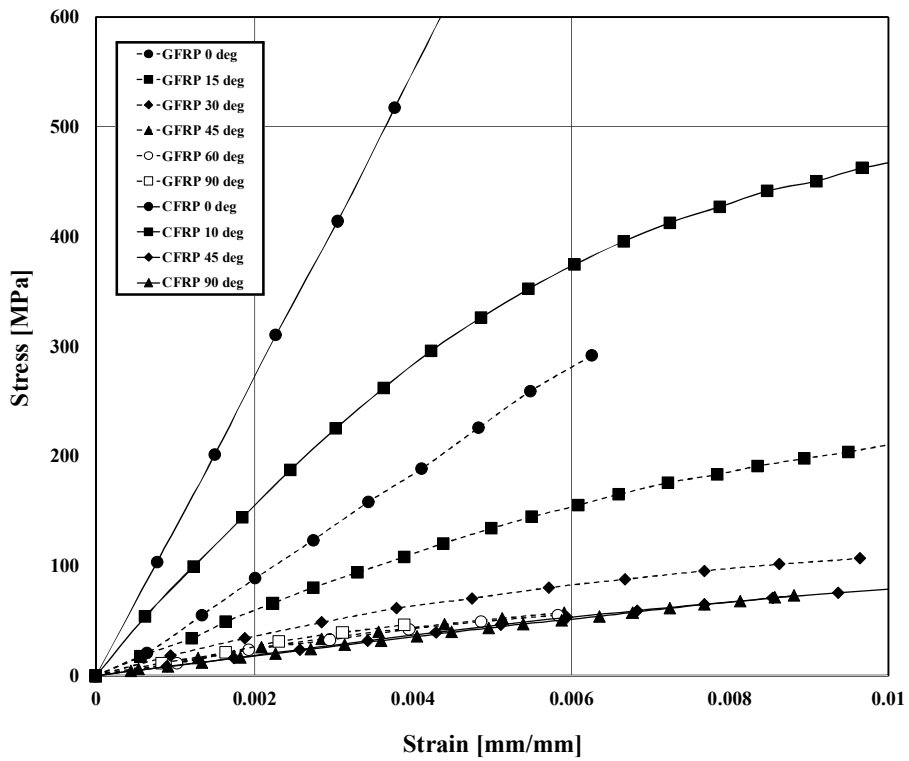

Fig. 2.1 Stress/strain curves for various off-axis coupons of the UD GFRP (S2-glass/8553-40) [30] and CFRP (IM7/977-2) [17]

Fig. 2.2 presents stress-strain curves by a static and monotonic tensile tests for $[\pm 45°]_{2S}$ coupon of the UD T300/914 thermoset material. The monotonic test presented by the dotted line is to obtain residual stiffness values, which is executed

with several quasi-static loading/unloading sequences. It is shown that the in-plane shear modulus gradually decreases in accordance with increasing strain.

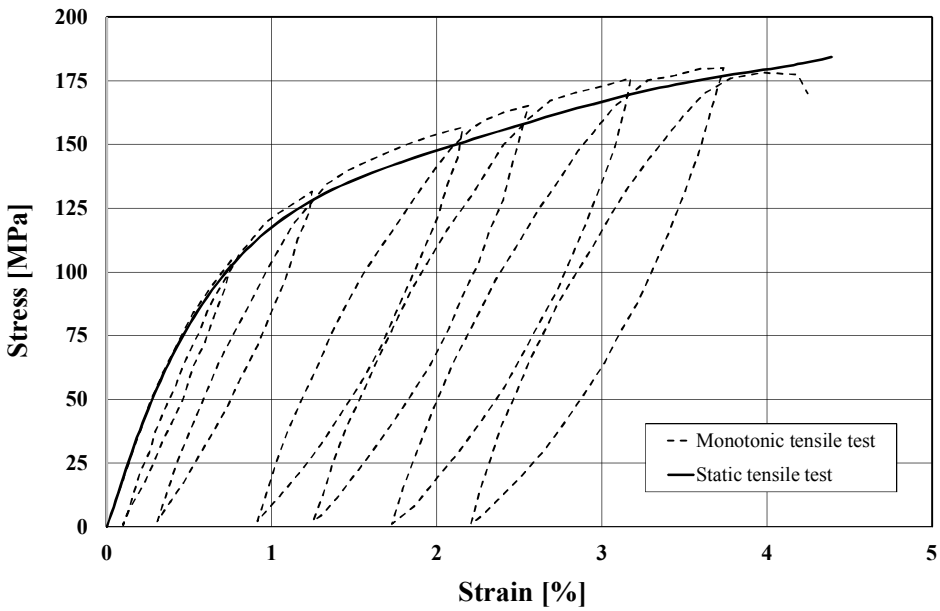

Fig. 2.2 Stress/strain curves by monotonic and static tensile tests for the T300/914 $[\pm 45°]_s$ laminate [22]

Fig. 2.3 shows the change in the matrix crack number and the average crack length with respect to applied stress, σ_{xx}, which were observed by X-ray photographs. The X-ray observation is not for detecting micro-cracks, but visible cracks. The initial crack is observed about 110 MPa and very few cracks are presented when the applied stress is less than about 150 MPa. The initiation and

evolution of cracks are rapidly increasing at 150 MPa of applied stress.

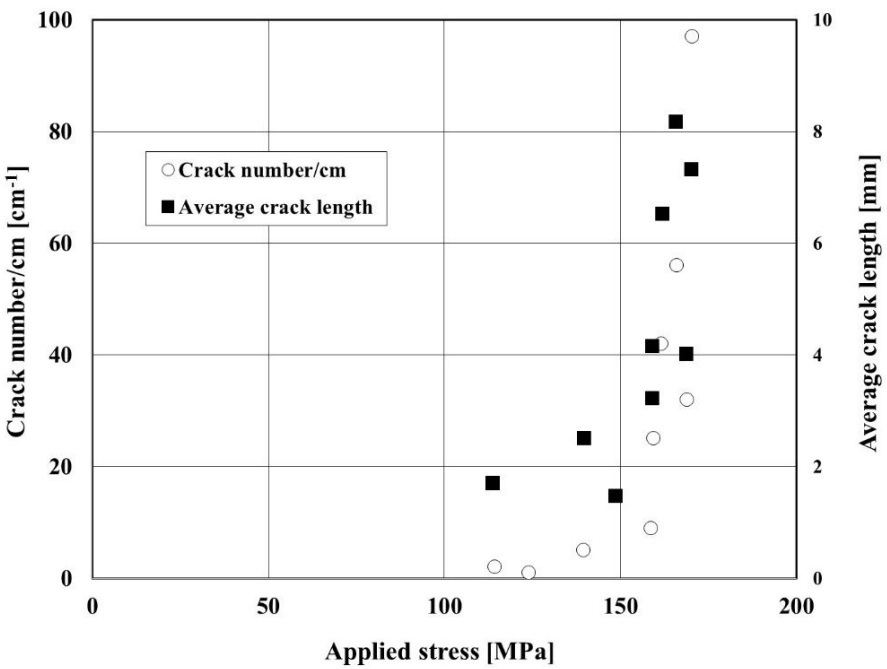

Fig. 2.3 Change in matrix crack number and average crack length with applied stress for the T300/914 $[\pm 45°]_s$ laminate [22]

Fig. 2.4 depicts the change in ply strains and matrix shear strain with respect to laminate applied stress, where solid lines present the strains in lamina level and the dotted line shows the calculated strain in matrix using the rule of mixture (ROM). Material properties of fibers, matrices and laminates to calculate the strains in

matrix are listed in Table 2.1. The 914 epoxy resin system reaches the ultimate shear strain (2.75%) at about 125 MPa of applied axial stress in Fig. 2.4 [73]. The strain calculated by the ROM represents the averaged value, where we can estimate that the matrix shear failure will develop at around 125 MPa. Therefore, the crack initiation at 110 MPa of applied axial stress, could be interpreted as a results of the shear failure of resin.

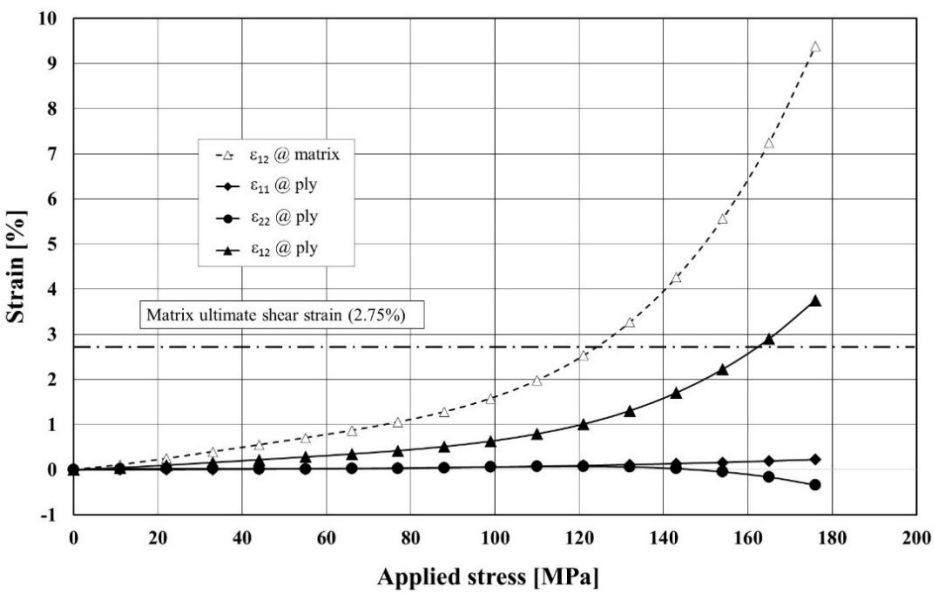

Fig. 2.4 Change in ply strains and the matrix shear strain with the laminate applied stress for the T300/914 $[\pm 45°]_s$ laminate [22]

Table 2.1. Mechanical properties of constituents and lamina of the T300/914

Material	Longitudinal elastic modulus [GPa]	Transverse elastic modulus [GPa]	Poisson's ratio, ν_{12}	Initial shear modulus [GPa]	Ultimate shear strain [%]	Fiber volume fraction
Matrix						
914 [73]	4.0	-	0.37	1.5	2.75	-
Fiber						
T300 [74]	233	16.7	0.20	24	-	-
Lamina						
T300/914 [75]	135	9.2	0.37	4.9	-	0.57

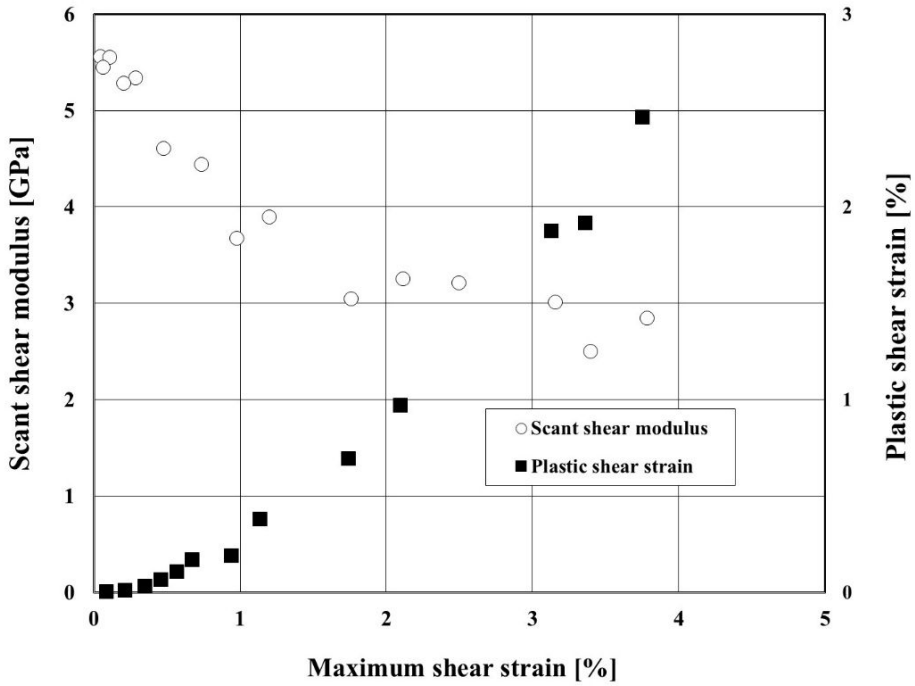

Fig. 2.5 Scant shear modulus, G_{12} and plastic shear strain versus max. shear strain for the T300/914 $[\pm 45°]_s$ laminate [22]

Fig. 2.5 presents the scant shear modulus, G_{12}, and the plastic shear strain with maximum shear strain. The scant shear modulus starts decreasing when the maximum shear strain is over 0.2%. This change can be observed in the plastic shear strain data. About 0.2% of shear strain of lamina at 40 MPa of applied stress in Fig. 2.4 can be estimated, and we can find that the nonlinear stress-strain behavior begins at this stress level in Fig. 2.2. Consequently, we can assume that other principal source(s) in intra-ply may exist before visible matrix cracks, then it

effects the in-plane stiffness degradation of composite laminates. This assumption matches up with the discussion in Puck and Shurmann [23] that the main reasons for the nonlinear behavior are the viscoplastic behavior of the matrix and, probably, micro-cracks in the matrix or at the fiber/matrix interface long before visible "matrix cracks". Therefore, in this study, the nonlinear behavior of UD composite materials under in-plane shear loading is simulated by means of the appropriate elastic damage model represented the initiation and evolution of micro-cracks and the viscoplastic model for polymeric composite materials which is coupled with the damage model.

2.1.3 Rate-dependent behavior of polymeric composite laminates

The rate-dependent behavior of polymers is originated from viscoelasticity, viscoplasticity, and variation of failure strength versus strain-rates. Polymers are known to have a rate-dependent deformation response that is nonlinear in range of one or two percent strain. As increasing strain rate, the elastic modulus of polymers typically rises up, while the failure strain of polymers falls off [3]. It is assumed that polymers tend to fail in a brittle manner at high strain rates.

Since carbon fibers is not rate-dependent, the deformation in fiber direction exhibits neither non-linearity nor strain-rate dependence. However, the polymeric composite materials have an equivalent level of rate-dependent properties in matrix dominant directions, presented in Fig. 2.6 [1].

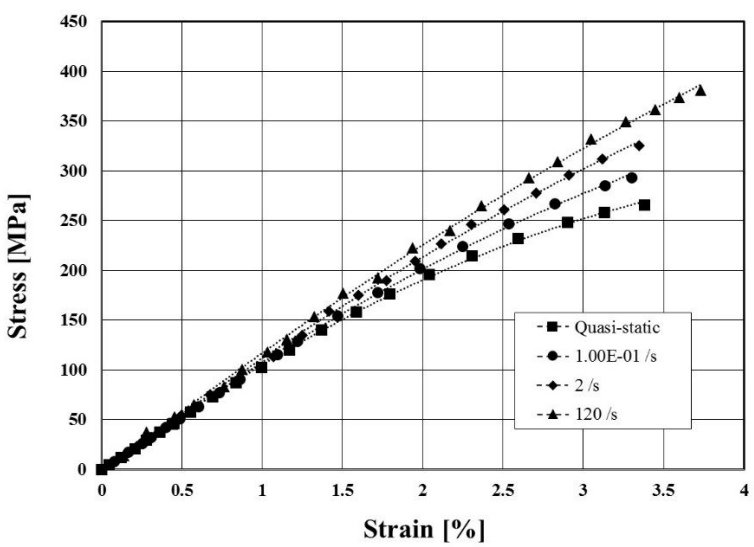

(a)

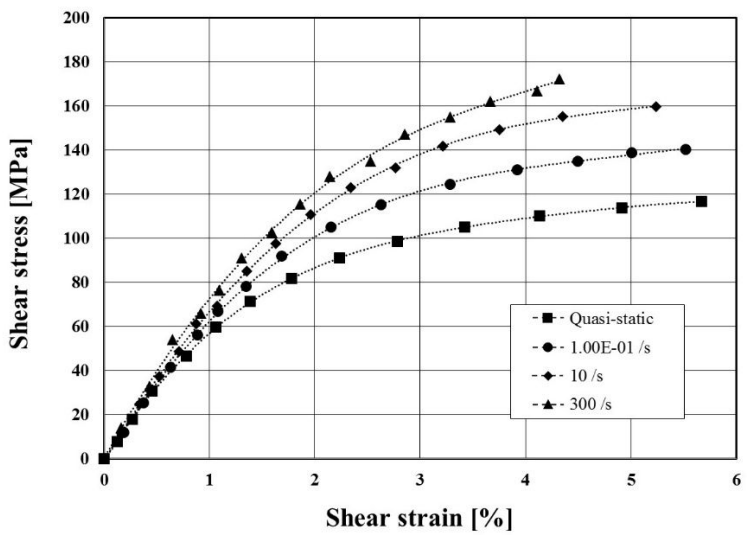

(b)

Fig. 2.6 UD carbon/epoxy composite under quasi-static and strain rate compressive loading: (a) transverse loadings; (b) 30deg of off-axis loadings [1]

Thiruppukuzhi and Sun [32] proposed the model to present change of failure strength with respect to strain-rate through the experimental study for glass fiber composite materials. The strength parameter k_{cr} can be expressed a function of strain rate, $\dot{\varepsilon}$, as:

$$k_{cr} = k_{cr}^{*}\left(\frac{\dot{\varepsilon}}{\dot{\varepsilon}^{*}}\right)^{\beta} \tag{2.1}$$

where the * quantities correspond to the reference strain rate and β is material constant determined by the dynamic coupon test. Goldberg [17] and Zheng [21] have applied the rate-dependent strength function to carbon/epoxy composite

materials.

2.2 Rate-dependent polymer model

The isotropic elasto-plastic constitutive equation is applied to the rate-dependent polymer model. Temperature and moisture effects are not considered. The nonlinear strain recovery observed in polymers during unloading is not simulated, and small strain theory is assumed to apply. Phenomena such as creep, relaxation and high cycle fatigue are not accounted for within the equations. The elasto-plastic strain-rate equation can be expressed as:

$$\dot{\varepsilon}_{ij} = \dot{\varepsilon}^{e}_{ij} + \dot{\varepsilon}^{I}_{ij} \tag{2.2}$$

The total strain rate, $\dot{\varepsilon}_{ij}$, is composed from the elastic component, $\dot{\varepsilon}^{e}_{ij}$, and the inelastic component, $\dot{\varepsilon}^{I}_{ij}$. Since the stresses are only proportioned to the elastic strain, Eq. (2.2) can be written as:

$$\dot{\varepsilon}^{e}_{ij} = \dot{\varepsilon}_{ij} - \dot{\varepsilon}^{I}_{ij} \tag{2.3}$$

Eq. (2.3) can be substituted into the strain components in the constitutive relationship for polymers, then the polymer's constitutive equation can be written

as:

$$\dot{\sigma}_{ij} = C_{ijkl}\left(\dot{\varepsilon}_{kl} - \dot{\varepsilon}^{I}_{kl}\right) \qquad i,j,k,l = 1 \dots 6 \tag{2.4}$$

The rate-dependent behavior of polymers is implied into the stiffness matrix, C_{ijkl}, as variable elastic modulus by the viscoelastic model for polymers. The inelastic strain rate tensor in Eq. (2.4) is expressed by the viscoplastic model for polymers.

2.2.1 Viscoelastic model for polymer

The rate of increasing of an elastic modulus tends to vary in accordance with a range of strain rates [7,19,76]. This tendency is accounted for by means of definition of the proper viscoelastic model at the lower and upper ranges of strain rates, in this study. The reference strain rate for dividing of the range of strain rates is determined as 200 /s.

The viscoelastic model at the lower range can be expressed as:

$$E = E_0 exp(C_1 \dot{\varepsilon}) \tag{2.5}$$

Above equation is generated from the dynamic coupon tests for the M015

epoxy resin system produced by TB Carbon Company. The dynamic coupon tests were conducted using the constant stroke machine (Instron VHS 8800 High strain rate systems). Dog-bone shaped specimens were used for the dynamic tensile tests with a gage length of 30 mm [33].

E is the elastic modulus at the effective strain rate, $\dot{\varepsilon}$, E_0 is the reference elastic modulus, and C_1 is the scaling material constant of the viscoelastic model at the lower range.

To account for the change of the elastic modulus at the upper range of strain rate, we utilize the Johnson-Cook model commonly used to describe the behavior of metals at high strain rates [21, 77]. The viscoelastic model at the upper range for polymers is written as:

$$E = E_0\left(1 + C_2\, ln\frac{\dot{\varepsilon}}{\dot{\varepsilon}_0}\right) \tag{2.6}$$

C_2 is the scaling material constant of the viscoelastic model at the upper range. The effective strain rate, $\dot{\varepsilon}_0$, is assumed to equal 1/s in this study.

The effective strain rate, $\dot{\varepsilon}$, can be expressed as:

$$\dot{\varepsilon} = \sqrt{\frac{2}{3}[(\dot{\varepsilon}_{11} - \dot{\varepsilon}_m)^2 + (\dot{\varepsilon}_{22} - \dot{\varepsilon}_m)^2 + (\dot{\varepsilon}_{33} - \dot{\varepsilon}_m)^2 + 2\dot{\varepsilon}_{12}^2 + 2\dot{\varepsilon}_{23}^2 + 2\dot{\varepsilon}_{13}^2]} \quad (2.7)$$

where

$$\dot{\varepsilon}_m = \frac{1}{3}(\dot{\varepsilon}_{11} + \dot{\varepsilon}_{22} + \dot{\varepsilon}_{33})$$

Fig. 2.7 shows the variation of the elastic modulus with respect to strain rate and the comparison with experimental results and prediction results for the M015 epoxy. The viscoelastic model at the lower range is in good agreement with experimental data up to the reference strain rate, then beyond this value, the viscoelastic model at the upper range is relatively accurate.

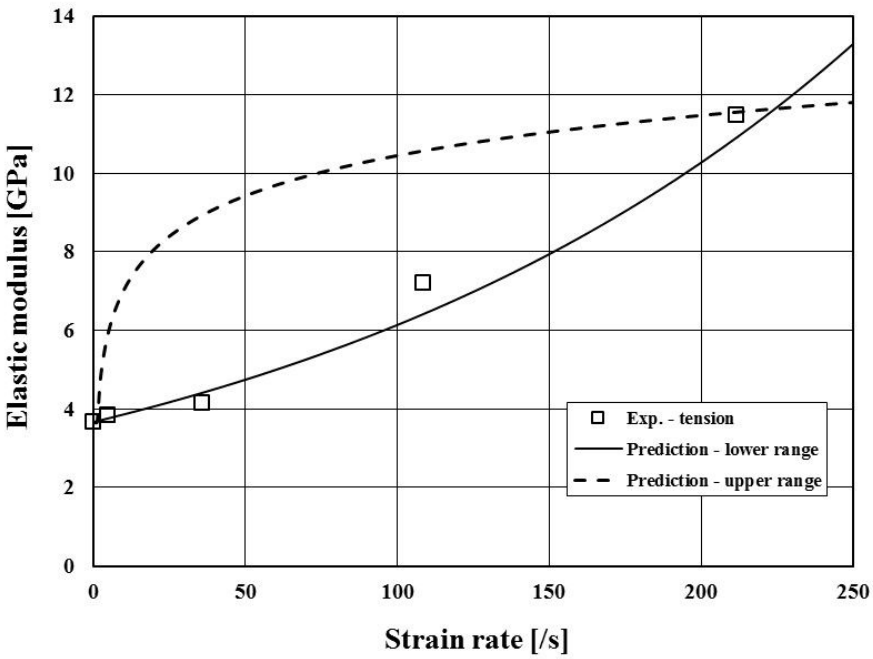

Fig. 2.7 Variation of tensile modulus versus strain rate for the M015 epoxy

2.2.2 Viscoplastic model for polymer – State variable constitutive equation

To account for the viscoplastic behavior of polymers, the modified Bodner-Partom viscoplastic state variable model, which was originally developed to analyze the viscoplastic deformation of metals above one-half of the melting temperature, is adopted as a viscoplastic model [14]. In the state variable model, a single unified strain variable is defined to represent all inelastic strains. Furthermore, in the state variable approach there is no defined yield stress, Inelastic strains are assumed to be present at all values of stress, the inelastic strains are just

assumed to be very small in the "elastic" range of deformation. State variables, which evolve with stress and inelastic strain, are defined to represent the average effects of deformation mechanisms [78]. Since there is no yielding condition, this model is very useful to employ into a numerical analysis method. The viscoplastic constitutive equation for polymers in this study is written as:

$$\dot{\varepsilon}_{ij}^{I} = 2D_0 exp\left[-\frac{1}{2}\left(\frac{Z}{\sigma_e}\right)^{2n}\right]\left(\frac{S_{ij}}{2\sqrt{J_2}} + \alpha\delta_{ij}\right) \tag{2.8}$$

The components of the inelastic strain rate tensor, $\dot{\varepsilon}_{ij}^{I}$, are defined as a function of the deviatoric stress components, S_{ij}, the second invariant of the deviatoric stress tensor, J_2, and the isotropic state variable, Z, which represents the resistance to molecular flow. D_0 and n are both material constants, with D_0 representing the maximum inelastic strain rate and n controlling the rate dependence of the material. The effective stress, σ_e, is defined as:

$$\sigma_e = \sqrt{3J_2} + \sqrt{3}\alpha\sigma_{kk} \tag{2.9}$$

where α is a state variable controlling the level of the hydrostatic stress effects and σ_{kk} is the summation of the normal stress components which equals three times the mean stress.

The rate of evolution of the internal stress state variable, Z, and hydrostatic stress effect state variable, α, are defined follows:

$$\dot{Z} = q(Z_1 - Z)\dot{e}_e^I \tag{2.10}$$

$$\dot{\alpha} = q(\alpha_1 - \alpha)\dot{e}_e^I \tag{2.11}$$

where q is a material constant representing the "hardening" rate, and Z_1 and α_1 are material constants representing the maximum value of Z and α, respectively. The initial values of Z and α are defined by the material constants Z_0 and α_0. The effective deviatoric inelastic strain rate, $\dot{e}_e^I$, is defined as:

$$\dot{e}_e^I = \sqrt{\frac{2}{3}\dot{e}_{ij}^I \dot{e}_{ij}^I} \tag{2.12}$$

where, $\dot{e}_{ij}^I$ represents the effective deviatoric inelastic strain rate and $\dot{\varepsilon}_m^I$ is the mean inelastic strain rate.

$$\dot{e}_{ij}^I = \dot{\varepsilon}_{ij}^I - \dot{\varepsilon}_m^I \delta_{ij} \qquad (i = j = 1,2,3) \tag{2.13}$$

$$\dot{\varepsilon}_m^I = \frac{1}{3}(\dot{\varepsilon}_{11}^I + \dot{\varepsilon}_{22}^I + \dot{\varepsilon}_{33}^I)$$

In many state variable constitutive models developed to analyze the behavior of

metals [60], the total inelastic strain and strain rate used in the evolution laws and are assumed to be equal to their deviatoric values. Since hydrostatic stresses contribute to the inelastic strains in polymers, indicating volumetric effects are present, the mean inelastic strain rate is accounts for in Eq. (2.13), unlike in the inelastic analysis of metals.

2.2.3 Viscoplastic model for polymer – Material constants determination

The material constants in the above state variable constitutive equations that need to be determined including D_0, n, Z_0, Z_1, α_0, α_1 and q. All of procedure and description have been referred from Goldberg et al. [14] and Zheng [21].

It is often necessary to determine the inelastic strain rate as part of the process to find the material constants. The inelastic strain can be determined from Eq. (2.3) using the stress and strain histories, elastic modulus and Poisson's ratio of matrix materials. The inelastic strain rate is then determined from the slope of a sliding spline fit of several time-inelastic strain pairs.

The parameter D_0 is correlated with the maximum inelastic strain rate. Typically, it is assumed to equal to a value of 10^4 times the maximum expected

strain rate. For example, $D_0 = 10^6$ /s or greater for high rate loading and wave propagation applications.

To determine the values of n and Z_1, Eq. (2.8) is simplified to the case of pure shear loading, so that the hydrostatic stress constant α can be ignored as follow:

$$\frac{\dot{\gamma}^I}{2} = D_0 exp\left[-\frac{1}{2}\left(\frac{Z}{\sqrt{3}|\tau|}\right)^{2n}\right]\frac{\tau}{|\tau|} \tag{2.14}$$

where, $\dot{\gamma}^I$ represents the engineering inelastic shear strain rate, τ is the shear stress. Rearrange Eq.(2.14) as follow:

$$-2\ln\left(\frac{\dot{\gamma}^I}{2D_0}\right) = \left[\left(\frac{Z}{\sqrt{3}|\tau|}\right)^{2n}\right] \tag{2.15}$$

Then the natural logarithm of both sides of the resulting expression is taken. The values of the inelastic shear strain rate, shear stress, and state variable Z at "saturation", which is the point where the stress-strain curve flattens out and becomes horizontal, are substituted into Eq.(2.15), leading to the following:

$$\ln\left[-2\ln\left(\frac{\dot{\gamma}_0^I}{2D_0}\right)\right] = 2n\ln(Z_1) - 2n\ln\left(\sqrt{3}\tau_s\right) \tag{2.16}$$

where τ_s equals the saturation shear stress, $\dot{\gamma}_0^I$ is the total engineering shear strain rate in a constant strain rate shear test, which is assumed to equal the inelastic

strain rate at "saturation". With a set of shear stress-shear strain curves obtained from different constant strain rate tests, data pairs of the total strain rate $\dot{\gamma}_0^I$ and the saturation shear stress τ_s are taken. For each strain rate, the data values are substituted into Eq. (2.16), and represent a point on a master curve. A least squares regression analysis is then performed on the master curve. As suggested by Eq. (2.16) and shown in Fig. 2.8, the slope of the best-fit line is equal to -2n. The intercept of the best-fit line is equal to $2n\ln(Z_1)$.

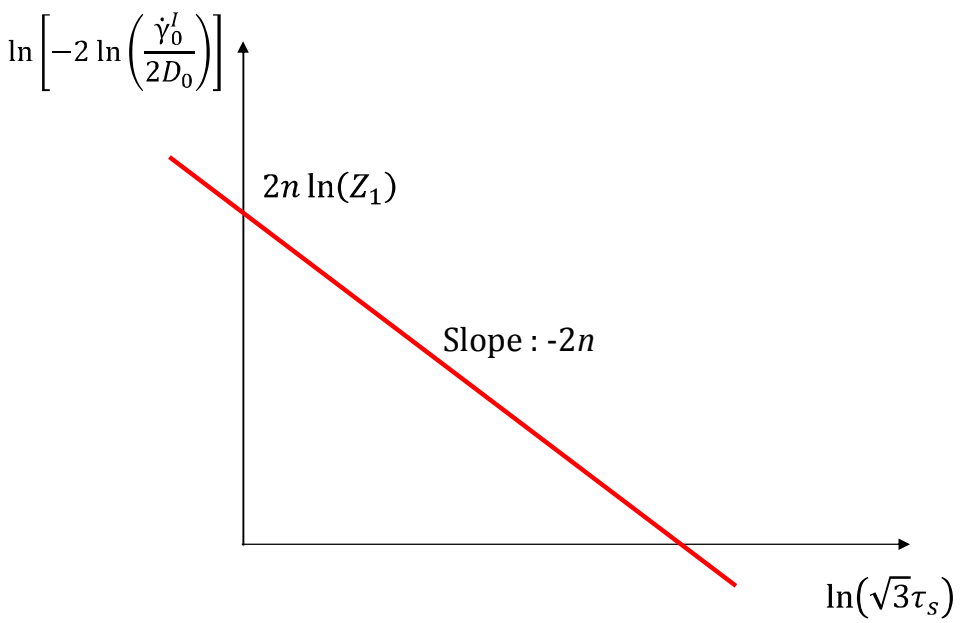

Fig. 2.8 Determination of n and Z_1

To determine the value of q, Eq. (2.10) is integrated for the case of pure shear loading, leading to the follow:

$$\mathrm{Z} = Z_1 - (Z_1 - Z_0)\exp\left(\frac{-q}{\sqrt{3}}\gamma^I\right) \tag{2.17}$$

where γ^I is the inelastic shear strain. At saturation, the value of the internal stress Z is assumed to approach Z_1, resulting in the exponential term approaching zero. Assuming that saturation occurs when the following condition is satisfied:

$$\exp\left(\frac{-q}{\sqrt{3}}\gamma_s^I\right) = 0.01 \tag{2.18}$$

The equation is solved for q, where γ_s^I is the inelastic shear strain at saturation.

To obtain the values of α_0 and α_1, Eq. (2.9) is used in combination with stress-strain data from constant strain rate uniaxial tensile tests and constant strain rate shear tests. It is assumed that at a particular strain rate the effective stress at saturation under uniaxial tensile loading is equal to the effective stress at saturation under pure shear loading. Assuming the value of α at saturation is equal to α_1 as follow:

$$\sigma_s\left(1 + \sqrt{3}\alpha_1\right) = \sqrt{3}\tau_s \tag{2.19}$$

where σ_s and τ_s are the tensile and shear stresses at saturation, respectively. Similarly, assuming the value of α at the point ate stress-strain curve becomes nonlinear is equal to α_0 gives:

$$\sigma_{nl}\left(1+\sqrt{3}\alpha_0\right)=\sqrt{3}\tau_{nl} \tag{2.20}$$

where σ_{nl} and τ_{nl} are the tensile and shear stresses at the point where the respective stress-strain curves become nonlinear status, respectively. Then the values of α_1 and α_0 can then be determined from these equations.

2.2.4 Viscoplastic model for polymer – Compressive loading consideration

It is known that there are two nonlinear behaviors such as a nonlinear elastic behavior in the fiber direction [61,62,63] and a hydrostatic stress effect in the matrix direction under compression [8,9,14], when polymeric composite materials have exerted the compressive loading. The nonlinear elastic deformation in fiber direction is caused by the fiber micro- buckling, namely, "Kinking" which is occurred by the misaligned fiber with compressive loading.

In this study, the nonlinear elastic behavior in compression is considered as the following equation [62]:

$$E_{11} = E_{11}^{0} + \delta\varepsilon_{11}H^{-}(\varepsilon_{11}) \tag{2.21}$$

with $\begin{cases} \mathrm{H}^{+}(x) = 1 & if\ x \geq 0;\ otherwise\ \ \mathrm{H}^{+}(x) = 0 \\ \mathrm{H}^{-}(x) = 1 & if\ x \leq 0;\ otherwise\ \ \mathrm{H}^{-}(x) = 0 \end{cases}$

where, E_{11} and E_{11}^{0} present the lamina fiber directional elastic modulus at certain strain value and the initial value of elastic modulus, respectively. δ is a material parameter which governs the loss of rigidity in compression, and this value can be acquired by the compressive coupon test. Through applying Eq. (2.21), the tensile deformation in fiber direction remains elastic, linear and brittle manner, with the elastic, nonlinear and brittle manner in compression.

The hydrostatic stress influences the elastic modulus, yield strength, and fracture strength of polymers [8,9,63]. The elastic modulus of polymers increases with increasing hydrostatic pressure in tension, compression, and shear in either a linear or piece-wise linear manner. The yield strength also increases with applied hydrostatic pressure, however, the pressure dependence of the yield strength usually differs from that of the modulus [63]. Finally, the ultimate tensile strengths of polymers always increase with increasing hydrostatic stress. This is known as the effects of pressure on molecular mobility. At high pressures the molecular chains are forced closer together, decreasing mobility, so that higher stresses are

necessary to produce a given strain. The ultimate strength is often affected by pressure in the same manner as the yield strength [64].

In this viscoplastic state variable constitutive equation, the hydrostatic stress effect is accounted for by the state variable α. Previously described Eq. (2.11-13) are related with the hydrostatic stress effect in the governing equation. Goldberg et al. [14] suggested the original form of the effective inelastic strain rate, $\dot{e}_{ij}^{I}$, however it had shear inelastic strain rate terms, so it could show unrealistic hydrostatic behavior under pure shear loading conditions. To improve the phenomenology of hydrostatic stress, Zheng [21] proposed the corrected effective inelastic strain rate expression which had only normal stress components. In Eq.(2.13), the corrected form is applied in this study.

2.3 Composite micromechanical model

The behavior of polymeric fiber reinforced composite materials is derived from the responses of the individual constituents. Especially, in case of carbon/epoxy composite materials, the strain rate and hydrostatic stress dependent deformations of the polymeric matrix should be considered with the linear and rate-independent

behaviors of the carbon fiber simultaneously. To analyze the effectively rate-dependent and nonlinear behaviors of polymeric composite materials, the micromechanical approach has been applied [14]. In order to improve the accuracy of the prediction of in-plane shear stress, the enhanced micromechanical model using the modified slicing algorithm has been proposed in this study.

2.3.1 Original micromechanical model – Slicing algorithm

In the micromechanical model, the unit cell is employed to compute the stress-strain behavior and material properties of a composite lamina. The unit cell is defined to consist of a single fiber with a circular cross section and its surrounding matrix with a square section. The fiber is assumed to be transversely isotropic, linear elastic, and rate independent, because the carbon fiber which is not rate-dependent, is only considered in this study. The matrix is assumed to be an isotropic, rate dependent, and elasto-plastic material described previously. Because the unit cell is a quadrant symmetry, only one-quarter of the unit cell is necessary to be analyzed. The UD composite lamina is assumed to have a periodic, square fiber packing and a perfect interfacial bond. The unit cell is assumed to measure one unit in length by one unit in height, the dimension of a fiber can be determined

by the fiber volume fraction of the overall composite laminate.

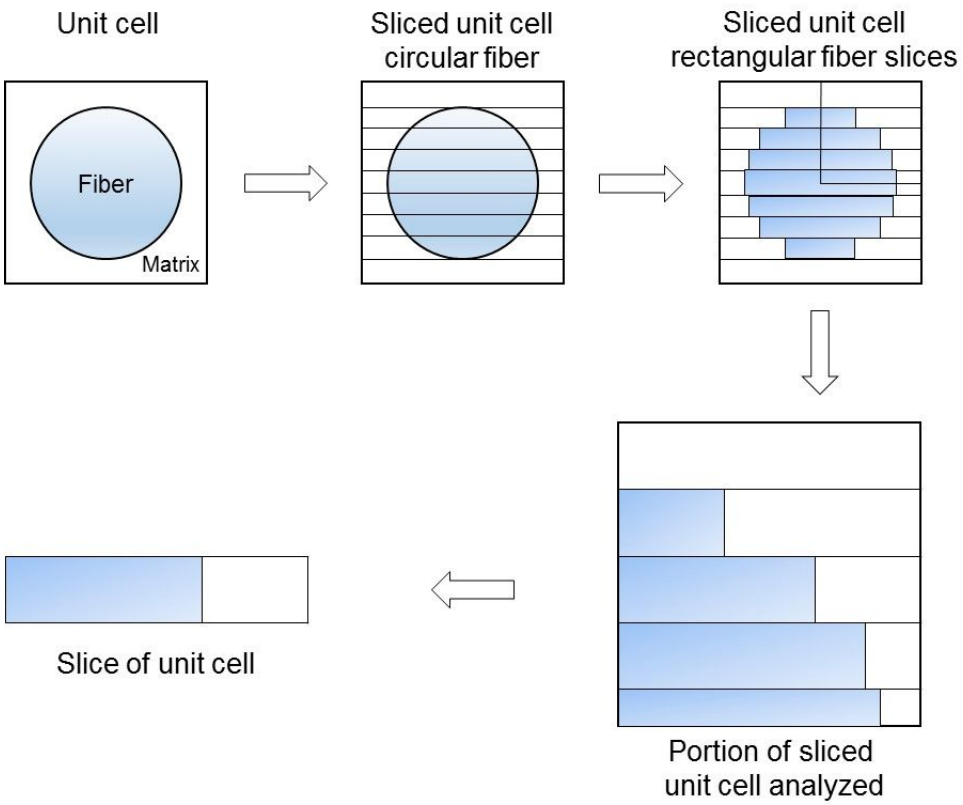

Fig. 2.9 Schematic showing relationship between unit cell and slices for micromechanics [19,78,79]

Fig. 2.9 presents the unit cell and slices for the micromechanical approach [19,78, 79]. Although it improve the accuracy of prediction, as many slices as possible, in this study, totally nine rectangular slices, to ensure the computational

efficiency and enough accuracy for applying the explicit finite element analysis. The unit cell is divided into nine rectangular, horizontal slices and the top and bottom slices in the unit cell are composed of matrix material only. Then each slice is separated into two subslices, one composed of fiber material and the other composed of matrix material. The thickness of horizontal slices are same value except for pure matrix slices. The bottom slice in the analysis cell is one-half as thick as the remaining fiber slices due to symmetry. Each slice has a slice fiber volume fraction, V_f^i, which is defined for the volume average of strains or stresses. The assumptions for the in-plane behavior of the unit cell are made on two levels, the slice level and the unit cell level. At the slice level, along the fiber direction, the strains are assumed to be uniform in each subslice, and the stresses are combined using volume averaging. The in-plane transverse normal stresses and in-plane shear stresses are assumed to be uniform in each subslice, and the strains are combined using volume averaging. The out-of-plane strains are assumed to be uniform in each subslice. The volume average of the out-of-plane stresses in each subslice is assumed to be equal to zero, enforcing a plane stress condition on the slice level. In each slice, the relations between the local strain, ε_{ij}^F and ε_{ij}^M, and the local stresses, σ_{kl}^F and σ_{kl}^M, in the fiber and matrix, respectively, are described as follows:

$$\varepsilon_{ij}^{F} = S_{ijkl}^{F}\sigma_{kl}^{F} \qquad i,j,k.l = 1 \dots 6 \tag{2.22}$$

$$\varepsilon_{ij}^{M} = S_{ijkl}^{M}\sigma_{kl}^{M} + \varepsilon_{ij}^{IM} \qquad i,j,k.l = 1 \dots 6 \tag{2.23}$$

where S_{ijkl}^{F} and S_{ijkl}^{M}, represent the components of the compliance tensors of fiber and matrix materials, respectively. ε_{ij}^{IM} represents the inelastic strains of matrix material. The superscript *i* and *I* expresses the slice and the inelastic component, and *F* and *M* express fiber and matrix, respectively. The assumptions for stress and strain of each slice can be expressed follows:

$$\varepsilon_{11}^{iF} = \varepsilon_{11}^{iM} = \varepsilon_{11}^{i} \tag{2.24}$$

$$\sigma_{11}^{i} = V_f^i\sigma_{11}^{iF} + \left(1 - V_f^i\right)\sigma_{11}^{iM} \tag{2.25}$$

$$\varepsilon_{22}^{i} = V_f^i\varepsilon_{22}^{iF} + \left(1 - V_f^i\right)\varepsilon_{22}^{iM} \tag{2.26}$$

$$\sigma_{22}^{iF} = \sigma_{22}^{iM} = \sigma_{22}^{i} \tag{2.27}$$

$$\varepsilon_{12}^{i} = V_f^i\varepsilon_{12}^{iF} + \left(1 - V_f^i\right)\varepsilon_{12}^{iM} \tag{2.28}$$

$$\sigma_{12}^{iF} = \sigma_{12}^{iM} = \sigma_{12}^{i} \tag{2.29}$$

$$\varepsilon_{33}^{iF} = \varepsilon_{33}^{iM} = \varepsilon_{33}^{i} \tag{2.30}$$

$$\sigma_{33}^{i} = 0 = V_f^i\sigma_{33}^{iF} + \left(1 - V_f^i\right)\sigma_{33}^{iM} \tag{2.31}$$

At the unit cell level, the in-plane strains for each slice are assumed to be constant and equal to the equivalent in-plane strains of the unit cell. The equivalent in-plane stresses of the unit cell are computed using the classical laminate theory (CLT). The strains and stresses in the unit cell are described follows:

$$\begin{Bmatrix}\varepsilon_{11}\\ \varepsilon_{22}\\ \varepsilon_{12}\end{Bmatrix} = \begin{Bmatrix}\varepsilon_{11}^{i}\\ \varepsilon_{22}^{i}\\ \varepsilon_{12}^{i}\end{Bmatrix} \quad i = 1 \ \ldots N_f + 1 \tag{2.32}$$

$$\begin{Bmatrix}\sigma_{11}\\ \sigma_{22}\\ \sigma_{12}\end{Bmatrix} = \sum_{i=1}^{N_f+1} \begin{Bmatrix}\sigma_{11}^{i}\\ \sigma_{22}^{i}\\ \sigma_{12}^{i}\end{Bmatrix} h_f^i \tag{2.33}$$

where N_f and h_f^i represent the number of fiber slices in the analysis cell and the ratio of thickness of each slice, respectively. Solving a series of Eq. (2.24) ~ (2.31) and the fiber and matrix constitutive equations; Eq. (2.22) and (2.23), the effective constitutive equation of the unit cell are obtained as:

$$\begin{Bmatrix}\sigma_{11}\\ \sigma_{22}\\ \sigma_{12}\end{Bmatrix} = \begin{bmatrix}Q_{11} & Q_{12} & 0\\ Q_{21} & Q_{22} & 0\\ 0 & 0 & Q_{66}\end{bmatrix} \begin{Bmatrix}\varepsilon_{11} - \varepsilon_{11}^{I}\\ \varepsilon_{22} - \varepsilon_{22}^{I}\\ \varepsilon_{12} - \varepsilon_{12}^{I}\end{Bmatrix} \tag{2.34}$$

Similar two-level assumption are also proposed for the transverse shear behavior in the unit cell. Along direction 13 and 23, the stresses are assumed to be uniform in each slice, and the strains are combined using volume averaging. That is,

for the slice i, these assumptions are expressed as:

$$\sigma_{23}^{iF} = \sigma_{23}^{iM} = \sigma_{23}^{i} \tag{2.35}$$

$$\varepsilon_{23}^{i} = V_f^i \varepsilon_{23}^{iF} + \left(1 - V_f^i\right)\varepsilon_{23}^{iM} \tag{2.36}$$

$$\sigma_{13}^{iF} = \sigma_{13}^{iM} = \sigma_{13}^{i} \tag{2.37}$$

$$\varepsilon_{13}^{i} = V_f^i \varepsilon_{13}^{iF} + \left(1 - V_f^i\right)\varepsilon_{13}^{iM} \tag{2.38}$$

At the unit cell level, along direction 13, the strains are assumed to be uniform for all slices, and the stresses are combined using volume averaging. Along direction 23, the stresses are assumed to be uniform for all slices, and the strains are combined using volume averaging, these assumptions can be expressed using the follows:

$$\begin{Bmatrix} \sigma_{23} \\ \varepsilon_{13} \end{Bmatrix} = \begin{Bmatrix} \sigma_{23}^{i} \\ \varepsilon_{13}^{i} \end{Bmatrix} \quad i = 1 \ \ldots N_f + 1 \tag{2.39}$$

$$\begin{Bmatrix} \varepsilon_{23} \\ \sigma_{13} \end{Bmatrix} = \sum_{i=1}^{N_f+1} \begin{Bmatrix} \varepsilon_{23}^{i} \\ \sigma_{13}^{i} \end{Bmatrix} h_f^i \tag{2.40}$$

Including above transverse shear behavior, solving a series of equations describing the assumption (Eq.(24-33,35-40)) and the constitutive equations for the

fiber and matrix, we can rewrite Eq.(2.34) as follow:

$$\begin{Bmatrix}\sigma_{11}\\ \sigma_{22}\\ \sigma_{12}\\ \sigma_{23}\\ \sigma_{13}\end{Bmatrix} = \begin{bmatrix} Q_{11} & Q_{12} & 0 & 0 & 0 \\ Q_{21} & Q_{22} & 0 & 0 & 0 \\ 0 & 0 & Q_{66} & 0 & 0 \\ 0 & 0 & 0 & Q_{44} & 0 \\ 0 & 0 & 0 & 0 & Q_{55} \end{bmatrix} \begin{Bmatrix}\varepsilon_{11}-\varepsilon_{11}^{I}\\ \varepsilon_{22}-\varepsilon_{22}^{I}\\ \varepsilon_{12}-\varepsilon_{12}^{I}\\ \varepsilon_{23}-\varepsilon_{23}^{I}\\ \varepsilon_{13}-\varepsilon_{13}^{I}\end{Bmatrix} \tag{2.41}$$

Using the derived effective stiffness matrix, the effective elastic properties of an UD composite lamina can be obtained follows:

$$E_{11} = \frac{(Q_{11}Q_{22} - Q_{12}Q_{21})}{Q_{22}} \tag{2.42}$$

$$E_{22} = \frac{(Q_{11}Q_{22} - Q_{12}Q_{21})}{Q_{11}} \tag{2.43}$$

$$G_{12} = Q_{66} \tag{2.44}$$

$$v_{12} = \frac{(Q_{11}Q_{22} - Q_{12}Q_{21})^2}{Q_{12}Q_{22}} \tag{2.45}$$

The advantage of the presented micromechanical approach considerably reduced the complexity of the analysis with a high accuracy and efficiency of the computation. Due to this advantage, this model is suitable to apply on the transient structural analysis scheme.

2.3.2. Enhanced micromechanical model – Modified slicing algorithm

The in-plane shear stress mainly influences the nonlinear behavior of polymeric matrix composite materials. In order to enhance the accuracy of in-plane shear behavior prediction, the method for the improvement of the original slicing algorithm (OSA) is proposed in this study.

Fig. 2.10 depicts the limitation of the in-plane shear stress prediction using the OSA, and the modified slicing algorithm (MSA), which is to overcome this limitation. The dotted line in Fig. 2.10 (a) presents the shear strain of the subslice with a rectangular fiber subslice, γ_{rf}^{i}. The solid line presents the shear strain of the subslice with the circular fiber subslice, γ_{cf}^{i}, which is close to the actual behavior. Actually, it can be assumed the existence of "fusion area", where coexists a fiber material with a matrix material and is illustrated as the envelope by double dotted dash line in Fig. 2.10 (b). Therefore, the fusion area may have the different shear modulus, which can be computed by means of the shear modulus and geometrical constants of two constituents. In the OSA, because fiber and matrix subslices are separated with a rectangular cross section based on the fiber volume fraction only in each slice, it leads to the over prediction of the shear deformation caused by

relatively large length of the subslice of pure matrix. Fig. 2.10 (b) shows the fusion area and the fusion volume fraction, V_{fu}^{i}, in each slice.

The volume average is employed to compute the shear modulus of the fusion area, G_{12}^{iFU}, which is defined as:

$$G_{12}^{iFU} = \frac{G_{12}^{F} A_{f}^{i} + G_{12}^{M} A_{m}^{i}}{A_{fu}^{i}} \tag{2.46}$$

where G_{12}^{F}, G_{12}^{M} represent the shear modulus of a fiber and a matrix, respectively. Then, A_{f}^{i}, A_{m}^{i}, and A_{fu}^{i} represent the area of fiber, matrix, and the sum of constituents in the fusion area, respectively. The computed shear modulus of the fusion area is used to generate the constitutive equation of a slice. The equation to compute the in-plane shear strain of each slice can be defined as:

$$\varepsilon_{12}^{i} = V_{f}^{i} \varepsilon_{12}^{iF} + V_{fu}^{i} \varepsilon_{12}^{iF} + \left(1 - V_{fu}^{i} - V_{f}^{i}\right) \varepsilon_{12}^{iM} \tag{2.47}$$

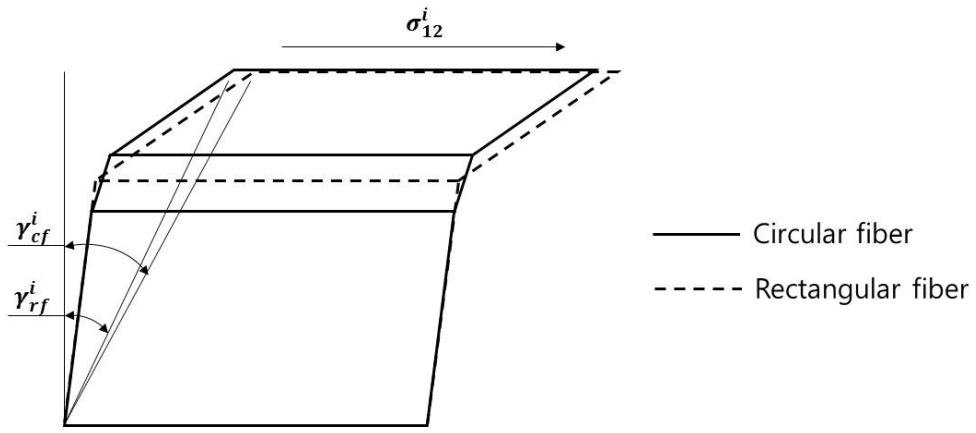

(a)

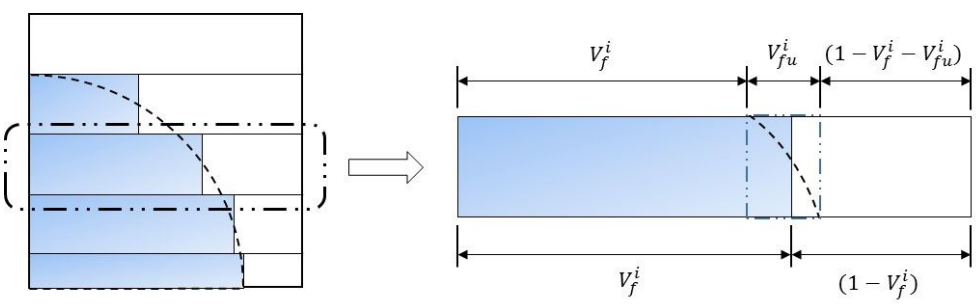

(b)

Fig. 2.10 Schematic showing the improvement of in-plane shear behavior prediction: (a) limitation of original slicing algorithm; (b) proposed slice composition

The material properties of carbon composite materials, which are to validate the proposed micromechanical model using the MSA, are listed in Table 2.2. Polymeric matrices are restricted within thermoset materials [19,21,80]. Table 2.3 lists the experimental data and predicted elastic constants using the OSA and MSA

for carbon UD composite materials with various fiber volume fractions [75,80,81]. The T700/M015 material examined for validation of presented analysis methods. The coupon tests for the T700/M015 are composed of the tensile and shear test. Tensile tests were carried out in accordance with ASTM D3039 [65] and the V-notched rail shear test in accordance with ASTM D7078 [66] was used for shear tests. Overall, the micromechanical model using slicing algorithm has fairly good predictions of effective elastic properties. Especially, we can find that the MSA improves the accuracy of the in-plane shear response of the micromechanical model.

Table 2.2 Material properties of fibers and matrices

Material	Longitudinal elastic modulus [GPa]	Transverse elastic modulus [GPa]	Poisson's ratio, ν_{12}	Initial shear modulus [GPa]
Matrix				
977-2 [19]	3.5	-	0.40	1.3
3501-6 [68]	4.8	-	0.34	1.8
M015	3.7	-	0.41	1.3
Fiber				
IM7 [19]	276	13.8	0.25	20
AS4 [68]	235	14.0	0.20	28
T700 [19]	230	10.0	0.20	17

Table 2.3 Comparison of elastic constants from predictions and tests

Elastic Constants	IM7/977-2 [81] (V_f = 0.66)			T300/914 [75] (V_f = 0.57)		
	OSA	MSA	Test	OSA	MSA	Test
E_{11} [GPa]	183	183	174.4	135	135	132
E_{22} [GPa]	9.8	9.8	9.6	10.0	10.0	9.2
G_{12} [GPa]	4.74	5.64	5.30	4.19	4.82	4.9
v_{12}	0.29	0.29	0.27	0.28	0.28	0.37
Elastic Constants	AS4/3501-6 [80] (V_f = 0.60)			T700/M015 (V_f = 0.63)		
	OSA	MSA	Test	OSA	MSA	Test
E_{11} [GPa]	142.95	142.95	142	146	146	147
E_{22} [GPa]	9.71	9.71	10.3	8.6	8.6	8.9
G_{12} [GPa]	5.56	6.44	7.6	4.24	4.92	4.9
v_{12}	0.26	0.26	-	0.29	0.29	0.29

2.4 Rate-dependent damage model prior to failure

In polymeric composite materials, after the micro-crack occurs in the matrix or at the fiber/matrix interface, the evolution of micro-cracks progresses with respect to applied stress, finally, throughout the ply thickness is smeared by them. The

damage originated from micro-cracks generates the stiffness degradation, which makes the in-plane nonlinear stress-strain response typically. The micro-crack in composite materials can be assumed a sort of the phenomenon of material failure, and the failure of polymers is rate-dependent as previously described. Therefore the damage caused by micro-cracks can be assumed that it will be changed with respect to strain-rate. The RDM presented in this study, starts from this assumption. The composite damage model proposed by Ladeveze [31], which calculates the damage values of each ply using applied stresses and material damage constants, is used as the basic reference damage model in the RDM. To account for the rate-dependence, the viscoplastic model for polymeric matrices using the micromechanical model as previously described, is applied into the RDM as the substitution of the isotropic hardening plastic model in the basic reference damage model.

2.4.1. Theoretical modeling of reference damage model

The damage process in the matrix is mainly caused by the transverse normal stress, σ_{22}, and in-plane shear stress, σ_{12}. The model assumes that the stress in fiber direction, σ_{11}, does not affect the damage state in the matrix. The basic

reference damage model proposed by Ladeveze [31] is theoretically based on the orthotropic continuum damage mechanics, only considers in-plane damages of the elementary ply. In the basic reference damage model, the damaged material strain energy is written as:

$$E_D = \left[\frac{\sigma_{11}^2}{E_{11}^0} - \frac{2v_{12}^0}{E_{11}^0}\sigma_{11}\sigma_{22} + \frac{\langle\sigma_{22}\rangle_+^2}{E_{22}^0(1-d_2)} + \frac{\langle\sigma_{22}\rangle_-^2}{E_{22}^0} + \frac{\sigma_{12}^2}{2G_{12}^0(1-d_6)}\right] \quad (2.48)$$

with $\begin{cases}\langle\sigma\rangle_+ = \sigma & if\ \sigma \geq 0;\ otherwise\ \ \langle\sigma\rangle_+ = 0\\ \langle\sigma\rangle_- = \sigma & if\ \sigma \leq 0;\ otherwise\ \ \langle\sigma\rangle_- = 0\end{cases}$

where d_2 and d_6 present the transverse and in-plane scalar damage variables, respectively, that remain constant throughout the ply thickness. The superscript *0* means the initial value, the elastic moduli are kept decreasing by the initiation and evolution of micro-cracks. If the transverse micro-cracks are loaded in compression, they close up and then have no effect on the transverse direction behavior. This explains splitting up the transverse energy into "tension" term and "compression" term in Eq. (2.48). The constitutive equations for the damaged composite lamina can be written as:

$$\begin{cases} \varepsilon_{11}^{e} = \dfrac{\sigma_{11}}{E_{11}^{0}} - \dfrac{v_{12}^{0}\sigma_{22}}{E_{11}^{0}} \\ \varepsilon_{22}^{e} = -\dfrac{v_{12}^{0}\sigma_{11}}{E_{11}^{0}} + \dfrac{\langle\sigma_{22}\rangle_{-}}{E_{22}^{0}} + \dfrac{\langle\sigma_{22}\rangle_{+}}{E_{22}^{0}(1-d_2)} \\ \varepsilon_{12}^{e} = \dfrac{\sigma_{12}}{2G_{12}^{0}(1-d_6)} \end{cases} \tag{2.49}$$

The associated forces, Y_2^d and Y_6^d, are associated with damage variables, d_2 and d_6, for dissipation, and they are defined follows:

$$Y_2^d = \frac{\partial\psi}{\partial d_2}|_{\tilde{\sigma},d_6:CST} = \frac{\partial E_D}{\partial d_2}|_{\tilde{\sigma},d_6:CST} = \frac{\langle\sigma_{22}\rangle_{+}^{2}}{2E_{22}^{0}(1-d_2)^2} \tag{2.50}$$

$$Y_6^d = \frac{\partial\psi}{\partial d_6}|_{\tilde{\sigma},d_2:CST} = \frac{\partial E_D}{\partial d_6}|_{\tilde{\sigma},d_2:CST} = \frac{{\sigma_{12}}^2}{2G_{12}^{0}(1-d_6)^2} \tag{2.51}$$

where ψ is the free-energy density and $\tilde{\sigma}$ presents the effective stress exerted on the changed sectional area by micro-cracks such as:

$$\tilde{\sigma} = \begin{Bmatrix} \sigma_{11} \\ \langle\sigma_{22}\rangle_{-} + \dfrac{\langle\sigma_{22}\rangle_{+}}{(1-d_2)} \\ \dfrac{\sqrt{2}\sigma_{12}}{(1-d_6)} \end{Bmatrix} \tag{2.52}$$

The damage of a ply is assumed to be governed by the variable *Y*. The damage variable, *Y*, is defined as

$$Y = sup_{\tau\geq t}\sqrt{Y_6^d(\tau) + bY_2^d(\tau)} \tag{2.53}$$

where *b* is a material constant which represents the coupling parameter between the

effect of the longitudinal and the transverse damaged strain energies. The damage-development laws are then very simple and are expressed follows:

$$d_2 = \frac{\langle Y - Y_2^0 \rangle_+}{Y_2^c} \tag{2.54}$$

$$d_6 = \frac{\langle Y - Y_6^0 \rangle_+}{Y_6^c} \tag{2.55}$$

Therefore, in the basic reference damage model, two directional damages are affected by each other with the material characteristics coupling quantity.

The basic reference damage model is based on the elasto-plastic with the "yield condition", the plastic strains are induced by damage. The plastic model is build up with the effective quantities. The effective plastic strain rate is given by:

$$\begin{cases} \tilde{\varepsilon}_{11}^p = 0 \\ \tilde{\varepsilon}_{22}^p = a^2 \dfrac{\tilde{\sigma}_{22}}{R(p) + R_0} \dot{p} \\ \tilde{\varepsilon}_{12}^p = \dfrac{\tilde{\sigma}_{12}}{2(R(p) + R_0)} \dot{p} \end{cases} \tag{2.56}$$

where

$$\dot{p} = \frac{\tilde{\sigma}_{12}\dot{\tilde{\sigma}}_{12} + a^2 \tilde{\sigma}_{22}\dot{\tilde{\sigma}}_{22}}{(R(p) + R_0)\dfrac{\partial R}{\partial p}}$$

The hardening is assumed to be isotropic, and the elasticity domain is defined

by the function, *f*, such as:

$$f = \sqrt{\tilde{\sigma}_{12}^2 + a^2\tilde{\sigma}_{22}^2} - R(p) - R_0 \tag{2.57}$$

The material yield conditions are $f = 0$ and $\dot{f} = 0$; otherwise $\dot{p} = 0$

In basic reference damage model, Y_2^0, Y_2^c, Y_6^0, and Y_6^c are the damage constants, represent the transverse damage initiation, transversely critical damage, in-plane shear damage initiation, and in-plane shear critical damage, respectively. $R(p) + R_0$ and a^2 are the material characteristic function for the material yield stress and material characteristics constant related to the accumulated plastic strain, respectively. These material constants can be acquired by the monotonic tensile coupon test such as:

- $[\pm 45°]_s$: Y_6^0, Y_6^c, $R(p) + R_0$

- $[\pm 67.5°]_s$: b, Y_2^0, Y_2^c, a^2

The composite damage model proposed by Ladeveze [31] predicts the nonlinear behavior under the in-plane shear loading using the damage developments laws with coupled damage value and the plasticity model which calculates the accumulated plastic strain after the material yield. In this damage

model, the inelastic behavior of polymeric matrix is considered within the material characteristic function, $R(p)+R_0$, and constant , a^2.

2.4.2. Development of rate-dependent damage modeling

To validate compatibility between the elastic damage model of the basic reference damage model and the viscoplastic model using the micromechanical approach, the initial RDM which was composed of two models, has been produced. After the analysis results using the initial RDM have compared with experimental results from quasi-static coupon tests, the elastic damage model was modified and applied in the RDM to agree with the experimental data. Fig. 2.11 presents the shear and transverse damage master curves for the T700/M015 to get material damage constants.

The quasi-static and monotonic tensile tests for the T700/M015 $[\pm 45°]_s$ and $[\pm 67.5°]_s$ coupons were carried out. The quasi-static tensile test is according to ASTM D3039 [65]. The shape of specimens and test procedure for the monotonic tensile test is referred to Ref. [22], because the monotonic tensile test for composite materials is not classified yet.

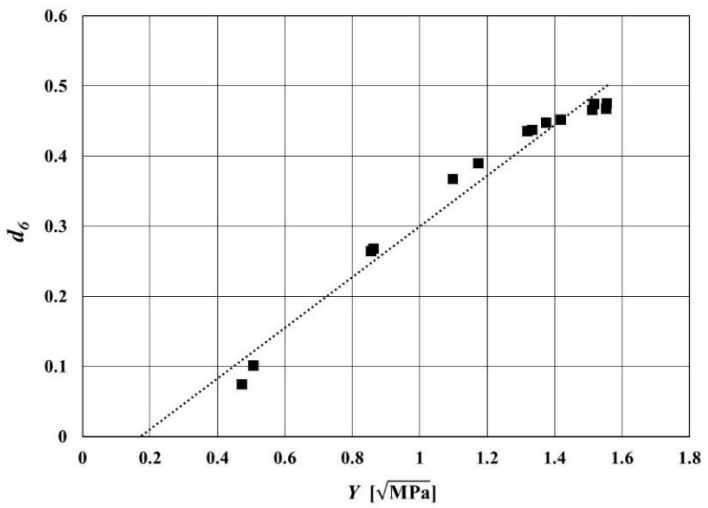
0.6
0.5
0.4
0.3
0.2
0.1
0
d_6
0
0.2
0.4
0.6
0.8
1
1.2
1.4
1.6
1.8
Y [$\sqrt{\text{MPa}}$]

(a)

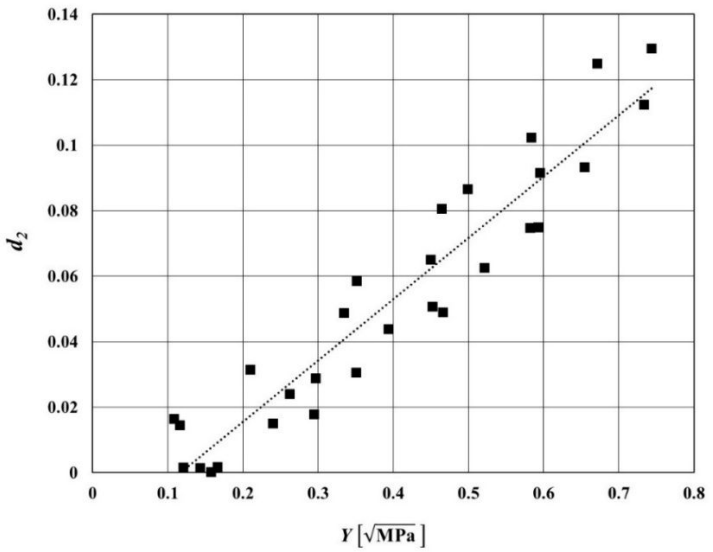
0.14
0.12
0.1
0.08
0.06
0.04
0.02
0
d_2
0
0.1
0.2
0.3
0.4
0.5
0.6
0.7
0.8
Y [$\sqrt{\text{MPa}}$]

(b)

Fig. 2.11 Damage master curve of elementary ply for the T700/M015:
(a) Shear; (b) Transverse

Fig. 2.12 presents the comparison between prediction and experimental results for the $[\pm 67.5°]_s$ angle-ply laminate. In Fig. 2.12 (a), prediction from the initial RDM with d_2 and d_6, and in Fig. 2.12 (b), the RDM with only d_6. The prediction is well up to the strain level of 0.3% in Fig. 2.12 (a). Beyond this point, prediction error starts to occur and increases by about 16% at the maximum strain level of 0.75%. While, in Fig. 2.12 (b), fairly good agreement between experimental and prediction results till the strain level of 0.5% is observed. Although prediction error starts to occur beyond this point, there is an only error of about 7%. It can be seen in the comparison between the experimental and prediction results for the [90°] laminate, as shown in Fig. 2.13. It has been known that the transverse behavior of composite materials is typically linear until the rupture, in case of the initial RDM, however, the nonlinear behavior and the increase of prediction error can be seen after a strain level of 0.2%. The prediction result from the RDM with only d_6, presents the very good correlation with the experimental result.

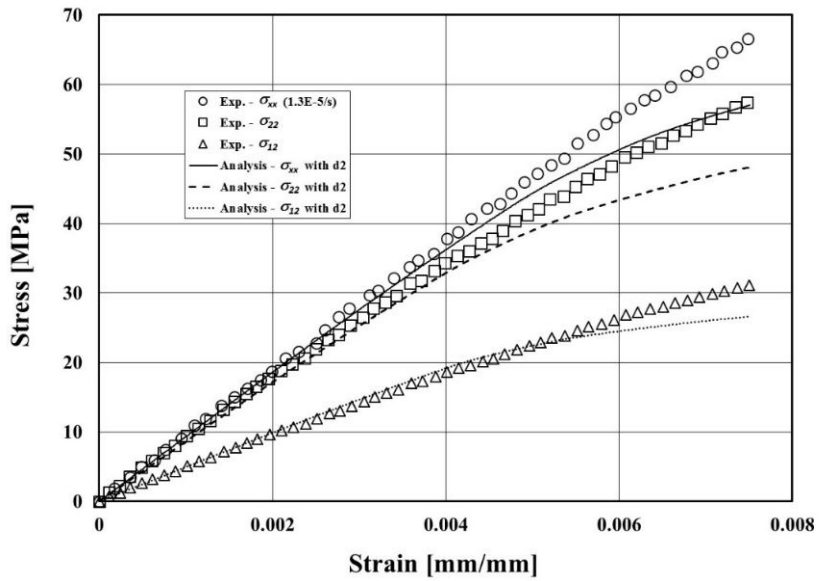

(a)

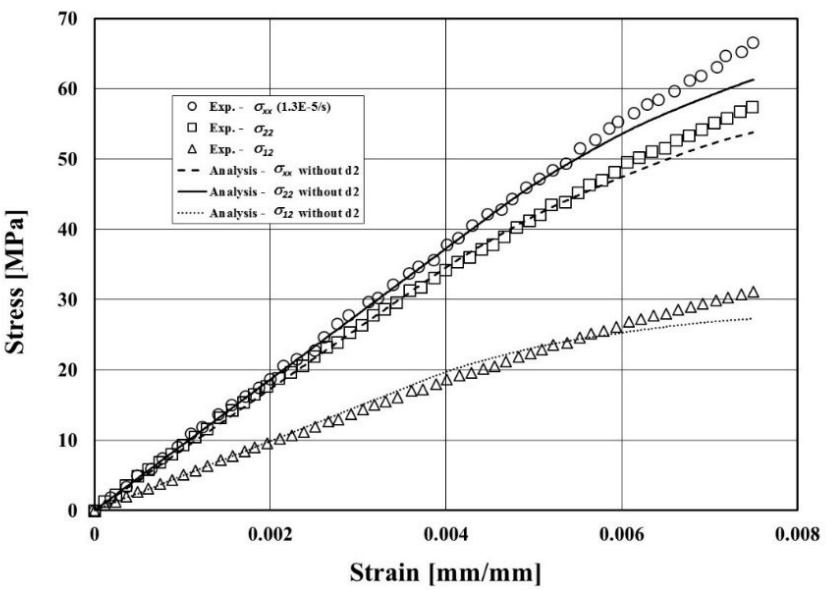

(b)

Fig. 2.12 Comparison of experimental and predicted stress-strain curves for the T700/M015 $[\pm 67.5°]_s$ laminate: (a) with transverse damage value (d_2); (b) without d_2

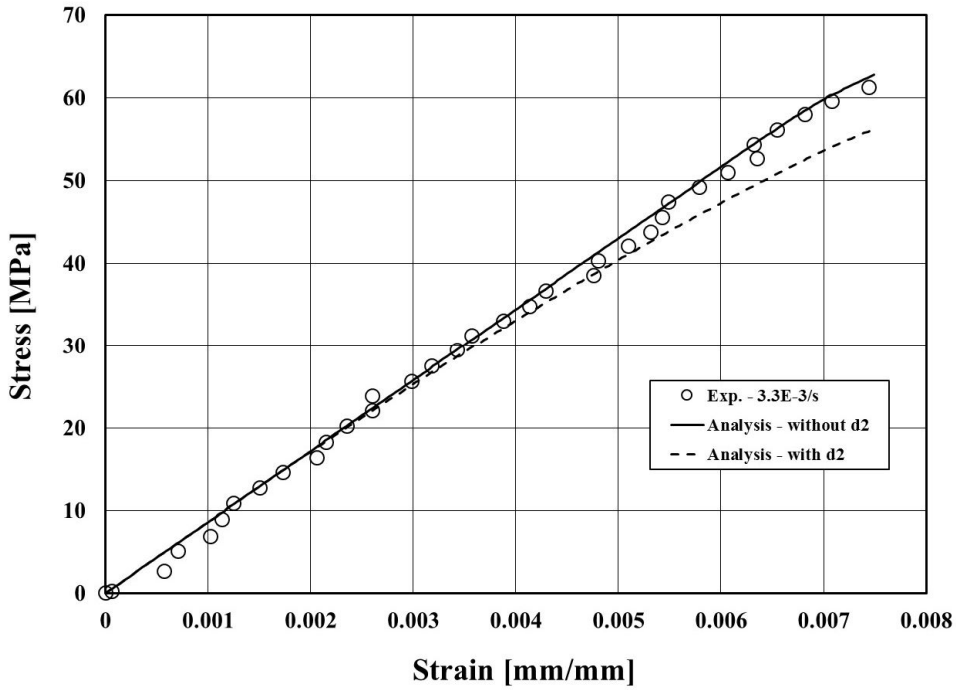

Fig. 12. Comparison of experimental and predicted stress-strain curves for the T700/M015 [90°] with d_2 and without d_2

Through validation of compatibility, these were observed that the initial RDM overpredicts the nonlinear behavior in transverse direction, and the RDM without d_2 has more accurate predictions. It can be assumed that the viscoplastic model presented in this study can sufficiently simulate not only the transverse nonlinear behavior but also the coupling effect with the in-plane shear behavior. Therefore, it is decided that the in-plane shear damage variable is only considered for the RDM, and the damage variable (Eq. (2.53)) and damage-development laws (Eq. (2.54-55))

in the basic reference damage model can be reduced follows:

$$\mathrm{Y} = sup_{\tau \geq t} \sqrt{Y_6^d(\tau)} \tag{2.58}$$

$$d_6 = \frac{\langle Y - Y_6^0 \rangle_+}{Y_6^c} \tag{2.59}$$

To account for change of the damage initiation with respect to strain rate, the in-plane shear initiation damage constant, Y_6^o, is defined follow:

$$Y_6^o = \sqrt{\frac{{\sigma_{12}^{th}}^2}{2G_{12}^0}} \tag{2.60}$$

The threshold stress of damage, σ_{12}^{th}, is employed to allow to Y_6^o with respect to strain rate. The rate-dependent strength function (Eq. (2.1)) is applied to obtain σ_{12}^{th} at different strain rates. The threshold stress of damage does not have physical meaning for the strength in the RDM.

To obtain the in-plane shear critical damage constant, Y_6^c, the associated force, Y_6^d, is expressed in terms of σ_{12}^r and d_6 in the following form:

$$Y_6^d = \frac{{\sigma_{12}^r}^2}{2G_{12}^0(1-d_6)^2} \tag{2.61}$$

and substituting Eq. (2.61) in Eq. (2.58), and then damage variable, *Y*, is substituted

in Eq. (2.59), we extract d_6 as a function of σ_{12}^r such as:

$$d_6 = \frac{\sigma_{12}^r}{Y_6^c\sqrt{2G_{12}^0}(1-d_6)} - \frac{Y_6^0}{Y_6^c} \tag{2.62}$$

At the ruptured shear stress, the quadratic equation for d_6 should have real roots, so we can apply the discriminant on Eq. (2.62). Finally, Y_6^c is written as:

$$Y_6^c = \frac{\frac{4\sigma_{12}^r}{\sqrt{2G_{12}^0}} - 2Y_6^0 + \sqrt{\left(2Y_6^0 - \frac{4\sigma_{12}^r}{\sqrt{2G_{12}^0}}\right)^2 - 4{Y_6^0}^2}}{2} \tag{2.63}$$

In Eq. (2.63), the rupture shear stress, σ_{12}^r, can be also computed by Eq. (2.1) with respect to strain rate, therefore, Y_6^c becomes the rate sensitive constant in the RDM.

3. PROGRESSIVE FAILURE ANALYSIS USING EDPM

The damage in composite structures is typically generated by the combination of matrix cracking, fiber breakage in tension and compression, and delamination. The first two damage modes, matrix cracking and fiber breakage in tension and compression, are called intra-laminar damage and the third damage mode, delamination, is called inter-laminar damage. Then, the progressive failure behaviors after the initiation of damage or failure are originated from the combined interaction between these damage modes within lamina or laminate. Therefore, the development of the PFA model is a complex task resulting in significant challenges at several steps of the procedure. One such step, which is also an active research area in PFA methodology development, is defining the material failure detecting criteria and degradation model for adjusting material properties or stresses to simulate composite damage progressive behaviors. The final step of the PFA is the element erosion according to the pre-defined limit values to improve the maturity of structural failure mechanisms.

For accounting for the PFA method for the explicit FE analysis in this study, it

is presented that the rate-dependent Hashin failure criteria as composite failure detecting and initiation method [21,59], the EDPM for the stiffness degradation and stress reduction after failure initiation, and the elimination conditions of failed elements in all of directions. The stiffness degradation into the micromechanical composite model is also introduced in this study [59].

3.1 Material failure detection model

The first step of the PFA methodology is the detection of material failure and the initiation of damage. Among many composite material failure criteria, the Hashin failure criteria is selected as the material failure detection model in this study, since this model have been validated through the usage of as the failure criteria on other studies and modified as rate-dependent type of failure criteria [21].

3.1.1. The Hashin composite failure criteria

The material failure detection model is based on the Hashin failure criteria [39,59]. The Hashin failure criteria are also interacting failure criteria as the failure criteria use more than a single stress component to evaluate different failure modes, The Hashin criteria were originally developed as failure criteria for unidirectional

polymeric composites. Hence, application to other laminate types or non-polymeric composite materials represents a significant approximation. Usually the Hashin criteria are implemented within a two-dimensional classical lamination approach for the point-stress calculations with ply discounting as the material degradation model. Failure indices for the Hashin criteria related to fiber and matrix failures and involve four failure mode. Additional failure indices result from extending the Hashin criteria to 2D shell element with transverse shear stress components. To consider the shear stress effect in fiber direction optionally, the weighting factor for shear term, γ_s, is included into original criteria. For $\gamma_s = 1$, we can get the original Hashin criteria in tensile fiber direction. For $\gamma_s = 0$, we can get the maximum stress criterion [58]. The failure modes included with the Hashin criteria [39,54] are as follows:

- Tensile fiber failure – for $\sigma_{11} \geq 0$

$$(e_1^t)^2 = \left(\frac{\sigma_{11}}{X_T}\right)^2 + \gamma_s \left(\frac{\sigma_{12}^2 + \sigma_{13}^2}{S_C^2}\right) = \begin{cases} \geq 1 & failure \\ < 1 & no\ failure \end{cases} \tag{3.1}$$

- Compressive fiber failure – for $\sigma_{11} \leq 0$

$$(e_1^c)^2 = \left(\frac{\sigma_{11}}{X_C}\right)^2 = \begin{cases} \geq 1 & failure \\ < 1 & no\ failure \end{cases} \tag{3.2}$$

- Tensile matrix failure – for $\sigma_{22} \geq 0$

$$(e_2^t)^2 = \left(\frac{\sigma_{22}}{Y_T}\right)^2 + \left(\frac{\sigma_{23}}{S_T}\right)^2 + \frac{\sigma_{12}^2 + \sigma_{13}^2}{S_C^2} = \begin{cases} \geq 1 & failure \\ < 1 & no\ failure \end{cases} \tag{3.3}$$

- Compressive matrix failure – for $\sigma_{22} \leq 0$

$$(e_2^c)^2 = \left[\left(\frac{Y_C}{2S_T}\right)^2 - 1\right]\left(\frac{\sigma_{22}}{Y_C}\right) + \left(\frac{\sigma_{22}}{2S_T}\right)^2 + \left(\frac{\sigma_{23}}{S_T}\right)^2 + \frac{\sigma_{12}^2 + \sigma_{13}^2}{S_C^2}$$
$$= \begin{cases} \geq 1 & failure \\ < 1 & no\ failure \end{cases} \tag{3.4}$$

where, X_T, X_C are lamina strength allowable values for tension and compression in fiber directions, respectively. Y_T, Y_C are lamina strength allowable values for tension and compression in matrix directions, respectively. S_C means the in-plane shear strength allowable value and S_T is the transverse shear strength allowable value. Failure indices for tension and compression are then compared to unity to determine whether failure initiation is predicted.

If any failure index $e_{1,2}^{t,c}$ exceeds unity, then failure initiation has occurred for that strain component at that material point and material degradation will be performed. That is, each failure mode may fail independently at different load levels, and the Hashin failure flags f_i^H are set accordingly:

$$f_i^H = \begin{cases} 0\ for\ e_i^{t,c} < 1 \\ \pm 1\ for\ e_i^{t,c} \geq 1 \end{cases} \quad \text{for } i = 1,2 \tag{3.5}$$

where if the material failure detection whether tension or compression, the Hashin failure flag is declared as unity following the same sign of stress. Failure flags is irreversible process and after they are determined as unity.

3.1.2. The Rate-dependent Hashin failure criteria

To account for the rate–dependent polymeric composites failure, the rate-dependent Hashin criteria which proposed in Zheng [21] is employed in this study. This criteria is referred to Thiruppukyzhi et al. [32], which modified the transverse strength with a rate-sensitive parameter for the matrix dominated failure modes. According to Ref. [21], Eq.(3.3) and Eq.(3.4) are written as follows:

$$(e_2^t)^2 = \left(\frac{\sigma_{22}}{Y_T}\right)^2 + \left(\frac{\sigma_{23}}{S_T}\right)^2 + \frac{\sigma_{12}^2 + \sigma_{13}^2}{S_C^2} = \begin{cases} \geq \left(\left|\frac{\dot{\varepsilon}_{22}}{\dot{\varepsilon}_0}\right|\right)^{2\beta} & failure \\ < \left(\left|\frac{\dot{\varepsilon}_{22}}{\dot{\varepsilon}_0}\right|\right)^{2\beta} & no\ failure \end{cases} \tag{3.6}$$

$$(e_2^c)^2 = \left[\left(\frac{Y_C}{2S_T}\right)^2 - 1\right]\left(\frac{\sigma_{22}}{Y_C}\right) + \left(\frac{\sigma_{22}}{2S_T}\right)^2 + \left(\frac{\sigma_{23}}{S_T}\right)^2 + \frac{\sigma_{12}^2 + \sigma_{13}^2}{S_C^2}$$

$$= \begin{cases} \geq \left(\left|\frac{\dot{\varepsilon}_{22}}{\dot{\varepsilon}_0}\right|\right)^{2\beta} & failure \\ < \left(\left|\frac{\dot{\varepsilon}_{22}}{\dot{\varepsilon}_0}\right|\right)^{2\beta} & no\ failure \end{cases} \tag{3.7}$$

where $\dot{\varepsilon}_0$ is the reference strain rate at which the values of the strengths are determined. $\dot{\varepsilon}_0$ is again assumed to be 1/s [21]. In Eq.(3.5), the Hashin failure flags is classified into fiber and matrix directions. For failure index in fiber direction, there is no change of conditions as strain rates. However, in matrix direction, the failure index is expressed as rate-dependent form as follow:

$$\begin{cases} f_2^H = \begin{cases} 0\ for\ e_i^{t,c} < 1 \\ \pm 1\ for\ e_i^{t,c} \geq 1 \end{cases} & if\ |\dot{\varepsilon}_{22}| < \dot{\varepsilon}_0 \\ f_2^H = \begin{cases} 0\ for\ e_i^{t,c} < \left(\left|\frac{\dot{\varepsilon}_{22}}{\dot{\varepsilon}_0}\right|\right)^{\beta} \\ \pm 1\ for\ e_i^{t,c} \geq \left(\left|\frac{\dot{\varepsilon}_{22}}{\dot{\varepsilon}_0}\right|\right)^{\beta} \end{cases} & if\ |\dot{\varepsilon}_{22}| \geq \dot{\varepsilon}_0 \end{cases} \tag{3.8}$$

Eq.(3.8) indicates that the failure index in matrix direction increases with increasing of the strain rate of matrix direction, except for lower values than the reference strain rate. β is the parameter that determines the rate sensitivity of strengths and can be approximated with the transverse strength values obtained at

different strain rates, as being written as follow:

$$\frac{Y_{T,C}}{Y_{T_0,C_0}} = \left(\left|\frac{\dot{\varepsilon}_{22}}{\dot{\varepsilon}_0}\right|\right)^{\beta} \tag{3.9}$$

where, Y_{T_0,C_0} is the transverse tensile or compressive strength value at (or lower than) the reference strain rate, and $Y_{T,C}$ is the value at the strain rate corresponding to $\dot{\varepsilon}_{22}$.

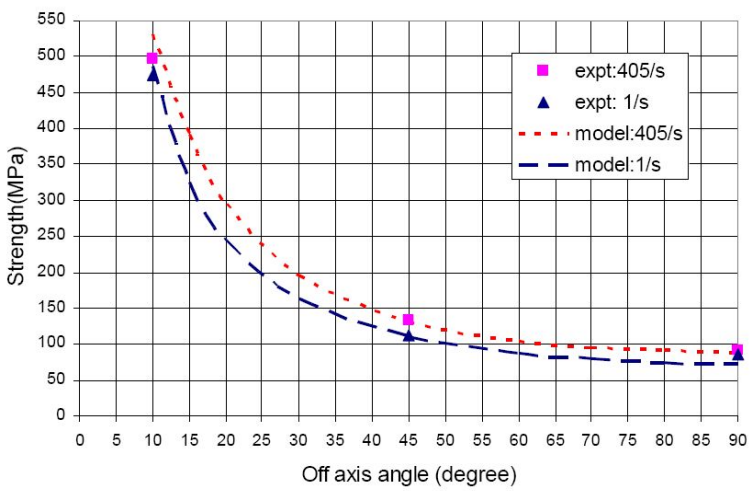

Fig. 3.1 Model predictions of the failure envelops for the UD IM7/977-2 composite at various strain rates (β = 0.065) [21]

Fig. 3.1 shows the model prediction of the failure envelopes at strain rates of 1/s and 405/s are compared with the experimental data [21]. As can be seen from

figure, the model predictions are in good agreement with the experiment, implying that the single rate-sensitive parameter β captures the rate-dependent failure strength reasonably accurate.

3.2 Damage progression after material failure

For laminate composite materials, the progressive failure is very difficult to predict or simulate caused by the complex and complicated interactions of intra-laminar and inter-laminar damage modes. For the analysis using 2D FE model, the progression of composite damage including delamination is barely estimated without special analysis schemes such as VCCT (Virtual Crack Closure Technique) and DCZM (Discrete Cohesive Zone Model) [82]. FE analyses for the structural analysis of aerospace structures are typically carried out using the two dimensional shell meshes caused by their thin and slender structures. In case of crash or impact analyses, 2D FE model, especially for composite materials is commonly used in simulation, because of the necessary for heavy computing resource. Therefore, appropriate method to the composite damage progression should be introduced and implemented into the explicit FE analysis to enhance the efficiency and accuracy of the crashworthiness analysis.

In this study, the hybrid material degradation method is employed to simulate the damage progression after material failure, which method is composed of the ply-discounting method with the damage model based on a CDM approach using internal state variables. To improve the applicability and accuracy of PFA, the EDPM based on the Yen's model is proposed in this study. The material degradation of corresponding to each constituent is adopted within composite micromechanical model, and the decreasing of stress is embodied with the level of micromechanics.

3.2.1. Material degradation model – micromechanical approach

In this study, to analyze the effectively rate-dependent and nonlinear behaviors of polymeric composite materials, the micromechanical approach has been applied. The increments of stresses and inelastic strains at current time step are calculated through the composite micromechanical model. Therefore, in this study, the adjustment of compliance matrix of each constituent is introduced to achieve the degradation of stiffness [59].

As previous description in chapter 3.1, the rate-dependent Hashin model is used

as the failure criteria. Once composite material failure is detected and initiated, the stresses and material properties are modified according to the damage model based on a CDM approach using internal state variables. For each failure mode, an appropriate degradation rule is defined. These degradation rules are empirical and including some assumptions related to engineering constrains, so their physical meanings are not always obvious [59].

Fig. 3.2 shows the material coordinate system and inter-fiber failure mode of UD composite materials [23]. The material coordinate system (x_1, x_2, x_3) is fixed to fiber direction (x_1), matrix direction (x_2), and thickness direction (x_3). According to Mohr's strength theory, the inter-fiber fracture is influenced by three stresses σ_n, τ_{nt}, τ_{nl}, only, as depicted in Fig. 3.2 [23]. We can inversely proceed on this hypothesis that three stresses σ_n, τ_{nt}, τ_{nl} can be influenced by the fracture. According to above assumption, we can specify the degradation rules like as; the fiber failure modes are related to the normal stress, σ_{11}, and the shear stresses, σ_{12} and σ_{13}. The matrix failure modes are related to the normal stresses, σ_{22}, and the shear stresses, σ_{12} and σ_{23}.

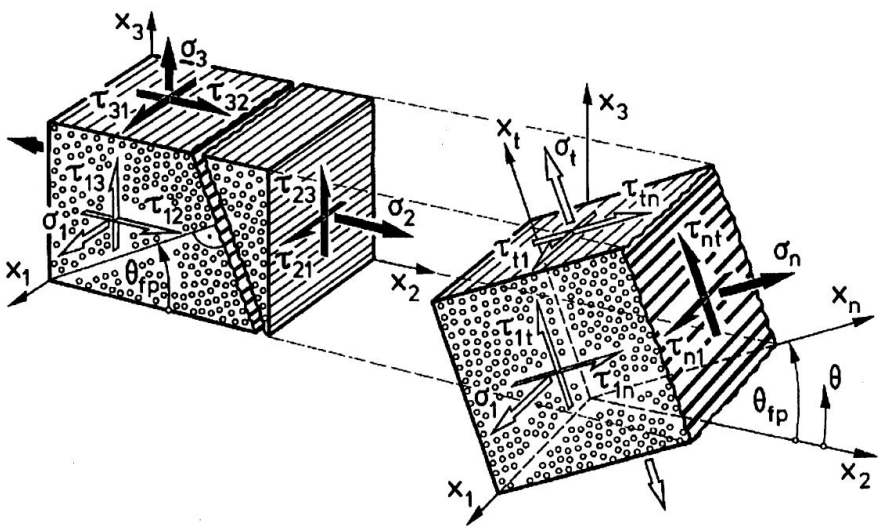

Fig. 3.2 Schematic showing of material coordinate system and inter-fiber failure mode of UD composite materials [23]

For intra-lamina failure modes, the degradation rule is divided into the case of tensile and compressive model. When the tensile failure mode is observed, the stresses in the unit cell (lamina) and the compliance matrices of the fiber and matrix constituents are adjusted appropriately. Oppositely, for the compressive failure mode, there is the adjustment of stresses only without the change of the compliance matrices of constituents, because the failure plane is closed. At this instance, the composite material still has the capability to support the compressive stresses [59].

Tensile Fiber Failure Mode

When the fiber tensile failure is observed by Eq.(3.1), the material degradation is applied with aspect of appropriate stresses and compliance matrices of constituents. The original compliance matrices, $\boldsymbol{S}_F$ and $\boldsymbol{S}_M$, of the fiber and matrix materials are listed as follows:

$$\boldsymbol{S}_F = \begin{bmatrix} \frac{1}{E_{11}^F} & -\frac{v_{21}^F}{E_{11}^F} & -\frac{v_{21}^F}{E_{11}^F} & 0 & 0 & 0 \\ -\frac{v_{12}^F}{E_{11}^F} & \frac{1}{E_{22}^F} & -\frac{v_{23}^F}{E_{22}^F} & 0 & 0 & 0 \\ -\frac{v_{12}^F}{E_{11}^F} & -\frac{v_{23}^F}{E_{22}^F} & \frac{1}{E_{22}^F} & 0 & 0 & 0 \\ 0 & 0 & 0 & \frac{1}{G_{23}^F} & 0 & 0 \\ 0 & 0 & 0 & 0 & \frac{1}{G_{12}^F} & 0 \\ 0 & 0 & 0 & 0 & 0 & \frac{1}{G_{12}^F} \end{bmatrix} \tag{3.10}$$

$$\boldsymbol{S}_M = \begin{bmatrix} \frac{1}{E^M} & -\frac{v^M}{E^M} & -\frac{v^M}{E^M} & 0 & 0 & 0 \\ -\frac{v^M}{E^M} & \frac{1}{E^M} & -\frac{v^M}{E^M} & 0 & 0 & 0 \\ -\frac{v^M}{E^M} & -\frac{v^M}{E^M} & \frac{1}{E^M} & 0 & 0 & 0 \\ 0 & 0 & 0 & \frac{1}{G^M} & 0 & 0 \\ 0 & 0 & 0 & 0 & \frac{1}{G^M} & 0 \\ 0 & 0 & 0 & 0 & 0 & \frac{1}{G^M} \end{bmatrix} \tag{3.11}$$

where, E_{11}^F, E_{22}^F, G_{12}^F, and G_{23}^F are the fiber elastic modulus in fiber direction, fiber elastic modulus in matrix direction, fiber in-plane shear modulus, and fiber transverse shear modulus, respectively. v_{12}^F, v_{21}^F, and v_{23}^F are Poisson's ratio of fiber in each direction. As isotropic material, the elastic modulus of matrix, E^M, Poisson's ratio of matrix, v^M, and in-plane shear modulus of matrix can be calculated as follow:

$$G^M = \frac{E^M}{2(1+v^M)} \tag{3.12}$$

Once the fiber tensile failure occurs, the coupling between the fiber direction and matrix direction and thickness direction disappears. The damaged compliance matrix of fiber constituent, $\boldsymbol{S}_F^d$, can be written as follows:

$$\boldsymbol{S}_F^d = \begin{bmatrix} \frac{1}{(1-\omega_1)E_{11}^F} & 0 & 0 & 0 & 0 & 0 \\ 0 & \frac{1}{E_{22}^F} & -\frac{v_{23}^F}{E_{22}^F} & 0 & 0 & 0 \\ 0 & -\frac{v_{23}^F}{E_{22}^F} & \frac{1}{E_{22}^F} & 0 & 0 & 0 \\ 0 & 0 & 0 & \frac{1}{G_{23}^F} & 0 & 0 \\ 0 & 0 & 0 & 0 & \frac{1}{(1-\omega_1)G_{12}^F} & 0 \\ 0 & 0 & 0 & 0 & 0 & \frac{1}{(1-\omega_1)G_{12}^F} \end{bmatrix} \tag{3.13}$$

where, ω_1 is the internal state variable for damage in fiber direction. The internal state variables are determined by the EDPM based on the MLT model.

The damaged compliance matrix of matrix constituent, $\boldsymbol{S}_M^d$, can be written as follows:

$$\boldsymbol{S}_M^d = \begin{bmatrix} \frac{1}{(1-\omega_1)E^M} & 0 & 0 & 0 & 0 & 0 \\ 0 & \frac{1}{E^M} & -\frac{v^M}{E^M} & 0 & 0 & 0 \\ 0 & -\frac{v^M}{E^M} & \frac{1}{E^M} & 0 & 0 & 0 \\ 0 & 0 & 0 & \frac{1}{G^M} & 0 & 0 \\ 0 & 0 & 0 & 0 & \frac{1}{(1-\omega_1)G^M} & 0 \\ 0 & 0 & 0 & 0 & 0 & \frac{1}{(1-\omega_1)G^M} \end{bmatrix} \quad (3.14)$$

Once the tensile failure mode is observed, the damaged stresses, $\boldsymbol{\sigma}^d$, in the unit cell (lamina) are reduced with the level of macroscopic as follows:

$$\boldsymbol{\sigma}^d = \begin{bmatrix} (1-\omega_1) & 0 & 0 & 0 & 0 \\ 0 & 1 & 0 & 0 & 0 \\ 0 & 0 & (1-\omega_1) & 0 & 0 \\ 0 & 0 & 0 & 1 & 0 \\ 0 & 0 & 0 & 0 & (1-\omega_1) \end{bmatrix} \begin{Bmatrix} \sigma_{11} \\ \sigma_{22} \\ \sigma_{12} \\ \sigma_{23} \\ \sigma_{13} \end{Bmatrix} \quad (3.14)$$

Compressive Fiber Failure Mode

When the fiber compressive failure is observed by Eq.(3.2), there is only the

adjustments of stresses in the unit cell. Kyriakides et al. [83] studied the compressive failure behavior of UD composite materials through the experimentation and analysis. In this study, it was introduced that dropped stress after the initiation of compressive failure in processing direction was maintained. It was known that this phenomenon was caused by the propagation of kink bands. The value of dropped stress can be determined through the experimentation.

In this study, the decrease of stress after initial compressive failure is included by means of strength reduction factors as follows:

$$\boldsymbol{\sigma}^{d} = \begin{bmatrix} 1 & 0 & 0 & 0 & 0 \\ 0 & 1 & 0 & 0 & 0 \\ 0 & 0 & (1-\omega_1) & 0 & 0 \\ 0 & 0 & 0 & 1 & 0 \\ 0 & 0 & 0 & 0 & (1-\omega_1) \end{bmatrix} \begin{Bmatrix} \max(\sigma_{11}, -k_F X_C) \\ \sigma_{22} \\ \sigma_{12} \\ \sigma_{23} \\ \sigma_{13} \end{Bmatrix} \tag{3.15}$$

where, k_F is the strength reduction factor under fiber compressive failure mode and the value of magnified k_F by the fiber compressive strength, X_C, is declared as maximum limited value. Shear stresses upon the failure surface are reduced same as the tensile fiber failure case.

Tensile Matrix Failure Mode

When the matrix tensile failure is observed by Eq.(3.6), the material

degradation is applied with aspect of appropriate stresses and compliance matrices of constituents same as the fiber tensile failure case. Once the matrix tensile failure occurs, the coupling between the matrix direction and thickness direction disappears. Original compliance matrices (Eq.(3.10, 3.11)) are adjusted as following. The damaged compliance matrix of fiber constituent, $\boldsymbol{S}_F^d$, can be written as follows:

$$\boldsymbol{S}_F^d = \begin{bmatrix} \frac{1}{E_{11}^F} & -\frac{v_{21}^F}{E_{22}^F} & -\frac{v_{21}^F}{E_{22}^F} & 0 & 0 & 0 \\ -\frac{v_{12}^F}{E_{11}^F} & \frac{1}{(1-\omega_2)E_{22}^F} & 0 & 0 & 0 & 0 \\ -\frac{v_{12}^F}{E_{11}^F} & 0 & \frac{1}{(1-\omega_2)E_{22}^F} & 0 & 0 & 0 \\ 0 & 0 & 0 & \frac{1}{(1-\omega_2)G_{23}^F} & 0 & 0 \\ 0 & 0 & 0 & 0 & \frac{1}{(1-\omega_2)G_{12}^F} & 0 \\ 0 & 0 & 0 & 0 & 0 & \frac{1}{(1-\omega_2)G_{12}^F} \end{bmatrix} \quad (3.16)$$

where, ω_2 is the internal state variable for damage in matrix direction. The internal state variables are determined by the EDPM based on the MLT model.

The damaged compliance matrix of matrix constituent, $\boldsymbol{S}_M^d$, can be written as follows:

$$\boldsymbol{S}_M^d = \begin{bmatrix} \frac{1}{E^M} & -\frac{v^M}{E^M} & -\frac{v^M}{E^M} & 0 & 0 & 0 \\ -\frac{v^M}{E^M} & \frac{1}{(1-\omega_2)E^M} & 0 & 0 & 0 & 0 \\ -\frac{v^M}{E^M} & 0 & \frac{1}{(1-\omega_2)E^M} & 0 & 0 & 0 \\ 0 & 0 & 0 & \frac{1}{(1-\omega_2)G^M} & 0 & 0 \\ 0 & 0 & 0 & 0 & \frac{1}{(1-\omega_2)G^M} & 0 \\ 0 & 0 & 0 & 0 & 0 & \frac{1}{(1-\omega_2)G^M} \end{bmatrix} \quad (3.17)$$

Once the tensile failure mode is observed, the damaged stresses, $\boldsymbol{\sigma}^d$, in the unit cell (lamina) are reduced with the level of macroscopic as follows:

$$\boldsymbol{\sigma}^d = \begin{bmatrix} 1 & 0 & 0 & 0 & 0 \\ 0 & (1-\omega_2) & 0 & 0 & 0 \\ 0 & 0 & (1-\omega_2) & 0 & 0 \\ 0 & 0 & 0 & (1-\omega_2) & 0 \\ 0 & 0 & 0 & 0 & (1-\omega_2) \end{bmatrix} \begin{Bmatrix} \sigma_{11} \\ \sigma_{22} \\ \sigma_{12} \\ \sigma_{23} \\ \sigma_{13} \end{Bmatrix} \quad (3.18)$$

Compressive Matrix Failure Mode

Same as for the fiber compressive failure, it is also only the adjustments of stresses in the unit cell, when the matrix compressive failure is observed by Eq.(3.7). The adjustment of stress in the unit cell is expressed as follow:

$$\boldsymbol{\sigma}^{d} = \begin{bmatrix} 1 & 0 & 0 & 0 & 0 \\ 0 & 1 & 0 & 0 & 0 \\ 0 & 0 & (1-\omega_2) & 0 & 0 \\ 0 & 0 & 0 & (1-\omega_2) & 0 \\ 0 & 0 & 0 & 0 & (1-\omega_2) \end{bmatrix} \begin{Bmatrix} \sigma_{11} \\ \max(\sigma_{22}, -k_M Y_C) \\ \sigma_{12} \\ \sigma_{23} \\ \sigma_{13} \end{Bmatrix} \tag{3.15}$$

where, k_M is the strength reduction factor under matrix compressive failure mode and the value of magnified k_M by the matrix compressive strength, Y_C, is declared as maximum limited value. Shear stresses upon the failure surface are reduced same as the tensile matrix failure case.

3.2.2. Enhanced damage progression model (EDPM)

Traditionally, in the explicit finite element analysis, ply-discounting material degradation models are based on the degradation (or discounting) of the elastic material stiffness. In this study, the UMAT in LS-DYNA is developed to use in the scheme of a multi-integration shell for the representation of laminate composite materials. In this scheme, each ply has a surface integration point, and total quantity of integration points is same as the quantity of plies in the laminate. If the failure initiated ply reaches at the condition to eliminate, the failed ply will be discounted within the laminate. After ply-discounting, the local material stiffness coefficients are re-computed using the degraded laminate condition. The process

for ply-discounting material degradation is executing in the main core of LS-DYNA, not in the UMAT. In the UMAT, the behavior of an integration point (present a ply in laminate) is determined using the RDM and PFA module.

The material degradation using the EDPM in the UMAT subroutine is related to the rate of material degradation during the damage progression, which is most effective for not only the avoidance of some of the numerical instability issues associated with an instantaneous local change in material stiffness, but also the simulation of the progressive failure behavior caused by complex interactions of laminate or (and) delamination. The EDPM in this study, is a derivation of the MLT damage model, and it has one more factor to adjust the shape of material degradation than the Yen's model.

MLT damage model

The MLT damage model based on the CDM models generally describes the internal damage in the material by defining one or more internal state variables. As the characteristic of many CDM models, the MLT approach uses a single mathematical expression to describe the damage evolution as function of strain over the entire loading range. Combining this with a linearly varying modulus

reduction as a function of the damage results in a nonlinear stress-strain curve (corresponding to a damaging material) over the entire range of strains.

The internal state variables introduced by the MLT model vary from zero (indicating no damage) to unity (indicating complete damage). These internal state variables increase from zero as the local strain level increases and serve as indicators of the local reduction in load carrying capability of a lamina. This reduction is caused by failure of weaker material or the coalescence of local defects within the lamina. Within a lamina, some fiber bundles are statistically stronger while others are weaker than the average fiber bundle, and the ultimate strength for the lamina is the accumulation of all fiber bundle strengths. As the strain level increases, the weaker fiber bundles fail and the total number of fiber bundles available to carry load decreases. However, those fiber bundles that remain are the statistically stronger fiber bundles. This behavior is accounted for in the MLT model by the Weibull-distribution assumption for the stress-strain curve. A reduction in the number of load-carrying fiber bundles relates to a reduction in the effective lamina cross-sectional area. Hence, a possible physical interpretation of the MLT internal state variables is that they represent the fractional loss of load-carrying capability in a particular mode or direction within an individual lamina.

The damage growth of the MLT model is based on a Weibull-distribution of strengths, commonly associated with the strength of fiber bundles with initial defects. The MLT model is expressed as follow:

$$\omega = 1 - \exp\left(-\frac{1}{me}\left(\frac{\varepsilon}{\varepsilon_f}\right)^m\right) \tag{3.16}$$

where ε is the current strain and ε_f is the strain at failure, and the exponent m, namely, Weibull number, controls the shape of the stress-strain curve. The damage growth with the strain increase is plotted in Fig. 3.3 with various values of m component. It can be seen that with a small m, the damage variable ω increases fast at the beginning and keeps a slowly decreasing growth rate; while with a large m, ω keeps a small value at the beginning and then increases abruptly to a large value. This implies that a high value of m will result in a brittle manner and a low one gives a materials a more ductile manner.

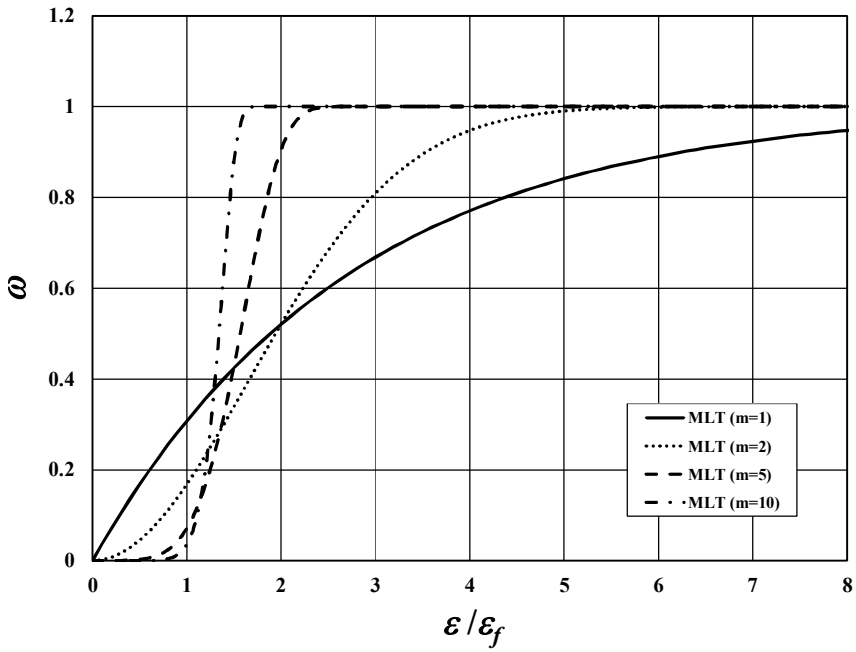

Fig. 3.3 Effect of *m* on the damage growth in the MLT model

The overall approach for the MLT model involves a series of key steps. The first step is selecting appropriate values of the input parameters that affect the MLT stress-strain representation. For example, in a one-dimensional uniaxial problem, five sets of parameters need to be assigned by the user: a *pseudo* initial tensile modulus, the ultimate tensile strength values, ultimate strain values, stress limit factors after ultimate stress, and maximum strain limits. The first three sets of parameters can be used to match measured stress-strain behavior up to ultimate including bimodulus material behavior and nonlinearity in the pre-ultimate

response. The last two sets of parameters can be tuned to match the final damage state. Thus, an empirically derived material model can be defined one that matches the stress-strain response up to the ultimate strength values in tension and compression and is empirically correlated to the post-ultimate response.

The next steps are associated with a sequence of computations performed for the MLT model. Based on a computed strain state, a trial stress state is determined using the constitutive relations. The material failure detection (Hashin criteria) process is evaluated using these trial stresses where the failure indices are turned on. Once the initiation of failure is recognized, then the material degradation by computing internal state variable are evaluated and new trial stresses are determined.

The MLT model is implemented into the MAT58 of LS-DYNA as the PFA methodology. Fig. 3.4 presents the stress-strain behavior near ultimate failure stress simulated by MAT 58. It can be seen in the figure that the degradation of stress at the ultimate strain, ε_f, is executed after the material failure detection by initial trial stress. At least, stress reaches to the ultimate strength beyond ε_f. The strain at which the ultimate strength is reached, is defined as the effective failure strain, ε_q.

In MAT58, exponent m is defined as follow:

$$m = \frac{1}{ln\left(\varepsilon_q / \varepsilon_f\right)} \tag{3.17}$$

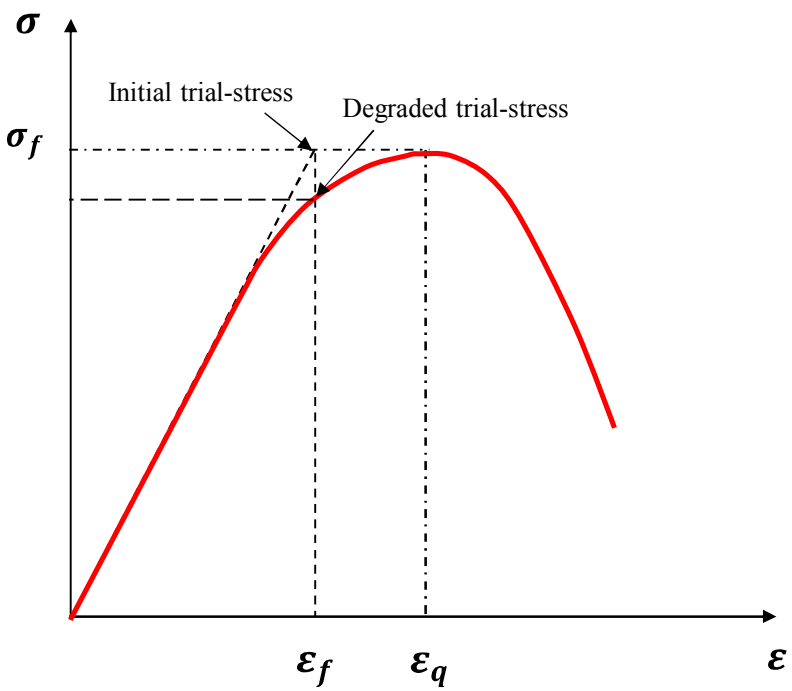

Fig. 3.4 Stress-strain behavior near ultimate failure stress simulated by MAT 58

In Fig. 3.5, the effect of damage exponent m on the tensile stress-strain curve is presented. As previously described, large m drives the brittle manner of behavior. σ_f and ε_f are same as 1.35 GPa and 0.015, respectively. For m = 1, ε_q is same as 0.041, then we can find, Eq.(3.17) is validated. As previously described, increasing

of exponent *m* is enlarging the brittle behavior, oppositely, small exponent m generates more strong nonlinearity as well as ductile behavior. It should be noted that in MAT58, all of nonlinearity is assumed to be due to damage.

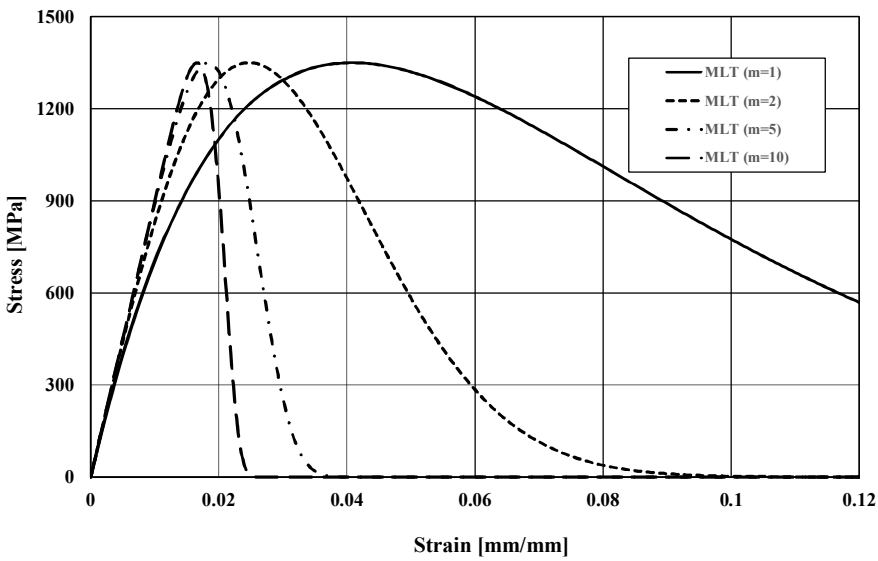

Fig. 3.5 Effect of exponent *m* on the stress-strain curve in MAT58

The MLT model has some distortion of phenomenon near failure strength as presented in Fig. 58, although it is assumed as due to the damage in fiber bundle. The point of view at the lamina, this nonlinear behavior almost can't be observed because of its brittle and abrupt failure, especially, UD carbon composite materials. Thus, we can infer that the MLT model is more suitable for all through-the-

thickness material points at a specific surface-integration point for two-dimensional finite elements. Moreover, in this study, the rate-dependent behavior and failure strength can lead to change the exponent *m*, and unexpected computation result.

Yen's damage model

An alternative damage growth law was proposed by Yen [77] in which the damage starts to grow after the material failure detection, which damage model was implemented into MAT162 in LS-DYNA. In this model, the damage variable, ω, are calculated as follow:

$$\omega = 1 - \exp\left(\frac{1}{m}\left(1 - \left(\frac{\varepsilon}{\varepsilon_f}\right)^m\right)\right) \qquad , |\varepsilon| \geq |\varepsilon_f| \tag{3.18}$$

The effect of the damage exponent *m* on the damage growth is shown in Fig. 3.6. It can be seen that the damage growth with different exponent *m* follows the same shape, while a larger *m* results in a faster damage growth and represents more brittle manner of deformation. It can be seen in Eq.(3.18) that the damage growth by Yen's damage model begins after the initiation of material failure, immediately. Thus, there is no nonlinear behaviors caused by this damage model before material failure detection. At the point of view in layer, this is more reasonable behavior of

failure for UD carbon composite materials.

The damage growth law of Yen's model is more straight forward and consistent than the MLT model [21]. The Yen's damage model is adopted into the composite model by Zheng [21]. The shape of damage curve is more abruptly decreased than the MLT model, so this model is more suitable for the UD carbon composite materials with multi integration point shell elements.

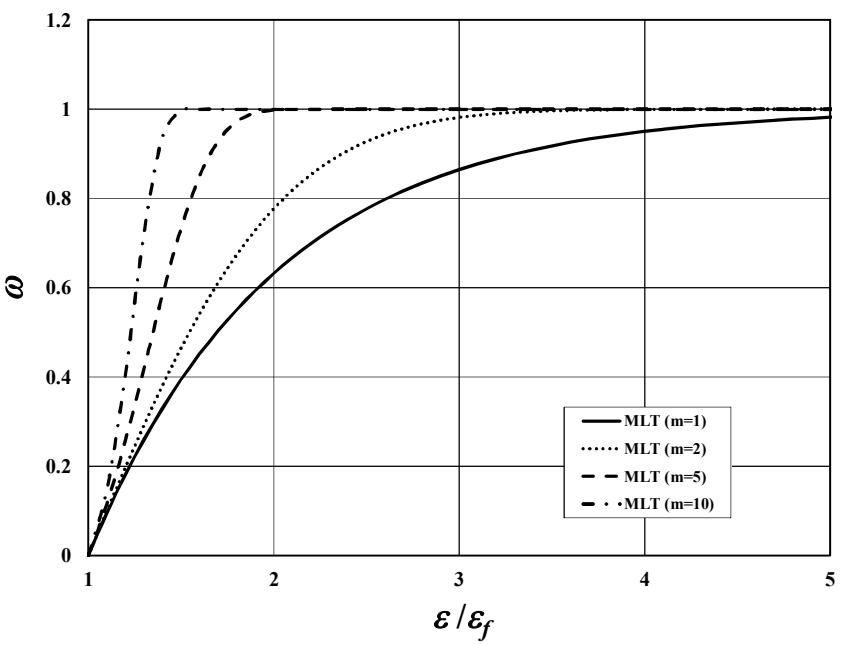

Fig. 3.6 Effect of *m* on the damage growth in the Yen's model

Enhanced damage progression model (EDPM)

In this study, more versatile damage progression model is proposed to capture more reasonable and precise post failure behavior of composite materials at various strain rates, also appropriate for multi integration point shell elements in the explicit FE analysis.

The proposed damage model, namely, the EDPM, is based on the CDM models generally describes the internal damage in the material by defining one or more internal state variables, same as the MLT model. However, to improve the applicability in the explicit FE analysis with multi integration point shell elements, it is triggered by the initiation of material failure, same as the Yen's damage model. Moreover, to complement the weak points in the Yen's model which is too brittle manner of the damage growth, the function of the adjustment of the damage growth rate is included into the damage model by means of the additional variable, λ which controls the shape of curve based on the Yen's model.

In the EDPM, the damage variable, ω, are calculated as follow:

$$\begin{cases} \omega = 1 - \exp\left(\dfrac{1-\left(\dfrac{\varepsilon}{\varepsilon_f}\right)^m}{\lambda\left(\dfrac{\varepsilon}{\varepsilon_f}\right)-\left(\dfrac{\varepsilon}{\varepsilon_f}-1\right)m''}\right) & if \ \dfrac{\varepsilon}{\varepsilon_f} < \dfrac{-m''}{\lambda - m''} \\ \omega = 1 & if \ \dfrac{\varepsilon}{\varepsilon_f} \geq \dfrac{-m''}{\lambda - m''} \end{cases}, |\varepsilon| \geq |\varepsilon_f| \qquad (3.19)$$

where

$$m'' = \frac{m - \lambda m'}{1 - m'}, \quad m' = \sqrt[m]{1 + 7m}$$

In Eq.(3.19), two variables influence the degradation curve after material failure detection. Exponent m controls the range of strain from at the failure initiation to at the zero stress, and λ adjusts the shape of the degradation curve which controls the rate of damage growth. Therefore, in contrast with above two damage models, the EDPM can control the range of strain until the perfect failure and the rate of damage growth with equal range of strain, respectively. The conditions for the calculation of the internal state variable in Eq.(3.19) are derived from the numerical stability of exponential functions.

The damage models based on a CDM approach using internal state variables typically force to adjust the strains and stresses depended on the damage growth law, and then, this adjustment can lead to break the energy balance condition and the numerical instability. Thus, to avoid this phenomenon, the process should be

accomplished as soon as possible. However, as previously described in the Yen's damage model, the rate of damage growth is controlled by only the range of strain until zero stress value as exponent *m*. Therefore, the Yen's model cannot help to get the limitation to simulate ductile behaviors of composite materials.

The effect of *m* and λ on the damage growth in the EDPM is shown in Fig. 3.7. It can be seen that the shape and range of curves are varied with respect to the variation of *m* and λ. With fixed value of $m = 2$, the effect of λ on the damage growth is presented in Fig. 3.8. It can be seen that the curves with same *m* meet at the same point of $\omega = 1$. As λ is larger, larger strain energy is necessary to reach at the point of $\omega = 1$. This implies that a high value of λ will result in a ductile behavior and a low one gives a materials a more brittle behavior. In Fig. 3.9, with fixed value of $\lambda = 10$, the effect of *m* on the damage growth is depicted. Almost same as previous damage models, a lager *m* makes a more ductile behavior, and this is an inverse effect of λ.

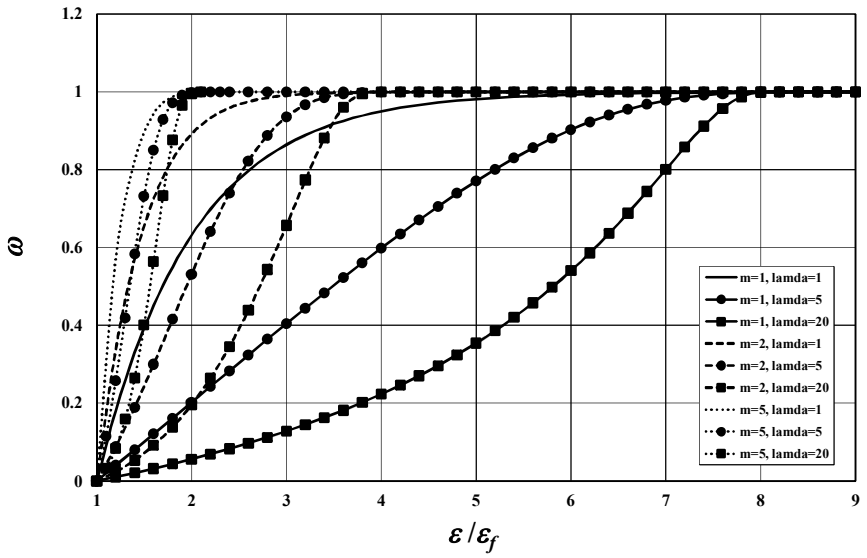

Fig. 3.7 Effect of m and λ on the damage growth in the EDPM

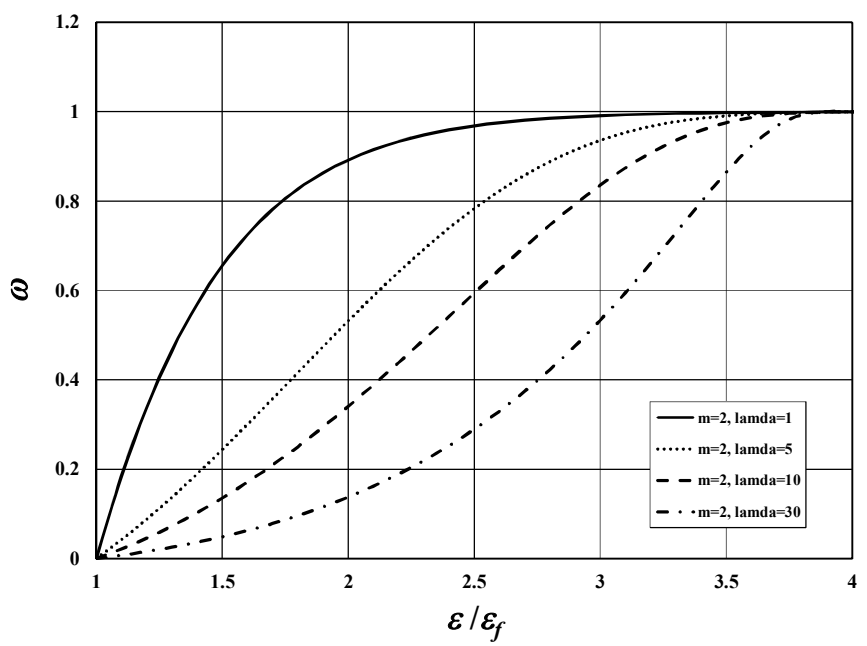

Fig. 3.8 Effect of λ with fixed m on the damage growth in the EDPM (m = 2)

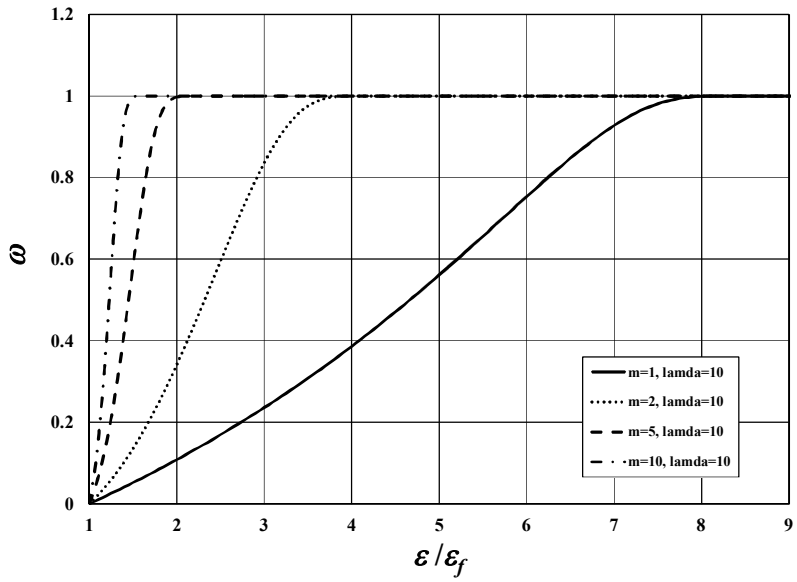

Fig. 3.9 Effect of m with fixed λ on the damage growth in the EDPM ($\lambda = 10$)

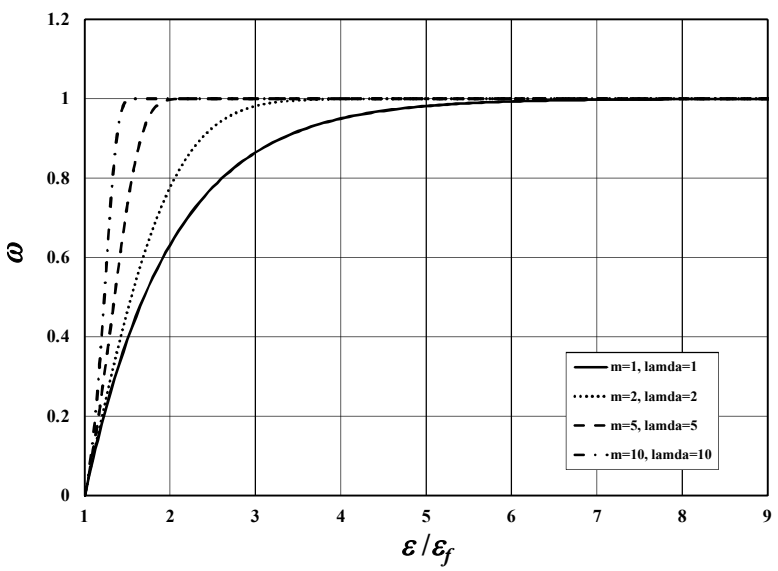

Fig. 3.10 Effect of m with fixed λ on the damage growth in the EDPM ($\lambda = m$)

With fixed value of $\lambda = m$, the effect of m on the damage growth is presented in Fig. 3.10. It can be seen that the curves are same as damage growth curves of the Yen's model in Fig. 3.6. It shows that the EDPM includes the Yen's damage model when $\lambda = m$ is applied.

The strain after the initiation of material failure is main variable to compute the damage growth in the EDPM. In this damage model, the strain value which is calculated in the EDPM not the main core of LS-DYNA, is used to compute the material degradation. Approximately, the damage growth in this study is employed in accordance with the time after material failure. To consider the strain rate dependency of the PFA in this study, the increase of strain is determined as a function of average strain rate of the corresponding element until the damage initiation and the time after failure, and the strain is calculated as follow:

$$\varepsilon = \varepsilon_f + S_s\left(TT - T_f\right)\dot{\varepsilon}_{ave} \tag{3.20}$$

where ε is the current strain, ε_f is the strain at material failure, and S_s is the scaling factor for strain calculation which has the physical meaning of the ratio of the time required to the elongation before the material failure initiation and the perfect fracture after the failure. TT is the current time, T_f is the time at the

material failure initiation, and $\dot{\varepsilon}_{ave}$ is the average strain rate until failure detection.

3.3 Damaged element deletion

The final step of the PFA is the material erosion according to the pre-defined limit values to improve the maturity of structural failure mechanisms. The criteria of element erosion is composed of the element and integration point (Gauss point) deletion.

The integration point will be eliminated when fiber and matrix directional failure are achieved and it has sufficient elongated with fiber or matrix direction. The application of the strain value as elimination criteria is to get more robust and stable results. The numerical instability can be occurred by a smaller stress value degraded by the PFA procedure. The criteria of the element erosion is "All of integration points have been failed." The element which is satisfied all of criteria, will be eroded by the main code of LS-DYNA.

4. IMPLEMENTATION AND MODEL VERIFICATION

The damage models for viscoplastic polymeric composite materials proposed in this study, are implemented into the dynamic explicit finite element code LS-DYNA as a UMAT. LS-DYNA has a user defined material option where a user can implement his or her own material model into the code through the use of a UMAT. The advantage of the usage of LS-DYNA is the making efficient use of the proven explicit finite element scheme like as numerical scheme for dynamics, imbedded materials, contact algorithms, adding the static & dynamic boundary condition, etc. The disadvantage of that is the absence of the interaction between elements. The recognition of the status of adjacent elements offers the crashfront strength reduction and the effect of delamination progression.

To validate proposed damage models and its implementation within FE code, two representative polymeric composite materials, T700/M015 and IM7/977-2 were analyzed using LS-DYNA with damage models, and the computed stress-strain curves, material failure, and post failure behaviors were compared to experimental results obtained test and Ref. [33]. As part of this study, the

T700/M015 is examined for a wide range of strain rates, and this material behaves in somewhat brittle manner. The IM7/977-2 have been frequently used in rate-dependent composite material studies, and it is known that this material has a good toughness property.

4.1 Implementation in the FE element analysis

The structure of the UMAT subroutine in this study is shown in Fig. 4.1. The LS-DYNA code calculates the strain increments for a time step and passes them to the UMAT subroutine at the beginning of each time step. The material constants, such as fiber and matrix moduli, viscoelastic and viscoplastic constants, and failure strength values, are read from the LS-DYNA input file by the subroutine. The previously calculated stresses and history variables such as Z, α, status of failure, and stresses at matrix, are flowed into the UMAT subroutine.

The UMAT subroutine is composed of the RDM module and the PFA module. The RDM module has a role of the calculation of stress increments and total stresses. The total stresses calculated RDM module come into the PFA module, then the material failure and post failure behavior are determined by this step. In

case of material failure, damage values (ω_1, ω_2) are handed over the RDM module to degrade the stiffness. If the criteria for element erosion is satisfied, corresponding element will be eliminated. Finally, the total stresses, inelastic strains, and history variables are resulted and returned into the main code.

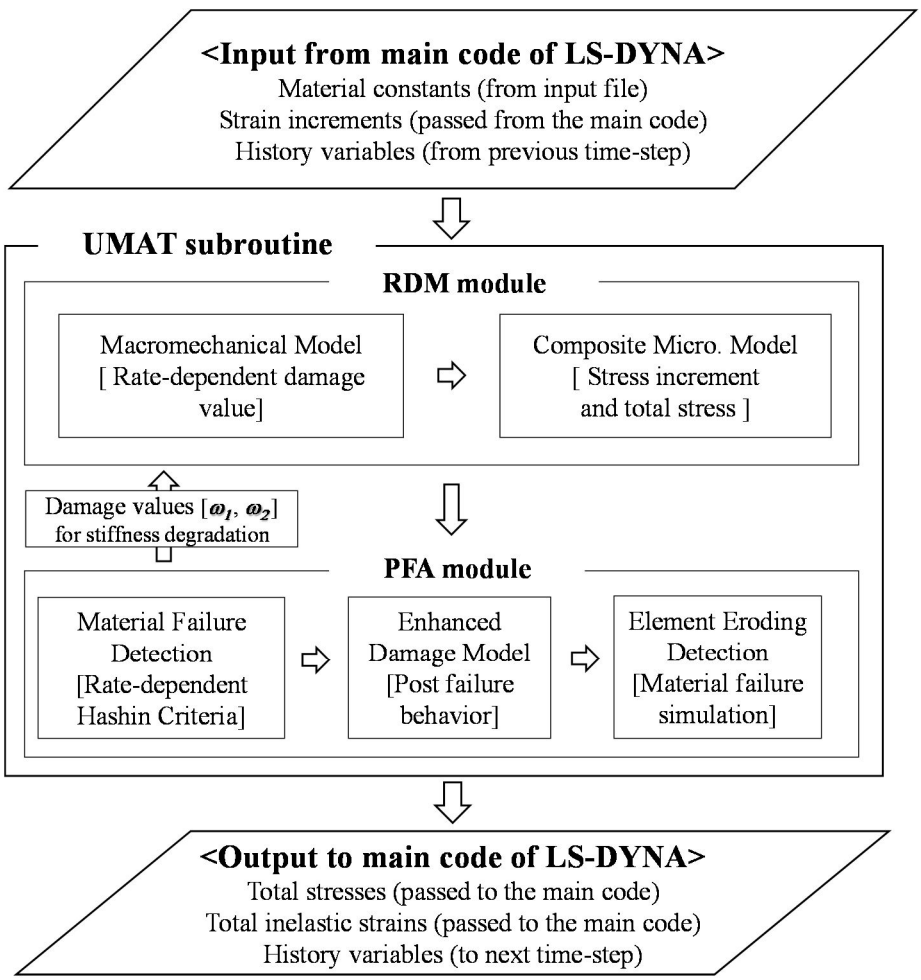

Fig. 4.1 Flowchart of user defined subroutine used to implement material model within LS-DYNA finite element code

4.1.1. Implementation of RDM using multi-scale approach

To compute the rate-dependent nonlinear behaviors of polymeric composite materials based on the response of the individual constituents, a micromechanical approach is employed into the RDM. The elastic damage value caused by micro-cracks in the matrix or at the matrix/fiber interface is calculated using the ply stresses at the macromechanical level.

Fig. 4.2 shows the flowchart of the RDM for the implementation of LS-DYNA as a UMAT using the multi-scale approach. In the flowchart, the macromechanical and micromechanical models are weakly coupled at same time step by the damage value that is computed using the strain rate at current time step and ply stresses at the previous time step. Material failure and post failure progression procedures are not included in Fig. 4.2.

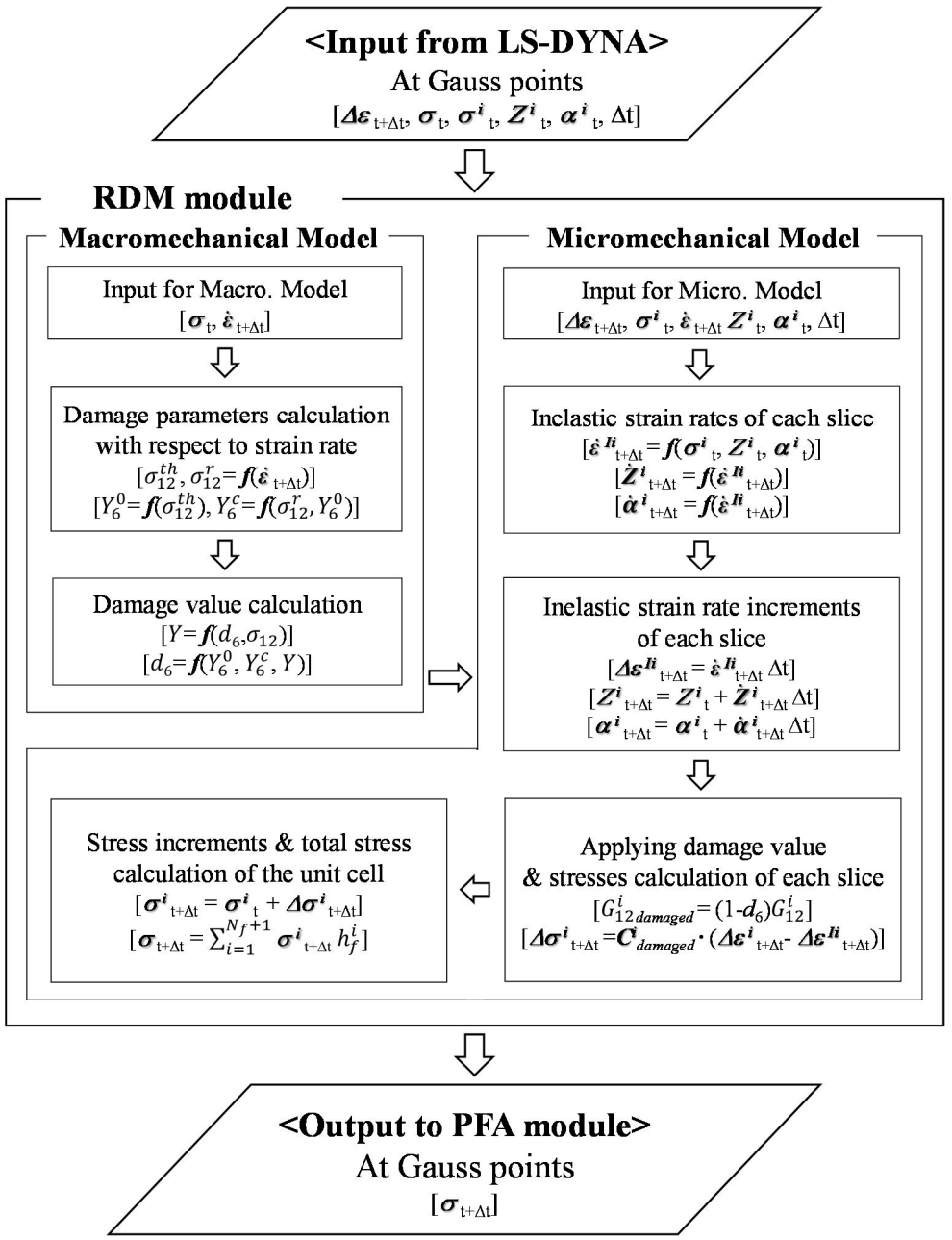

Fig. 4.2 Flowchart of the RDM for the implementation of LS-DYNA as a UMAT using the multi-scale approach

4.1.2. Implementation of PFA

The PFA is composed of the part for material failure detection, damage value calculation, and examination of element deletion. The stresses, strains, total time, time step, and history variables about failure indices are flowed from the RDM module to PFA module. If material failure already occurred at the previous time step, this part will be bypassed to next part. The material failure detection part is divided into the step for fiber failure and matrix failure. In each directional step, rate-dependent Hashin failure criteria is applied to determine the failure. In case of matrix direction, the failure strengths of matrix under tension or compression is calculated with respect to strain rate (Eq. (3.6,3.7)), and these values are implied into the examination of matrix failure.

In case of the occurrence of material failure, the internal state variables for damage are calculated with the enhanced damage model proposed in this study. Same as the part of material failure detection, this part is also decomposed into the fiber direction and matrix direction. Calculated internal state variables are used to reduce the stress and degrade the stiffness, and the degradation of stiffness is started to next step after the failure occurrence.

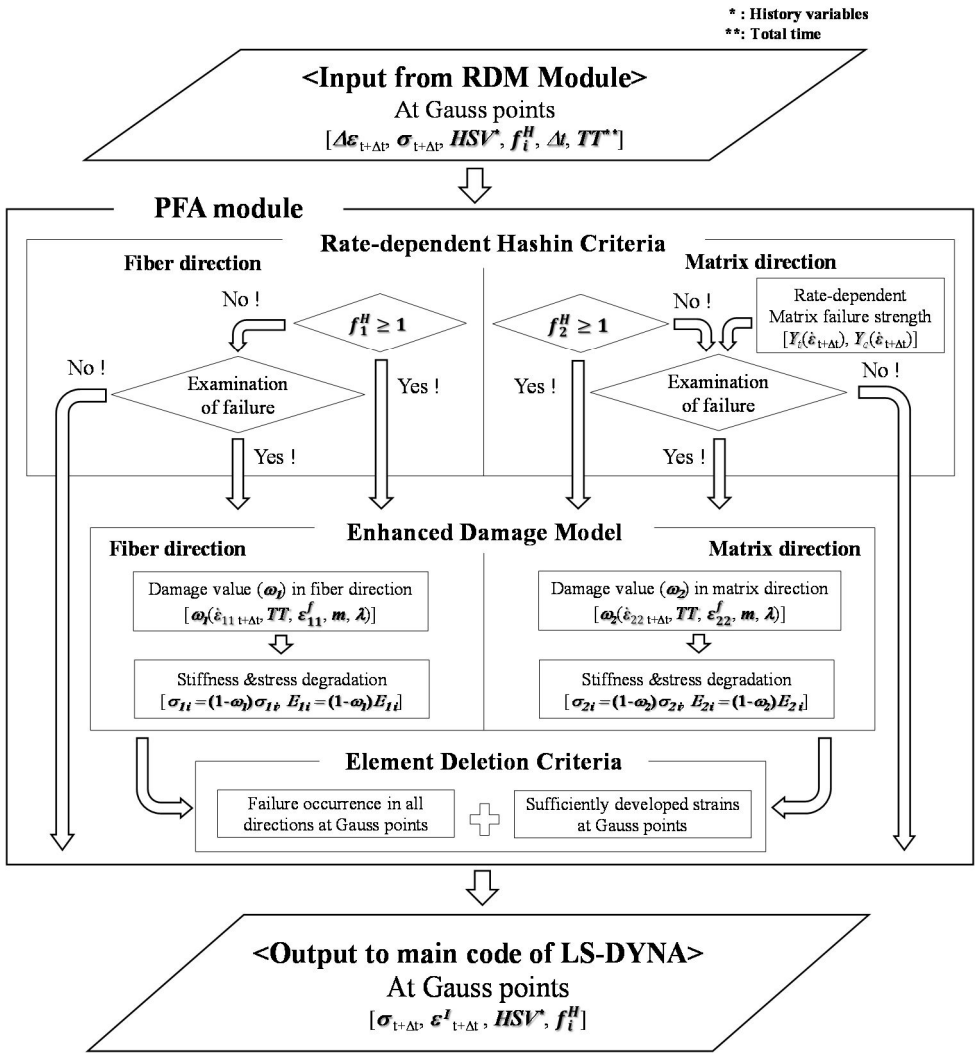

Fig. 4.3 Flowchart of the PFA for the implementation of LS-DYNA as a UMAT

The final part of the PFA module is to present the elimination of integration points. The criteria of element deletion is defined as all of directional failure and sufficiently small value of stress in fiber and matrix direction. In the UMAT in LS-

DYNA, elimination condition can be declared as the quantity of failed integration points. In case of the usage of reduced integration scheme such as Belytschko-Tsay shell element, just one integration point per layer can be granted [58]. Therefore, the declaration as the same quantity with layers can make element eliminate. However, when the fully integrated shell element is using, four times of the quantity of layers should be declared to eliminate an element [58].

4.2 Model verification

The verification of the RDM is carried out through the comparison with experimental results of off-axis and angle-plies, because these type of laminates quite well represent the characteristics of in-plane shear behavior as well as rate-dependent matrix behavior. The PFA model is verified with a sort of practical composite laminates which composed of 0°, ±45°, and 90°. All of experimental data are acquired or referred as static and various strain rates conditions.

4.2.1. Verification for RDM

To verify the RDM, experimental results are compared with analysis results for the T700/M015 and IM7/977-2 materials [33]. Table 4.1 lists the material constants for the viscoelastic and viscoplastic behaviors of the M015 and 977-2 materials. The damage constants for the RDM are listed in Table 4.2. To validate the phenomenological maturity and the improvement of the RDM, the analysis results with the elastic damage model ("with DM" in the figure) and without the elastic damage model ("without DM" in the figure), are compared with experimental results.

Table 4.1 Comparison of elastic constants from predictions and tests

Material	Viscoelastic constants			
	E_0 [GPa]	C_1	C_2	ν_m
977-2 [19]	3.5	-	0.17	0.40
M015	3.7	0.005	0.40	0.41

Material	Viscoplastic constants						
	D_0 [/s]	n	Z_0 [MPa]	Z_1 [MPa]	q	α_0	α_1
977-2 [19]	$1x10^6$	0.85	259.5	1131.4	150.5	0.129	0.15
M015	$1x10^6$	0.89	692.1	955.3	180.0	0.15	0.23

Table 4.2 Material damage constants for the RDM

Material	$\boldsymbol{\sigma_{12}^r}$ (X_S) [MPa]	β	$\boldsymbol{Y_6^0}$ $[\sqrt{\boldsymbol{MPa}}]$	$\boldsymbol{Y_6^c}$ $[\sqrt{\boldsymbol{MPa}}]$
IM7/ 977-2 [19]	95.0	0.065	0.16	3.66
T700/M015	75.0	0.16	0.17	2.73

Analysis results for T700/M015 material

The RDM is implemented into LS-DYNA as a UMAT presented in Fig. 4.2, a

single shell element model is used for validation of the model. The boundary conditions same as experiments are applied to the model, the constant strain rate is allowed in the model. Fig. 4.4 shows the single element FE model for the verification.

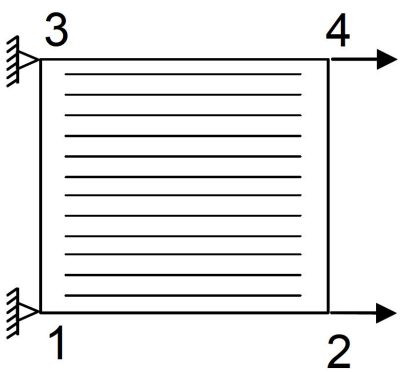

Fig. 4.4 Boundary and loading conditions for single element FE model (Tension)

Dynamic tensile tests for the laminate configuration $[\pm 45°]_s$ of the T700/M015 material were conducted at average strain rates of about 2.3E-4/s, about 15~20/s, and about 100~150/s, and these test strain rates represented a quasi-static, a medium, and a high speed condition, respectively. Quasi-static tests were carried out using a MTS 810 hydraulic testing machine. Dynamic tests were conducted using an Instron VHS 8800 High strain rate system. ASTM D3039 [65] is applied

on quasi-static tests. For dynamic test, to ensure the compatibility with the dynamic tensile test device, dog-bone shaped specimens in Ref. [33] are applied on these experimentations. Strain gages and an extensor-meter were used to measure the strain data of quasi-static tests, and the digital image correlation method using ARAMIS software was applied to measure the strain data of medium and high strain rate tests. In case of high strain rate tests in Fig. 4.5, although the considerable oscillation due to the dynamic effects of the load train of a testing machine is observed, the similar trend of response with other stress-strain curves can be estimated.

Fig. 4.5 presents the comparison between experimental results and prediction results of the analysis model with DM for the $[\pm 45°]_s$ angle-ply at strain rates of 2.3E-4/s, 18.3/s, and 113.6/s. The predicted results fairly agree with the experimental values at quasi-static and medium strain rates. The high strain rate result is somewhat under estimation up to the strain level of 1%, beyond this point, prediction correlates well with the tendency of non-linearity. Specifically, non-linearity and rate dependence of experimental results are captured well qualitatively at the entire range of strain rates.

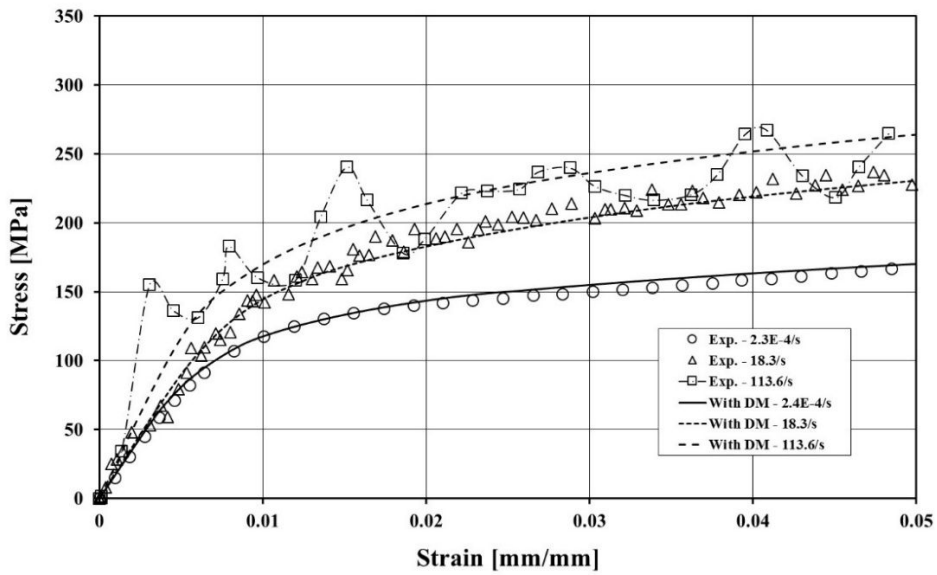

Fig. 4.5 Comparison of experimental and predicted stress-strain curves with damage model for the T700/M015 $[\pm 45°]_s$ laminate

Fig. 4.6 shows the comparison between experimental results and prediction results of the analysis model without DM. Overall, the analysis model overpredicts experimental results significantly beyond a strain level of 0.5%. Moreover, the errors between experimental and prediction results enlarge as increasing strain and strain rate.

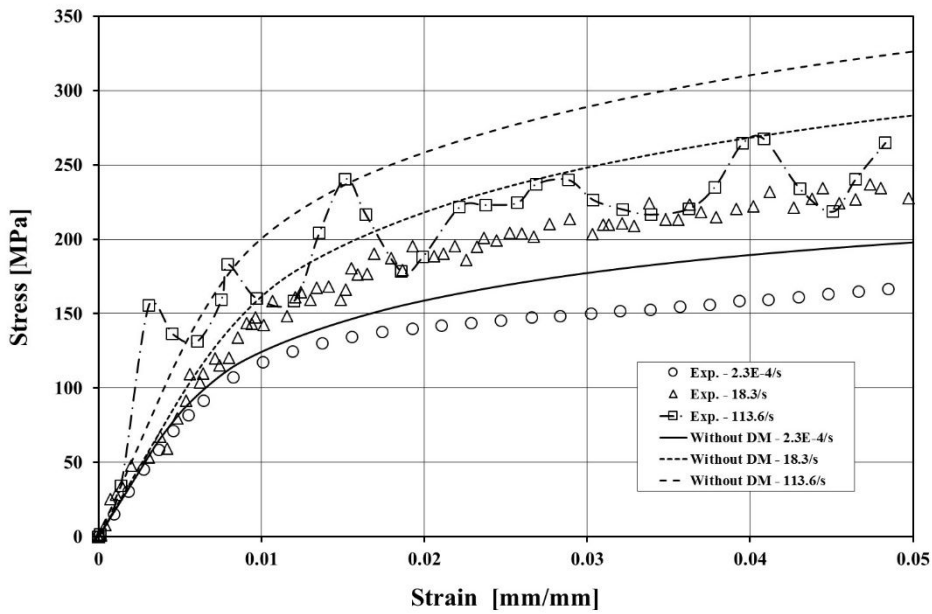

Fig. 4.6 Comparison of experimental and predicted stress-strain curves without damage model for the T700/M015 $[\pm 45°]_s$ laminate

Analysis results for IM7/977-2 material

Gilat et al. [33] have conducted the experimental study for the rate sensitivity of the IM7/977-2 material, and experimental data, was utilized as reference data in several analysis model development researches [19, 21]. Hence, we are willing to apply the IM7/977-2 material on the RDM to compare with other rate-dependent analysis models for polymeric composite materials.

The RDM needs the in-plane initiation damage constant, Y_6^o, which could be

obtained by the monotonic tensile coupon test for the $[\pm 45°]_s$ laminate as previously described. However, it is impossible to execute the monotonic tensile test with the same composite material, in this study, the value of Y_6^o is estimated through the analysis of the initiation of non-linearity for the $[\pm 45°]_s$ laminate tensile test data [33] with a assistance of FE analysis. The estimated value of Y_6^o is presented in Table. 4.2. The viscoelastic model written in Eq. (2.6) is only applied to the IM7/977-2 material at all of strain rates, because the scaling material constant, C_2, is just available.

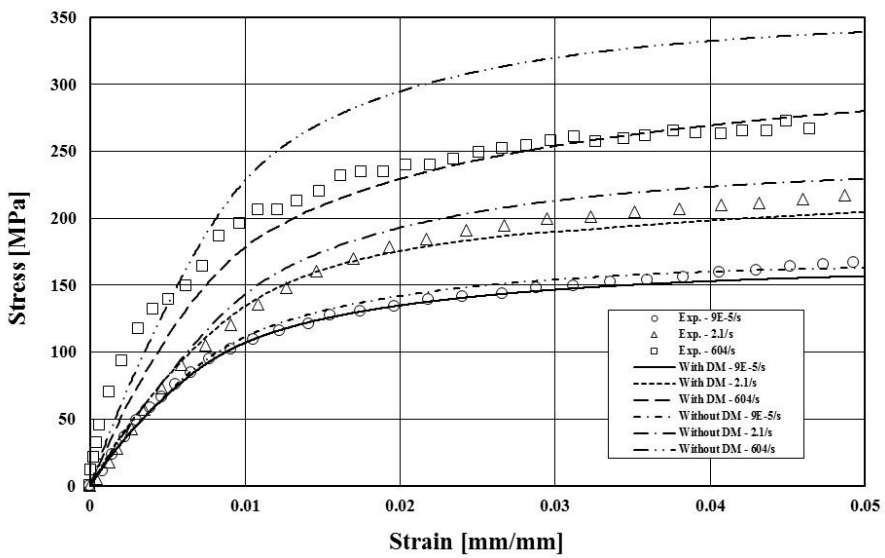

Fig. 4.7 Comparison of experimental [19] and predicted stress-strain curves with and without damage model for the IM7/977-2 $[\pm 45°]_s$ laminate

Fig. 4.7 shows the comparison between experimental results and prediction results of the analysis model with DM and without DM. Throughout all of strain rates, the analysis model with DM is more accurate than without DM. In case of with DM, the prediction results fairly agree with the experimental values for the quasi-static and medium strain rates up to the strain level of 2%. Beyond this point, the quasi-static result keeps a good correlation, while the medium strain rate is somewhat under prediction of the stress as increasing strain. At high strain rate, prediction result is somewhat under estimation up to the strain level of 3%, beyond this point, prediction correlates well with the experimental data.

In case of without DM, the errors of prediction results are grown up as increasing strain and strain rate, which results are same as the T700/M015 material.

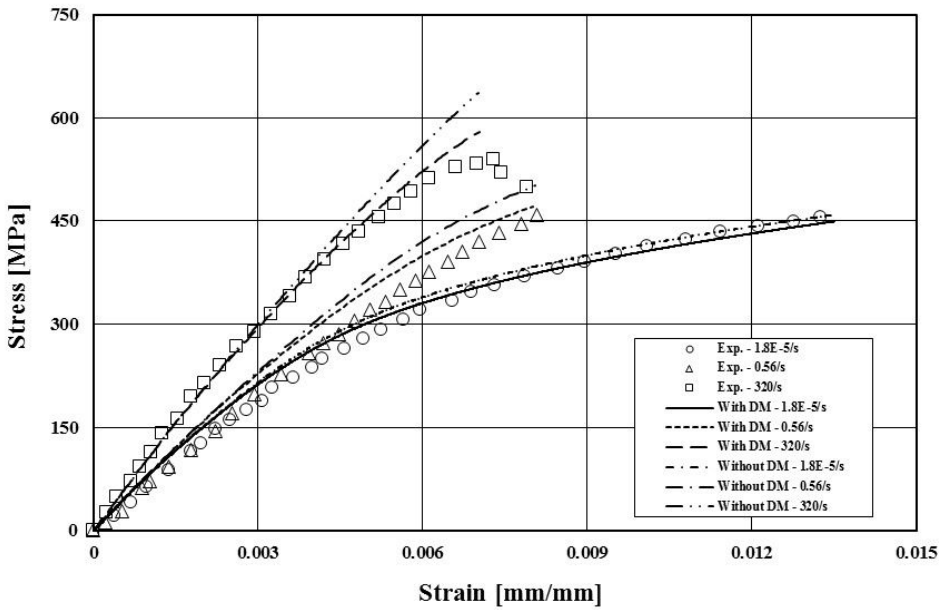

Fig. 4.8 Comparison of experimental [19] and predicted stress-strain curves with and without damage model for the IM7/977-2 [10°] laminate

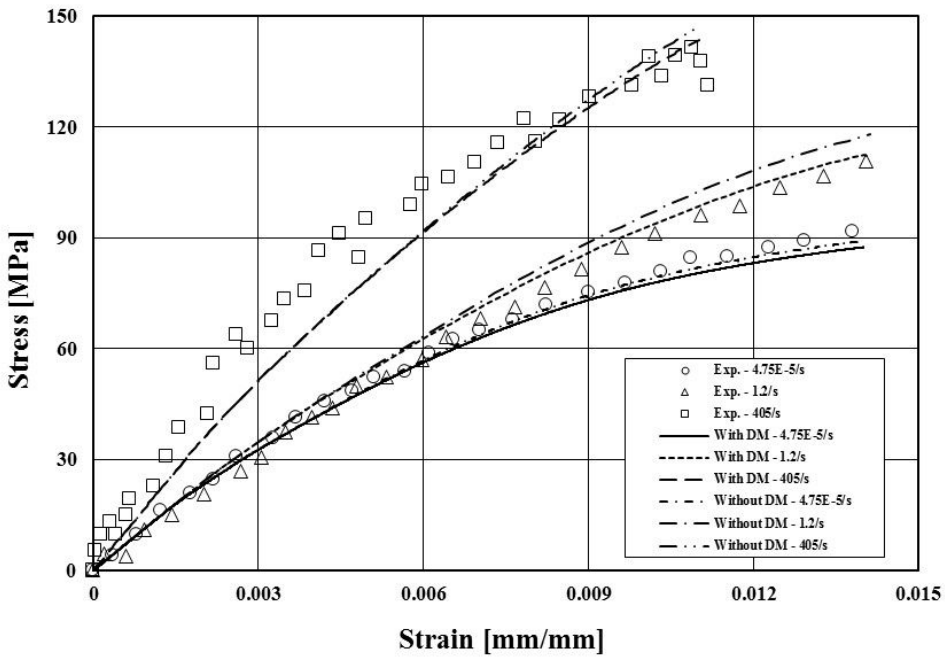

Fig. 4.9 Comparison of experimental [19] and predicted stress-strain curves with and without damage model for the IM7/977-2 [45°] laminate

Figs. 4.8 and 4.9 depict the verification results of off-axis loading conditions, and show the [10°] and the [45°], respectively. Two comparison results show that the analysis model with DM is more accurate than without DM. Though it is similar to previous comparison cases, predictions from two analysis models are similar to each other. Relatively little discrepancies between two analyses models are most likely due to a small range of strain.

In Fig. 4.8, at high strain rates, the analysis result fairly agrees with the experimental data, but the over estimations are observed at quasi-static and medium strain rates. Beyond a strain level of 0.8%, however, the quasi-static result is well correlation with the experimental data. In Fig. 4.9, at high strain rates, the analysis model is somewhat under prediction of stress up to 0.9%, while the prediction results at quasi-static and medium strain rates are in good agreement with experimental results.

4.2.2. Verification for PFA model

The PFA presented in this study, is for the impact and crash simulation of composite aircraft structures using the explicit FE analysis. Thus, the rate-dependency of the PFA model is focused on the validation procedure. To meet this condition, the model for verification is determined as the plain coupon configuration to consider wide range of strain rates from quasi-static loading condition to dynamic loading conditions.

To verify the PFA model, experimental results are compared with analysis results for the T700/M015 material. Experimentation for the verification is

composed of the quasi-static and dynamic coupon tests and both of tests have same geometry of coupon. Table 4.3 presents the test matrix for the verification of the PFA model. The numbers in the laminate configuration cell mean the percentage of 0, 45, 90 degrees of layup, and the parenthesized word below the numbers is a name of specimens. To promote the practicality, the test laminate and test specimen configurations referred to the Advanced General Aviation Transport Experiments (AGATE) test report for composite materials [83]. In this reference, the test laminate and test specimen configurations were selected to be representative of a wide range of typical airframe structures and were not intended to reflect structural details that were unique to a specific frame design.

Table 4.4 lists strength allowable values for the T700/M015 material. All of values are average values of coupon test results, and three specimen are used per each coupon. The value in parenthesis is representing the estimation.

The dog-bone shaped specimens in Ref. [33] also used to verify the PFA model, and it was applied static and dynamic tests. In contrast with the RDM verification, fully shaped FE model and boundary conditions are used in the PFA verification to identify failure modes. Thus, dynamic tensile tests are classified as the stroke speed

to accommodate the effect of strain rates. As listed in Table 4.3, 1, 3, 6 m/s of stroke speeds are determined and these test strain rates represented a quasi-static, a medium, and a high speed condition, respectively. Quasi-static tests were carried out using an Instron 5882 electromechanical material testing system. Dynamic tests were conducted using an Instron VHS 8800 High strain rate system. Dog-bone shaped specimens in Ref. [33] are applied on these experimentations. Strain gage was used to measure the strain data of quasi-static tests, and the digital image correlation method using ARAMIS software was applied to measure the strain data of dynamic tests.

Table 4.3 Test matrix for verification of the PFA model

Laminate configuration	**Stacking sequence**	**Loading condition (speed)**			
		quasi-static	1 [m/s]	3 [m/s]	6 [m/s]
10/80/10 (LE1)	$[45/-45/90/45/-45/45/-45/0/45/-45]_s$	3	3	3	3
25/50/25 (LE2)	$[45/0/-45/90/45/0/-45/90/45/0/-45/90]_s$	3	3	3	3
50/40/10 (LE3)	$[45/0/-45/90/0/0/45/0/-45/0]_s$	3	3	3	3

Table 4.4 Material strength allowable values for the T700/M015

Material	Strength allowable values					
	X_T [MPa]	X_C [MPa]	Y_T [MPa]	Y_C [MPa]	S_C [MPa]	S_T [MPa]
T700/M015	2,300	1,700	60	(150)	180	(65)

The details about the FE model and applied the boundary and loading (prescribed velocity) conditions are depicted in Fig. 4.10. The region in gage length is defined as more fine meshes than other regions to improve accuracy.

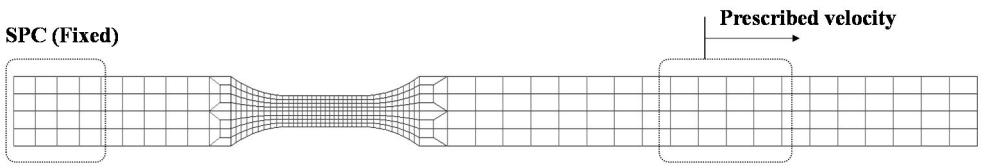

Fig. 4.10 Boundary and loading conditions of the FE model for the PFA verification

Fig. 4.11 presents the comparison between experimental result and prediction results of the Yen's model for the PFA with various *m* for the configuration of LE1 (10/80/10) of the T700/M015. It can be seen that even though a quit good correlation with experimental result before the saturation of stress-strain curve

around 450 MPa, the Yen's damage model cannot generate enough plateau stress-strain curve. As previously described, a smaller m yields the increase of ductile behavior, and it can be seen in Fig. 4.11. However, no longer possible to increase the value of *m*, because *m* less than 8 causes the numerical instability in the Yen's model.

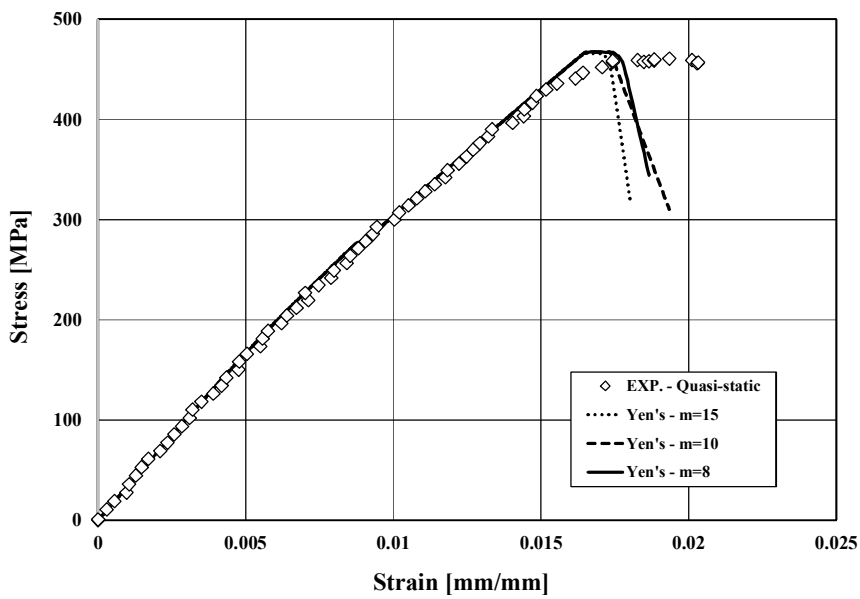

Fig. 4.11 Comparison of experimental and predicted stress-strain curves with Yen's model for 10/80/10 (LE1) configuration of the T700/M015 laminate

In Fig. 4.12, comparison of experimental and predicted stress-strain curves

using the EDPM as the PFA model is presented, and it contains the Yen's most ductile analysis result for comparison of two damage models. The results from the EDPM is showing longer saturation range than the Yen's model. A larger λ value yields the more ductile behavior. If λ is same as *m*, the analysis result from the EDPM will be same as the Yen's one. The maximum allowable λ and *m* are limited as 20 and 8, and values in excess of these values make the numerical instability. Both of results are showing the degradation of stiffness around 250 MPa, it is caused by the breakage of the pattern 90 degree in matrix direction.

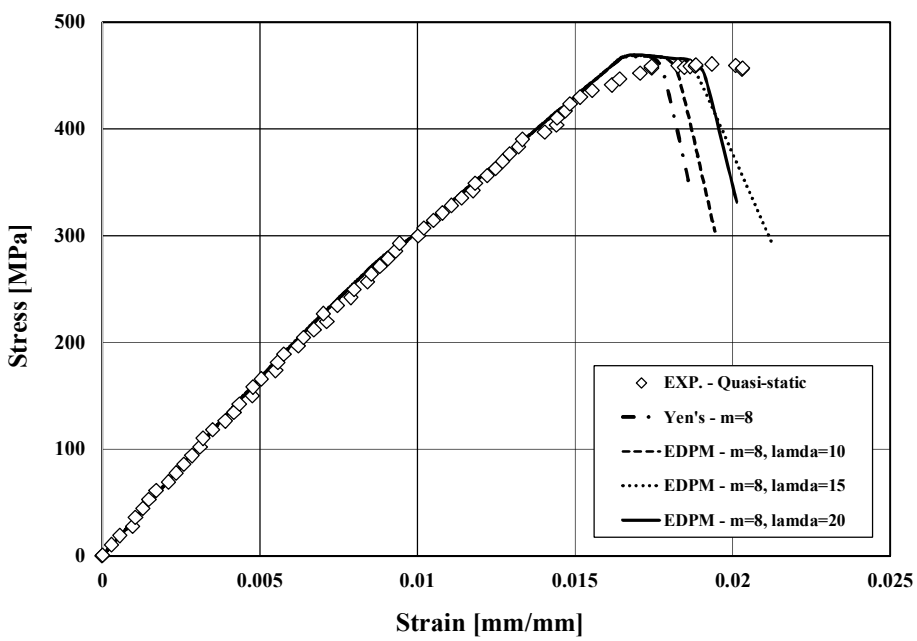

Fig. 4.12 Comparison of experimental and predicted stress-strain curves with

EDPM for 10/80/10 (LE1) configuration of the T700/M015 laminate

Fig. 4.13 presents the failed coupon shapes of the experimentation and analysis with the EDPM of LE1. It can be seen in the experimental result that the damaged and failed area are widely spread on the gage length region. In case of the result of analysis, almost elements in the gage length region are lost and scattered out. Through the comparison of two failed shapes, we can confirmed that the EDPM is capable to simulate the damage and failure behaviors.

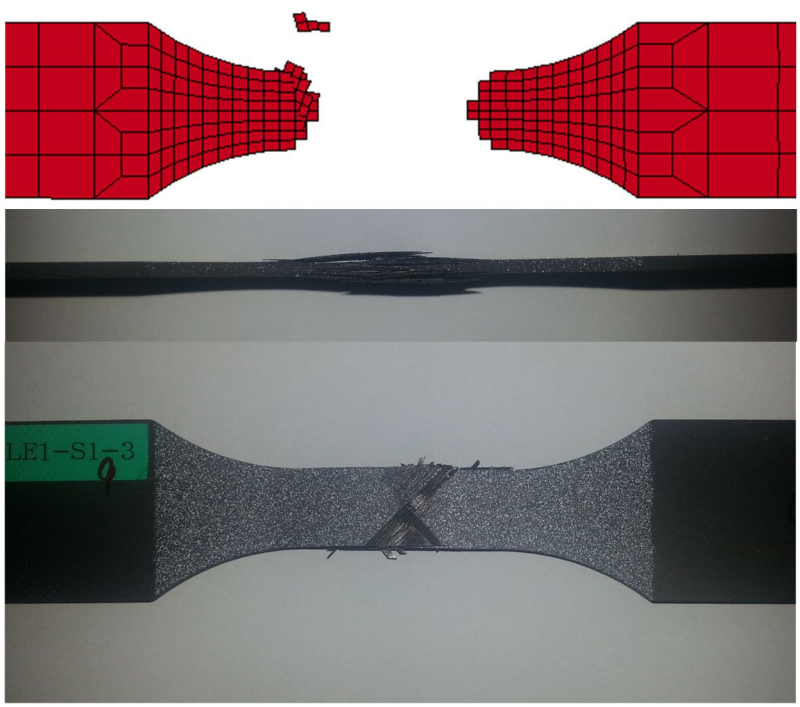

Fig. 4.13 Comparison of the failed coupon shapes of experimentation and

analysis with EDPM for 10/80/10 (LE1) configuration of the T700/M015 laminate

In Fig. 4.14, comparison of experimental and predicted stress-strain curves using the EDPM for LE1 configuration with various stroke speed. The variables for the EDPM is defined as $m = 8$ and $\lambda = 20$. Both of results present that the stiffness and strength tend to increase as the increasing of stroke speed. In case of experimental results, some dispersion appears in these data, but it can be found in the increasing tendency. For dynamic cases, approximately 5% of the strength of the error is estimated. The degradation around 0.75% of strain can be seen in every results as previously described.

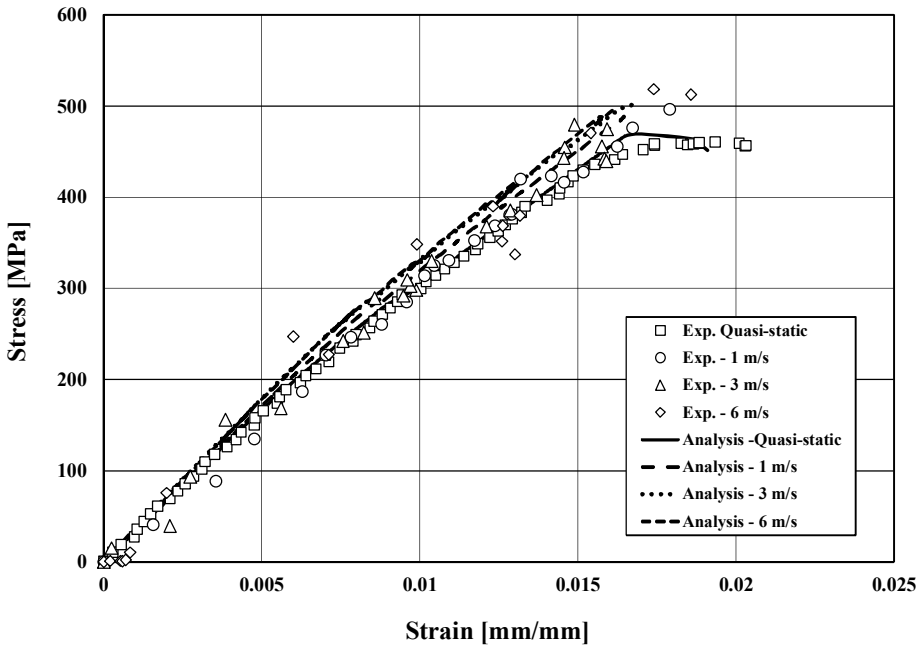

Fig. 4.14 Comparison of experimental and predicted stress-strain curves with EDPM (m = 8, λ = 20) for 10/80/10 (LE1) configuration with various stroke speed

In Fig. 4.15, comparison of experimental and predicted stress-strain curves using the EDPM for LE2 configuration with various stroke speed. The LE2 configuration is same as the quasi-isotropic laminate. The variables for the EDPM is same as previous analysis models. Unlike previous results of the LE1, both of results present that the stiffness and strength almost does not change as the increasing of stroke speed. It can be considered as the contribution of 0° laminas on the entire stiffness of laminate. For all of cases, approximately within 3% of the

strength and stiffness of the error can be estimated. The degradation around 0.8% of strain can be seen in every results, and it is also due to the failure of 90° laminas.

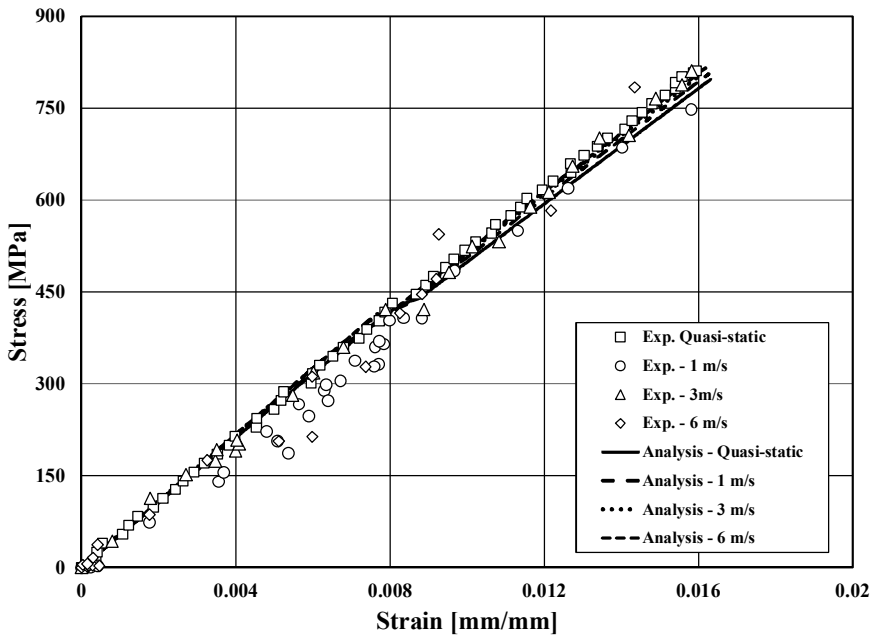

Fig. 4.15 Comparison of experimental and predicted stress-strain curves with EDPM (m = 8, λ = 20) for 25/50/25 (LE2) configuration with various stroke speed

In Fig. 4.16, comparison of experimental and predicted stress-strain curves using the EDPM for LE3 configuration with various stroke speed. The LE3 configuration is most stiffened laminate among laminate configurations in this study. The variables for the EDPM is same as previous analysis models. In the

results of analysis, the behaviors are almost rate-independent, even though some dispersion appears in experimental data. Through the results of LE2, we can be estimated that there are somewhat errors in the reduction of experimental data of dynamic cases. In case of the quasi-static case, within 3% of error is estimated on the stiffness and strength.

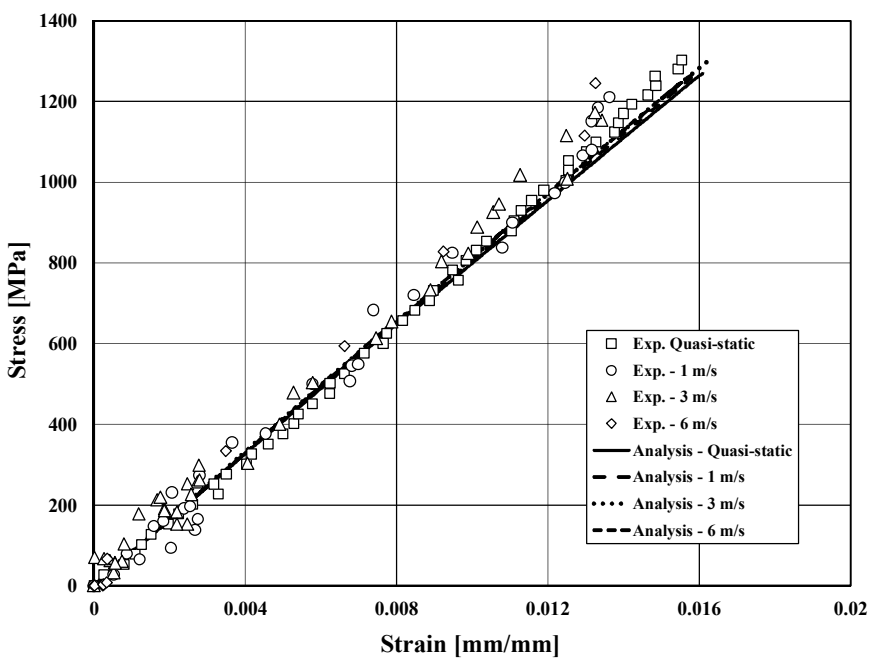

Fig. 4.16 Comparison of experimental and predicted stress-strain curves with EDPM (m = 8, λ = 20) for 40/50/10 (LE3) configuration with various stroke speed

5. DISCUSSION

The validation of the RDM using a multi-scale approach with experimental results of the T700/M015 and IM7/977-2 materials, shows that it precisely captures the non-linearity and rate dependence of polymeric composite materials with wide range of toughness, qualitatively and quantitatively. The rate-dependent elastic damage model in the RDM effectively works on degradation of the in-plane stiffness as increasing strain and strain rate.

Fig. 5.1 presents the shear damage master curves at all of strain rates, which curves are extracted from analysis results for the T700/M015 and IM7/977-2 $[\pm 45°]_s$ angle-ply. As increasing toughness of material, the slope of the curve decreases.

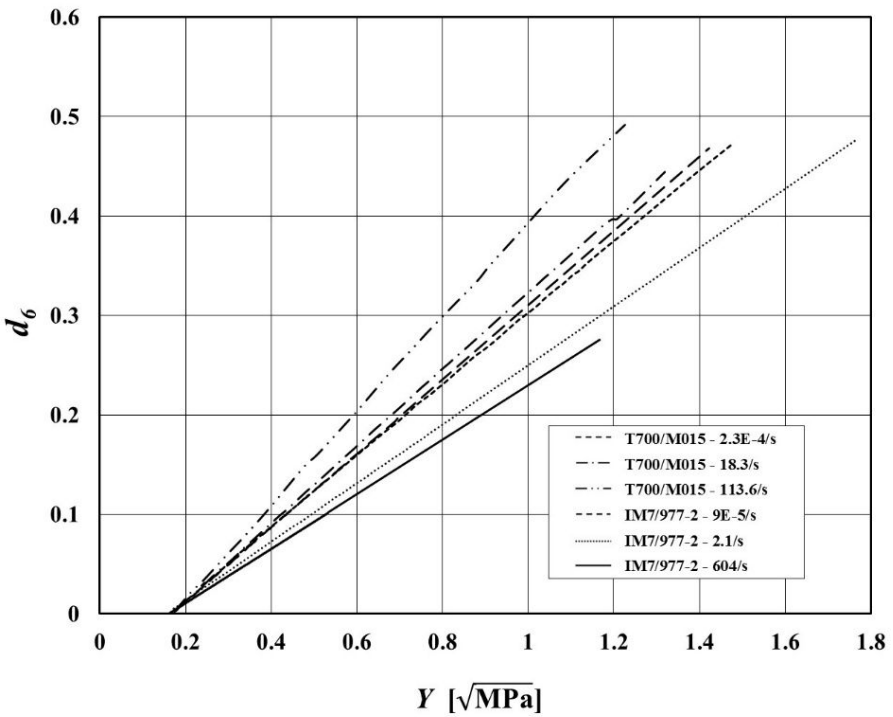

Fig. 5.1 Shear damage master curves from predictions using RDM for $[\pm 45°]_s$ laminate of the T700/M015 and IM7/977-2

This trend is shown in the slopes of the T700/M015 and IM7/977-2 materials. There is a remarkable point that the slope of the curve rises up in accordance with increasing strain rate. This phenomenon is similar to decrease of the plastic deformation and the failure strain of epoxy resins as increasing strain rate [7]. Such change of damage characteristics in the RDM can be materialized by the viscoelastic and viscoplastic models for polymeric matrices and the rate-dependent

in-plane damage constants. The shear damage master curve for the IM7/977-2 at a quasi-static condition shows that there is no matrix failure up to the strain level of 5% caused by the relatively high toughness. The shear damage master curve for the T700/M015 at a quasi-static condition is in good agreement with the experimental result presented in Fig. 2.11 (a).

To compare the performance of the damage growth model, the specific damage growth strain energy, E_{DG}, is introduced in this study. E_{DG} can be described as follow:

$$E_{DG} = \int_1^{r_c} (1-\omega)\, dr \tag{5.1}$$

where

$$r = \frac{\varepsilon}{\varepsilon_f} \quad , \quad r_c = \sqrt[m]{1+7m}$$

r is the strain ratio between the current and failure, and r_c means the critical strain ratio when ω is unity.

$$E_{DG} = \int_1^{r_c} \exp\left(\frac{1}{m}(1-r^m)\right) dr \tag{5.2}$$

$$E_{DG} = \int_1^{r_c} \exp\left(\frac{1-r^m}{\lambda r-(r-1)m''}\right) dr \tag{5.3}$$

where

$$m'' = \frac{m - \lambda m'}{1 - m'}, \quad m' = \sqrt[m]{1 + 7m}$$

Eq.(5.2) and (5.3) are the specific damage growth strain energy of the Yen's model and the EDPM presented in this study, respectively.

In Fig. 5.2, the specific damage growth strain energy of the EDPM and Yen's damage model are shown to compare the performance of the PFA. As previously mentioned, the cross point with curves of the Yen's model and the EDPM is occurred once the variable m and λ are same value in the EDPM. The Yen's model has a single value of E_{DG} corresponding to variable m, whereas, the EDPM has a range of value of E_{DG} corresponding to variable m by applying the variable λ. That means the EDPM can have a wide range of E_{DG} than the Yen's model in the same range of strain ratio, in other words, the EDPM has a flexibility to simulate the damage growth. Moreover, in case of the LE1 configuration presented in Fig. 4.12, in point of view about the numerical instability, the Yen's model just has 0.266 of E_{DG}, but the EDPM can represent 0.332 of E_{DG}. As a result, the EDPM can be affordable to simulate more ductile behavior of LE1 configuration, and we can consider that the EDPM proposed in this study, is the appropriate damage model to

more precisely simulate the damage progression for the crash and impact of composite structures using the explicit FE analysis with multi-integration shell elements.

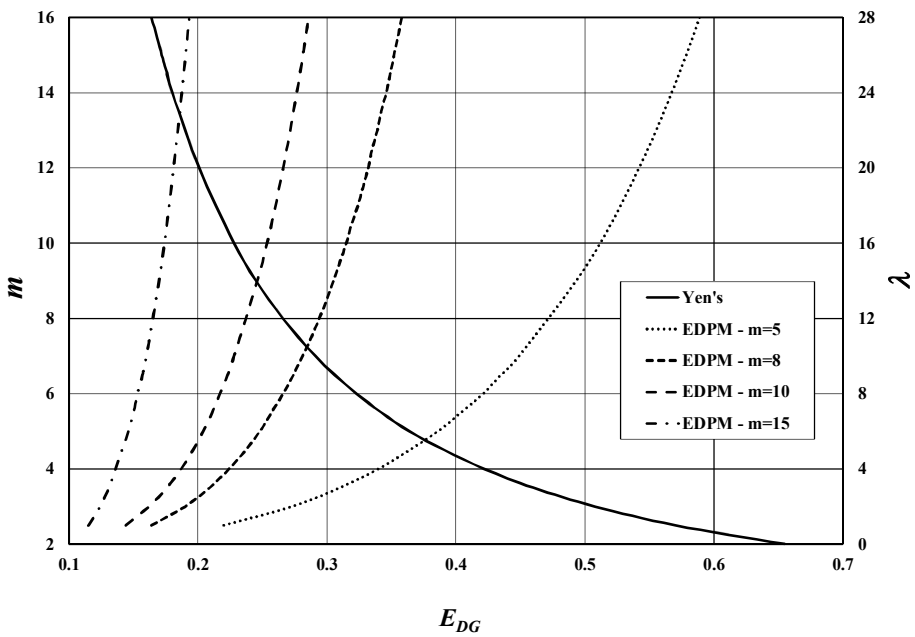

Fig. 5.2 Comparison of the specific damage growth strain energy of the EDPM and Yen's damage model

In Fig. 4.14, we can observe that the increasing of the stiffness and strength as larger stroke speed is remarkable than other stress-strain responses which are depicted in Fig. 4.15 and Fig. 4.16. The stiffness is increased by about 9% and the

increasing of strength is nearly 12%. For the LE2, the increasing of stiffness and strength is about 3%, and it is almost none in the LE3. Through these results, we can infer that this phenomenon is originated from the contribution of matrix material to the laminate. In case of the LE1, 90% of the laminate is a matrix dominant.

In the crash and impact environment, the loading direction is not always aligned as the static case. Therefore, in spite of the LE2 and LE2, the change of the stiffness and strength with respect to strain rate can be occurred. Fig. 5.3 presents the analysis results of the LE3 under 40 degree of inclined loading condition. Compare with the result in Fig. 4.16, the stiffness is reduced by 54%, and then it can be seen that the stiffness and strength are increased by about 5% with respect to the increase of stroke speed.

Fig. 5.4 shows the result of analysis for the LE2 under 40 degree of inclined loading, it can be seen that there is almost independent of strain rates, though inclined loading direction. It is estimated as the effect of quasi-isotropic lamination of the LE2 which is always same stiffness in any direction. Therefore, we can get the rate-independent composite structures once we use quasi-isotropic laminates.

Through above results of analyses and experimentations, the rate-dependent behavior of polymeric composite materials should be considered to get more precise prediction when the crash and impact analysis.

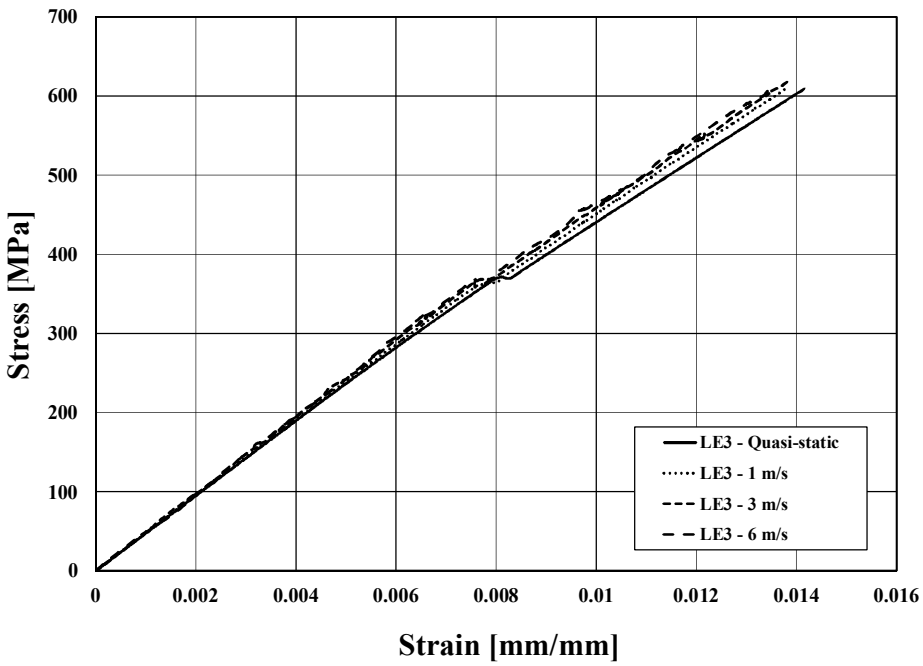

Fig. 5.3 Predicted stress-strain curves for 40/50/10 (LE3) configuration under 40° of inclined loading direction

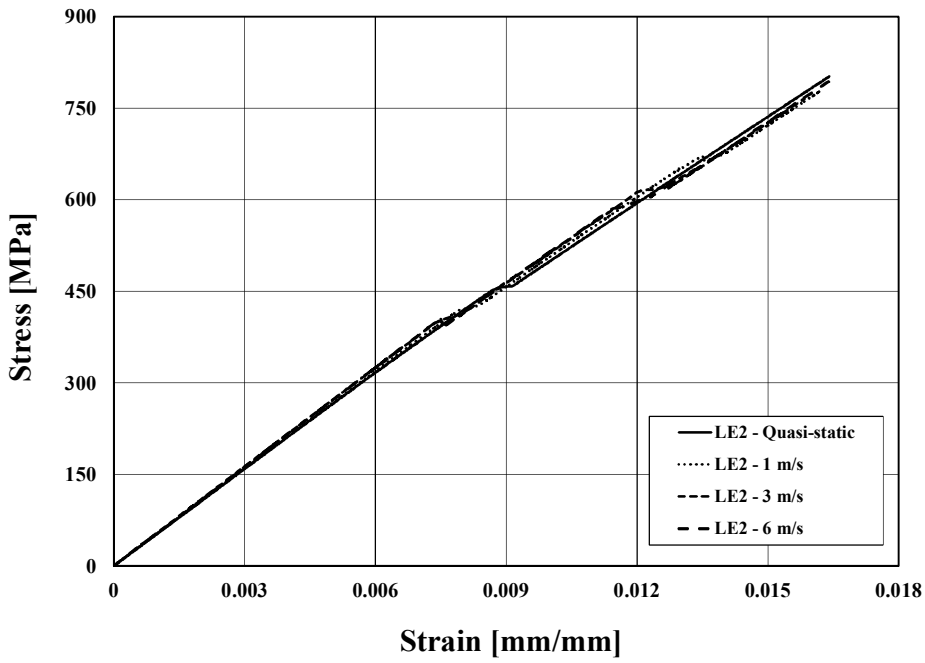

Fig. 5.3 Predicted stress-strain curves for 25/50/25 (LE2) configuration under 40° of inclined loading direction

6. CONCLUSIONS

In this work, it is aimed to develop the nonlinear damage models for the crash and impact simulation of polymeric composite materials using the explicit FEM.

In the first part of this study, the phenomenological inquiry for polymeric UD carbon composite materials is carried out with the sources of nonlinear deformations such as anisotropic behavior, rate-dependent characteristics, and the initiation and evolution of micro-cracks.

The viscoelastic and viscoplastic constitutive equations are employed to simulate the rate-dependence of polymers. The micromechanical approach is employed to consider the different response of constituents simultaneously. The enhanced micromechanical model using the modified slicing algorithm is proposed to improve the prediction of in-plane shear behavior, and the verification is carried out through comparisons with several coupon test results.

To account for the damage from the micro-cracks in the matrix and the matrix/fiber interface, the rate-dependent elastic composite damage model is introduced and modified as a simple form through validation to ensure

compatibility with the viscoplastic model using a micromechanical approach. Finally, the RDM using a multi-scale approach is developed, and then the implementation of LS-DYNA as a UMAT is carried out.

Through validation of the RDM using a multi-scale approach with experimental results of the T700/M015 and IM7/977-2 materials, it is confirmed that the RDM using a multi-scale approach precisely captures the non-linearity and rate dependence of polymeric composite materials with wide range of toughness under in-plane shear dynamic loading, qualitatively and quantitatively.

In the second part of this study, the PFA model for the crash and impact analysis of polymeric composite materials using the explicit FE analysis, is introduced, which model is composed of the rate-dependent composite failure detecting, damage progression after material failure, and elements elimination. In the PFA model presented in this study, the EDPM based on CDM for the composite damage growth is proposed to precisely simulate the post-failure behaviors of composite materials.

As the composite failure detection method with respect to strain rates, the rate-dependent Hashin failure model for two dimensional condition is applied into this

study. In matrix direction, the failure strength and the failure indices for initiation with respect to strain rates are employed to allow the rate-dependent criteria.

To account for the damage progression and post failure analysis, the hybrid material degradation method is employed, which method is composed of the ply-discounting method on the laminate with the damage model based on a CDM approach on each layer. The material degradation of corresponding to each constituent is adopted within composite micromechanical model, and the decreasing of stress is embodied with the level of micromechanics after the detection of material failure. The material degradation is achieved with corresponding to the failed surface and failure modes such as tension or compression.

To develop the EDPM, the MLT and Yen's models are reviewed briefly and the EDPM is generated from the Yen's model which is an original form. The EDPM adopts an additional variable λ which controls the shape of damage growth curve, and it can make more damage growth strain energy than the Yen's model.

Through validation of the PFA presented in this study with experimental results of the laminate configurations of the T700/M015 composite material, it is

confirmed that the PFA model is appropriate to apply into the explicit FE analysis using a multi-integration shell meshes. Also, we can find that the EDPM proposed in this study, is the appropriate damage model to more precisely simulate the damage progression for the crash and impact of composite structures.

Moreover, the comparison study with experimental results about the behavior of “pre-post” failure, it can be validated and approved that the performance to predict and simulate the rate-dependent and nonlinear behaviors of polymeric composite materials using the RDM and EDPM proposed in this study.

REFERENCES

[1] H. M. Hsiao and I. M. Daniel, Strain rate behavior of composite materials, Compos. Part B 29B (1998) 521–533.

[2] V. P. W. Shim, C. T. Lim and K. J. Foo, Dynamic mechanical properties of fabric armour, Int. J. Impact Eng. 25 (2001) 1-15.

[3] A. Gilat, R. K. Goldberg, Experimental study of strain rate dependent behavior of carbon/epoxy composite, Compos. Sci. Technol. 62 (2002) 1469-1476.

[4] T. Z. Blazynski, Materials at high strain rates, Elsevier Appl. Sci. Publishers LTD (1987) 133-186.

[5] T. E. Tay, H. G. Ang, V. P. Shim, An empirical strain rate dependent constitutive relationship for glass-fiber reinforced epoxy and pure epoxy, Compos. Struct. 33 (1995) 201-210.

[6] Z. H. Li, J. Lambros, Strain rate effects on the thermomechanical behavior of polymers, Int. J. Solid Struct. 38 (2001) 3549-3562.

[7] A. Gilat, R. K. Goldberg, Strain rate sensitivity of epoxy resin in tensile and shear loading, NASA/TM-2005-213595, Washington, DC, National Aeronautics and Space Administration, (2005)

[8] W. A. Spitzig, O. Richmond, Effect of hydrostatic pressure on the deformation behavior of polyethylene and polycarbonate in tension and in compression, Polym. Eng. Sci. 19 (1979) 1129-1139.

[9] I. M. Ward, J. Sweeney, An introduction to the mechanical properties of solid polymers, John Wiley and Sons LTD, 2nd ed. (2004)

[10] A. S. Wineman, K. R. Rajagopal, Mechanical response of polymers, Cambridge University Press, (2000)

[11] C. A. Weeks, C. T. Sun, Modeling non-linear rate-dependent behavior in fiber-reinforced composites, Compos. Sci. Technol. 58 (1998) 603-611.

[12] S. V. Thiruppukuzhi, C. T. Sun, Testing and modeling high strain rate behavior of polymeric composites, Compos. Part B 29B (1998) 535-546.

[13] C. M. Bordonaro, Rate dependent mechanical behavior of high strength plastics: Experiment and modeling, PhD Dissertation, Rensselaer Polytech. Inst., Troy, New York (1995)

[14] R. K. Goldberg, D. R. Gary, A. Gilat, Implementation of an associative flow rule including hydrostatic stress effects into the high strain rate deformation analysis of polymer matrix composites, NASA/TM-2003-212382, Washington, DC, National Aeronautics and Space Administration, (2003)

[15] S. J. Kim, J. T. Oden, Finite element analysis of a class of problems in the finite elastoplasticity based on the thermodynamical theory of materials of type N, Compos. Meths. Appl. Mech. Eng. 53 (1985) 277-302.

[16] S. J. Kim, J. Y. Cho, The role of matrix in viscoplastic behavior of thermoplastic composites at elevated temperature, AIAA J. 31(12) (1992) 2571-2573.

[17] R. K. Goldberg, Strain rate dependent deformation and strength modeling of a polymer matrix composite utilizing a micromechanics approach, NASA/TM-1999-209768, Washington, DC, National Aeronautics and Space

Administration, (1999)

[18] C.T. Sun, J. Chan, A micromechanical model for plastic behavior of fiber composites, Compos. Sci. Technol. 40 (1991) 115-129.

[19] R. K. Goldberg, Computational simulation of the high strain rate tensile response of polymer matrix composites, NASA/TM-2002-211489, Washington, DC, National Aeronautics and Space Administration, (2002)

[20] S. K. Mital, P. L. M. Murthy, C. C. Chamis, Micromechanics for ceramic matrix composites via fiber substructuring, J. Compos. Mater. 29 (1995) 614-633.

[21] X. Zheng, Nonlinear strain rate dependent composite model for explicit finite element analysis, PhD Dissertation, University of Akron, Akron, Ohio, (2006)

[22] M. C. Lafarie-Frenot, F. Touchard, Comparative in-plane shear behavior of long carbon-fiber composites with thermoset or thermoplastic matrix, Compos. Sci. Technol. 52 (1994) 417-425.

[23] A. Puck, H. Schrümann, Failure analysis of FRP laminates by means of physically based phenomenological models, Compos. Sci. Technol. 62 (2002) 1633–1662.

[24] P. H. Petit, M. E. Waddoups, A method of predicting the nonlinear behavior of laminated composites, J. Compos. Mater. 3 (1969) 2.

[25] H. T. Hahn, S. W. Tsai, Nonlinear elastic behavior of unidirectional composite laminae, J. Compos. Mater. 7 (1973) 102-108.

[26] Z. Hashin, D. Bagchi, B. W. Rosen, Nonlinear behavior of fiber composite laminates, NASA CR-2013, Washington, DC, National Aeronautics and

Space Administration, (1973)

[27] R. S. Sandhu, Nonlinear behavior of unidirectional and angle ply laminates, J. Aircraft 13(2) (1976) 104-111.

[28] Y. Surrel, A. Vautrin, On a modelling of the plastic response of FRP under monotonic lading, J. Compos. Mater. 23 (1989) 232-250.

[29] R. Vaziri, M. D. Olson, D. L. Anderson, A plasticity based constitutive model for fiber reinforced composite laminate, J. Compos. Mater. 25 (1991) 512-535.

[30] T. S. Gates, C. T. Sun, Elastic/viscoplastic constitutive model for fiber reinforced thermoplastic composites, AIAA J. 29(3) (1991) 457-463.

[31] P. Ladeveze, E. Le Dantec, Damage modelling of the elementary ply for laminated composites, Compos. Sci. Technol. 43 (1992) 257-267.

[32] S. V. Thiruppukuzhi, C. T. Sun, Models for the strain-rate-dependent behavior of polymer composites, Compos. Sci. Technol. 61 (2001) 1-21.

[33] A. Gilat, R. K. Goldberg, G. D. Roberts, Experimental study of strain-rate-dependent behavior of carbon/epoxy composite, Compos. Sci. Technol. 62 (2002) 1469-1476.

[34] C. A. Deenadayalu, A. Cahttopadhyay, X. Zhou, Constitutive modeling of progressive damage in composite laminates, 46th AIAA/ASCE/AHS/ASC Structures, Structural Dynamics & Material Conference, AIAA, Austin, Texas, (2005).

[35] S.W. Tsai, E.M. Wu, A General theory of strength for composite anisotropic materials, J. Compos. Mater. 5 (1971) 58-80.

[36] Y. S. Reddy, J. N. Reddy, Three-dimensional finite element progressive

failure analysis of composite laminates under axial compression, J. Compos. Technol. Res. 15(2) (1993) 73-87.

[37] S. B. Singh, A. Kumar, N. G. R. Iyengar, Progressive failure of symmetrically laminated plates under uni-axial compression, Struc. Eng. Mech. 5(4) (1997) 433-450.

[38] S. Huybrechts, A. Maji, J. Lao, P. Wegner, T. Meink, Validation of the quadratic composite failure criteria with out-of-plane shear terms, J. Compos. Mater. 36(15) (2002) 1879-1888.

[39] Z. Hashin, Failure criteria for unidirectional fiber composites, ASME J. App. Mech. 47(2) (1980) 329-334.

[40] F. Paris, A study of failure criteria of fibrous composite materials, NASA/CR-2001-210661, Washington, DC, National Aeronautics and Space Administration, (2001).

[41] P. D. Soden, M. J. Hinton, A. S. Kaddour, A comparison of the predictive capabilities of current failure theories for composite laminates, Compos. Sci. Technol. 58(7) (1998) 1225-1254.

[42] P. D. Soden, M. J. Hinton, A. S. Kaddour, Biaxial test results for strength and deformation of range of E-glass and carbon fiber reinforced composite laminates: Failure exercise benchmark data, Compos. Sci. Technol. 62(12-13) (2002) 1489-1514.

[43] P. A. Zinoviev, O. V. Levedeva, L. P. Tairova, Coupled analysis of experimental and theoretical results on the deformation and failure of laminated composites under a plane state of stress, Compos. Sci. Technol. 62(12-13) (2002) 1711-1723.

[44] A. Kuraishi, S. W. Tsai, K. Liu, A progressive quadratic failure criterion, Compos. Sci. Technol. 62(12-13) (2002) 1683-1695.

[45] C. T. Sun, J. Tao, A. S. Kaddour, Prediction of failure envelopes and stress-strain behavior of composite laminates: Comparison with experimental results, Compos. Sci. Technol. 62(12-13) 1673-1682.

[46] O. O. Ochoa, J. J. Engblom, Analysis of failure in composites, Compos. Sci. Technol. 28 (1987) 87-102.

[47] F. K. Chang, K. Y. Chang, A progressive damage model for laminated composites containing stress concentrations, J. Compos. Mater. 21(9) (1987) 834-855.

[48] Y. S. Reddy, J. N. Reddy, Three-dimensional finite element progressive failure analysis of composite laminates under axial compression," J. Compos. Technol. Res. 15(2) (1993) 73-87.

[49] D. W. Sleight, N. F. Knight, Jr., J. T. Wang, Evaluation of progressive failure analysis methodology for laminated composite structures, 38th AIAA/ASCE/AHS/ASC Structures, Structural Dynamics & Material Conference, AIAA, Kissimmee, FL, (1997).

[50] E. Moas, O. H. Griffin, Jr., Progressive failure analysis of laminated composite strcutres, 38th AIAA/ASCE/AHS/ASC Structures, Structural Dynamics & Material Conference, AIAA, Kissimmee, FL, (1997).

[51] C. G. Dávila, P. P. Camanho, C. A. Rose, Failure criteria for FRP laminates, J. Compos. Mater. 39(4) (2005) 323-345.

[52] J. Chen, M. Crisfield, A. J. Kinloch, E. P. Busso, F. L. Matthews, Y. Qiu, Predicting progressive delamination of composite material specimens via interface elements, Mech. Compos. Mater. Struct. 6(4) (1999) 303-317.

[53] P. P. Camanho, C. G. Dávila, D. R. Ambur, Numerical simulation of delamination growth in composite materials, NASA/TP-2001-211041, Washington, DC, National Aeronautics and Space Administration, (2001).

[54] N. F. Knight, Jr., User-defined material model for progressive failure analysis, NASA/CR-2006-214526, Washington, DC, National Aeronautics and Space Administration, (2001).

[55] A. Matzenmiller, J. Lubiliner, Jr., R. L. Taylor, A constitutive model for anisotropic damage in fiber-composites, Mech. Mater. 20 (1995) 125-152.

[56] W. Weibull, A statistical distribution function of wide applicability, ASME J. App. Mech. 18 (1951)

[57] T. S. Creasy, Modeling analysis of tensile tests of bundled filaments with a bimodal Weibull survival function, J. Compos. Mater. 36(2) (2002) 183-194.

[58] LS-DYNA Users Manual – Volume II (Material models, references and appendices), Version 971, Livermore Software Technology Corporation, Livermore, CA, (2007).

[59] L. Zhu, A. Chattopadhyay, R. K. Goldberg, Failure model for rate-dependent polymer matrix composite laminates under high-velocity impact, J. Aerospace Eng. 21(3) (2008) 133-139.

[60] D. C. Stouffer, L. T. Dame, Inelastic deformation of metals, models, mechanical properties and metallurgy, John Wiley and Sons, New York, (1996).

[61] O. Allix, H. Girard, P. Ladeveze, E. Vittecoq, Composites 2D á fibres haute résistance: caractérisation du comportement de compression, J.N.C.6 De. Pluralis, Paris, (1988) 515-526.

[62] O. Allix, P. Ladeveze, E. Vittecoq, Modelling and identification of the mechanical behavior of composite laminates in compression, Compo. Sci. Technol. 51 (1994) 35-42.

[63] S. S. Paul, A model for kinking in fiber composites-I. Fiber breakage via micro-buckling, Int. J. Solids Struct. 26(5) (1990) 549-561.

[64] P. R. H. Christopher, W. G. John, Jr., Effects of hydrostatic pressure on the mechanical behavior of composite materials, ARL-TR-727, Army Research Laboratory, (1995)

[65] Standard test method for tensile properties of polymer matrix composite

materials, ASTM Standard D3039/3039M-08, American Society for Testing of Materials, Philadelphia, PA, 2008

[66] Standard test method for shear properties of composite materials by V-notched rail shear method, ASTM Standard D7078/7078-08, American Society for Testing of Materials, Philadelphia, PA, 2008

[67] W. Y. You, J. H. Lim, D. W. Sohn, S. W. Kim, S. H. Kim, Prediction of the equivalent elastic properties of fiber reinforced composite materials and structural analysis of composite satellite panel, Aerospace Eng. Technol. 12(2) (2013) 48-56.

[68] C. T. Sun, R. S. Vaidya, Prediction of composite material properties from a representative volume element, Compos. Sci. Technol. 56 (1996) 171-179.

[69] J. Y. Jeong, S. K. Ha, Analysis of micromechanical behavior of fiber-reinforced composites, The Transactions of the Korean Society of Mech. Eng. A 28(10) (2004) 1435-1450.

[70] A. Matzenmiller, J. Lubliner, R. L. Taylor, A constitutive model for anisotropic damage in fiber-composites, Mech. Mater. 20(2) (1995) 125-152.

[71] C. Herakovich, Mechanics of fibrous composites, John Wiley and Sons LTD, 1st ed. (1998).

[72] P. Maim, P. Camanho, J. Mayugo, C. Dávila, A continuum damage model for composite laminates: Part I – Constitutive model, Mech. Mater. 39(10) (2007) 897-908.

[73] R. S. Zimmerman, D. F. Adams, D. E. Walrath, Investigation of the relations between neat resin and advanced composite mechanical properties: Volume I – Results, NASA/CR-172303, Washington, DC, National Aeronautics and Space Administration, (1984).

[74] C. L. Hwan, K. H. Tsai, C. H. Chiu, Y. S. Huang, Strength prediction of woven hybrid composite laminates each with a center hole, J. Compos. Mater. 0 (2013) 1-8.

[75] F. Pierron, A. Vautrin, Accurate comparative determination of the in-plane shear modulus of T300/914 by the iosipescu and 45° off-axis tests, Compos. Sci. Technol. 52 (1994) 61-72.

[76] A. D. Mulliken, Low to high strain rate deformation of amorphous polymers: Experiments and modeling, M.Sc. Dissertation, Massachusetts institute of technol., Cambridge, Massachusetts, (2004).

[77] C. F. Yen, Ballistic impact modeling of composite materials, Proceeding of the 7th int. LS-DYNA users conference, (2002).

[78] X. Zheng, R. K. Goldberg, W. K. Binienda, G. D. Roberts, LS-DYNA implementation of polymer matrix composite model under high strain rate impact, NASA/TM-2003-102633, Washington, DC, National Aeronautics and Space Administration, (2003).

[79] L. Zhu, A. Chattopadhyay, R. K. Goldberg, Multiscale analysis including strain rate dependency for transient response of composite laminates shells, J. Reinforced Plastics and Compos. 25(17) (2006) 1795-1831.

[80] C. T. Sun, R. S. Vaidya, Prediction of composite properties from a representative volume element, Compos. Sci. Technol. 56 (1996) 171-179.

[81] J. S. Welsh, J. S. Mayes, A. C. Biskner, Experimental and numerical failure predictions of biaxially-loaded quasi-isotropic carbon composites, Proceeding of the 16th Int. conference on Compos. Mater. (2007).

[82] T. E. Tay, G. Liu, V. B .C. Tan, X. S. Sun, D. C. Pham, Progressive failure

analysis of composites, J. Compos. Mater. 42(18) (2008) 1921-1966.

[83] Agate laminate material qualification of T700G/#2510, 150 g/m2 - UD tape, T700S/#2510, 190g/m2 – plan weave fabric, and Style 7781 finish 558/#2510, 295g/m2 – glass fiber fabric, TCQAL-T-1026, Toray Composites (America), INC., (2002).

초 록

항공기 경량화를 통한 운항효율을 증진시키기 위해 최근 폴리머 복합재료를 적용한 항공기 주 구조물의 개발이 보편화되고 있는 추세이다. 복합재료의 항공기 구조재료로의 적용 확대는 일반적인 항공기 운용 조건을 나타내는 선형, 정적 하중 하의 항공기 구조 설계 및 해석에 요구되는 해석 기법과 재료 물성확보 등 공학적 기법의 발전으로 이어졌다. 그러나 항공기 구조재료로 널리 적용되는 복합재료의 동적 거동 및 비선형 변형 등은 해석의 정확도가 선형, 정적 해석에 비해 상대적으로 높지 않으며, 특히 충격 또는 충돌에 의해 발생되는 비선형 거동의 해석적 방법을 통한 예측에는 한계를 나타내고 있다. 그러므로 이러한 비선형 거동과 충돌속도에 따라 변화하는 복합재료의 거동을 예측하기 적합한 해석 모델과 방법의 개발을 통해 항공기 구조물의 내추락 성능 향상이 가능할 것으로 판단할 수 있다.

본 연구는 외연적 유한요소해석기법에 적용하기 위한 변형률속도에

따라 변화하는 폴리머 복합재료의 비선형 손상 모델에 관한 것으로, 재료의 비선형 손상 거동을 효과적으로 예측하기 위해 수행되었다. 복합재료의 파손이 발생하기 전 거동을 예측하기 위한 손상 모델은 다중스케일 접근법을 이용한 폴리머 복합재료의 점탄성, 점소성 구성방정식으로 구성되어 있다. 현상학적으로, 면내 전단하중이 작용하는 복합재료의 비선형 변형 거동은 기질의 점소성 거동과 복합재 내부의 미세손상에 의한 손상거동에 의해 나타나는 것으로 알려져 있다. 동적 하중이 작용하는 경우 변형률속도의 변화는 복합재료 내 기질의 거동의 변화 뿐 아니라, 복합재 손상거동의 변화를 초래하게 된다. 면내 전단 거동에 대한 정확도가 향상된 미시역학모델의 적용을 통해 변형거동의 특성이 상이한 섬유와 기질의 거동을 동시에 고려하였다. 해석 모델의 정확도 향상을 위해 본 연구에서는 거시역학적 이방성 연속체 손상역학이론을 바탕으로 변형률속도에 따라 탄성손상모델의 상태변수가 변화하는 손상모델을 제안하였다.

본 연구에서 복합재 적층판내의 적층의 파손이 발생한 이후 재료 강성 및 강도의 변화를 나타내기 위한 손상 거동 모델을 적용하고 있다. 복합재 적층판 내의 복합재 적층의 파손 발생 예측은 Hashin 파손 모델

을 기본형태로 변형률속도에 따라 파손기준이 변화하는 파손 모델을 적용하였다. 복합재 적층판 내 복합재 적층의 파손에 의한 강성 및 작용 응력의 감소를 나타내기 위해 본 연구에서는 향상된 손상 진전 모델을 제안하고 있다. 이 손상 진전 모델은 기존 손상 진전 모델에 다양한 형태의 손상 거동 곡선을 나타내기 위한 변수를 추가함으로써 기존 모델에 비해 다양한 손상 거동을 모사할 수 있어, 외연적 유한요소해석을 이용한 복합재 점진적 파손해석에 적합한 모델이다.

본 연구에서 제안된 변형률속도에 따라 변화하는 손상 모델을 적용한 해석 결과는 다양한 변형률 속도에서의 시험치와 비교를 통해 검증되었으며, 높은 해석 정확도를 확인할 수 있었다. 또한 본 연구에서 제안된 손상 진전 모델은 외연적 유한요소기법을 위한 점진적파손해석기법에 매우 적합한 모델임을 확인할 수 있었다.

주요어 : 손상 진전 모델, 다중스케일 접근법, 폴리머 복합재료, 점진적 파손해석, 변형률속도 손상 모델

학 번 : 2010-30954